A HYDRODYNAMIC INVESTIGATION OF PLATINUM FLOTATION IN A PILOT FLOTATION PLANT

A Thesis Submitted To The Faculty Of
ENGINEERING AND THE BUILT ENVIRONMENT
of the
UNIVERSITY OF CAPE TOWN
In Fulfilment Of The Requirements Of The Degree Of
MASTER OF SCIENCE IN ENGINEERING

By
Jonathan Stretton Lewis
B.Eng. (Metallurgical Engineering) (RMIT)

Mineral Processing Research Unit
University of Cape Town
Rondebosch 7700
South Africa
March 2003

Abstract

Flotation cell hydrodynamics, driven by the central hydrodynamic variables of impeller speed and air flowrate, has a profound effect on flotation in mechanical flotation cells. However, comparatively little work has been performed on quantifying the effect of these variables in the flotation of platinum ores. This is despite the fact that, due to the effect of impeller speed and air flowrate on the power input, platinum producers regard hydrodynamic effects as having a large impact on the recovery of platinum in their flotation circuits. The aim of this thesis was to determine the effect of impeller speed and air flowrate on the flotation of platinum in mechanical flotation cells.

The testwork for this thesis was performed on the Baker Process Floatability Characterisation Test Rig (FCTR), under the auspices of the AMIRA P9 project. The FCTR is a fully instrumented, self-contained flotation pilot plant consisting of twelve mechanical flotation cells, six of which are 150 litre rougher cells and six are 50 litre cleaner cells. The testwork was conducted on-site at Lonmin's Eastern Platinum concentrator near Brits in the North-West Province of South Africa. Tests were conducted in the first four rougher cells of the FCTR using a central composite rotatable design (CCRD) statistical technique. Two plant streams were run through the FCTR; namely the primary rougher feed and the secondary cleaner tails. For each of these streams, fourteen tests were conducted at a variety of different settings of both impeller speed and air flowrate. The results of these tests were mass balanced and a statistical analysis was performed on the data. The results of this regression analysis were then used to calculate the flotation performance under each set of hydrodynamic conditions in terms of the recovery, flotation rate constant and concentrate grade.

In addition to the flotation tests, ancillary hydrodynamic data was collected at the various settings of impeller speed and air flowrate. This data was used to evaluate hydrodynamics, gas dispersion and solids suspension in the rougher cells. Hydrodynamic data was either evaluated using actual experimental measurements (e.g. power input, bubble size, superficial gas velocity) or used to determine various dimensionless numbers and other important hydrodynamic parameters (e.g. power number, Froude number, air flow velocity). In general, this hydrodynamic data was found to lie within, or just outside, the ranges of values observed in typical industrial platinum flotation cells. However, gas dispersion parameters were found to be towards the lower (poorer) end of this range and were fairly insensitive to changes in impeller speed and air flowrate.

Significant statistical error was observed in the CCRD regression analysis of the rougher feed results while the cleaner tails results were generally good. Hence, the major conclusions from the

flotation tests were derived largely from the cleaner tails results. Recovery was generally found to increase with increasing feed grade, impeller speed and air flowrate, which is commonly observed in the flotation literature. More significantly, however, is that no (clear) relationship between the flotation rate constant and bubble surface area flux was observed. This does not support the commonly observed k-S_b relationship, developed through the P9 Project, and suggest that this relationship does not hold for platinum.

A more positive finding from the flotation tests was that increasing the power intensity was found to have a beneficial effect on the rate of flotation of platinum, particularly in cells further down the bank. From this it was (tentatively) concluded that increasing the power intensity improves the rate of flotation of finer or slow floating material, which is a common opinion in the platinum industry. Unfortunately, increases in recovery and the flotation rate constant were generally accompanied by significant decreases in concentrate grade. This may have been due to simple factors, such as increases in entrainment, or due to increases in the rate of flotation of poorly liberated, slow floating particles at higher levels of agitation. This would have to be ascertained through a mineralogical study of the flotation concentrate, which was not done as part of this study, and represents an opportunity for future research.

Acknowledgements

I would like to express my sincere thanks to my supervisor, Dr Dave Deglon, for his invaluable advice and guidance in this study.

The help of the following people is also gratefully acknowledged:

My co-supervisor, Professor Cyril O'Connor, for his input and enthusiasm.

The staff at Lonmin and Eastern Platinum for their assistance with the FCTR campaign; in particular Bert Knopjes, Craig Goodall and Wilhelm De Beer.

Rob Coleman, for his assistance, support and friendship during the long days of the FCTR campaign.

JKMRC staff, Tim Napier-Munn, J-P Franzidis and Emmy Manlapig, for their assistance with the statistical design of the campaign.

My mother, Jean Lewis, for her encouragement and moral support over the years.

My wife, Meron, for her eternal patience and good humour, and for having the sense to remind me to wind up my window when there are ostriches about.

TABLE OF CONTENTS

List of Figures

List of Tables

Nomenclature

a_i	Coefficients estimated from the data (Equation 3.4)
α_{rot}	Distance of axial points from the centre for rotatability
ε	Specific power input
ε_u	Error which cannot be explained by the model (Equation 3.4)
γ_{LS}	Surface tensions at the liquid-solid interface
γ_{LV}	Surface tensions at the liquid-vapour interface
γ_{SV}	Surface tensions at the solid-vapour interface
λ	Parameter for orthogonality
μ_L	Liquid viscosity
v	Velocity
ρ	Pulp density
ρ_L	Liquid density
ρ_S	Solids denisty
τ	Pulp phase residence time
τ_g	Gas phase residence time
τ_s	Shear stress
τ_{con}	Contact between particle and bubble
τ_F	Film drainage time
τ_{In}	Inertial effect
τ_o	Induction time when kinetic hindrance to attachment is at a minimum
τ_{TPC}	Expansion time
c	Solids concentration
C	Impeller height above the bottom of the tank
d_b	Bubble diameter
d_p	Particle diameter
d_{32}	Sauter mean bubble diameter
D	Impeller diameter
E_c	Efficiency of collision between particles and bubbles
E_{id}	Ideal collision
E_s	Interception effect
E_{In}	Inertial effect
E_G	Gravitation effect

F	Resistive force per unit area
g	Gravitational forces
G	Concentrate grade
h	Depth of froth
H	Liquid depth
J	Baffle width
J_g	Superficial gas velocity in the flotation cell
k	First-order rate constant
k_a	Rate of particle attachment
k_d	Rate of particle detachment
L	Length of impeller blade
n_c	Number of factorial runs
n_a	Number of axial runs
n_0	Number of centre point runs
N	Impeller rotational speed
N_{JS}	Impeller speed necessary to just completely suspend particles
N_P	Power number
N_Q	Air flow number
N_{Fr}	Froude number
N_{Re}	Reynolds number
N_{We}	Weber number
N_{TOT}	Total number of experiments
P	Impeller power consumption
P_f	Particle floatability
Pa	Probability of attachment
Pc	Probability of collision
P_d	Probability of detachment
P_{coll}	Probability of collection
Q	Air flow rate
R	Recovery of mineral
S_b	Bubble surface area flux
T	Tank diameter
u(t)	Turbulent velocity
u_{mean}	Mean velocity
u'(t)	Fluctuating velocity
U_{tip}	Impeller tip speed
V	Cell volume

W	Width of impeller blade
x_i	Factors (Equation 3.4)
y	Equation response (Equation 3.4)

Abbreviations

AMIRA	Australian Mining Industry Research Association
CCRD	Central Composite Rotatable Design
FCTR	Floatability Characterisation Test Rig
JKMRC	Julius Kruttschnitt Mineral Research Centre
MPRU	Minerals Processing Research Unit (UCT)
OK	Outokumpu® (flotation cell manufacturer)
P9L	Project 9 Module L (AMIRA project numbering system)
PGM	Platinum group metals
PLC	Process logic controller
RPM	Revolutions per minute
RTD	Residence time distribution
SD	Standard deviation
SMD	Stirred media detritor
UBC	University of British Columbia
UCT	University of Cape Town
VSD	Variable speed drive

Chapter 1 Literature Review

This chapter presents a review and critique of the literature pertaining to the topics dealt with in this thesis. The chapter firstly presents a brief overview of the process of froth flotation and then discusses mechanical flotation cells. The chapter concludes with a detailed review of hydrodynamic effects in mechanical flotation cells after which the scope and objectives of the thesis are presented.

1.1 Froth Flotation

1.1.1 Overview of Flotation

Froth flotation is the most important technique in modern mineral processing. Existing as a patented process since 1906 (Wills, 1988), it has grown into the most widely used mineral separation process in the world today. Flotation has allowed low-grade orebodies, or orebodies containing finely disseminated minerals that would otherwise have been uneconomic, to be developed. Originally used to treat lead, zinc and copper sulphide ores, froth flotation is now applied to over one hundred different mineral species, including iron oxides, oxidised minerals such as malachite, and also non-metallic ores such as coal. The selectivity of the process also means that complex orebodies, such as those containing lead, zinc and silver-bearing minerals can be separated into specific concentrates.

The first patent involving mineral flotation was granted in 1860 to Haynes (anon., 1982) who recognised differences in the wettability of mineral particles by oil and water. This was the starting point for a number of "oil" flotation processes. Between 1890 and 1915, skin flotation was developed, and as early as 1902 Potter recognised the potential for using gas bubbles to carry sulphide mineral particles to the surface of an ore pulp. Froth flotation was first used commercially at Broken Hill to treat zinc-rich lead tailings in 1909 (Griffiths, 1998).

The process of flotation selectively separates different minerals by exploiting differences in the physical and chemical properties of the various species. The addition of flotation reagents selectively renders the surfaces of mineral particles either hydrophobic or hydrophilic. The hydrophobic particles become attached to air bubbles and are carried upwards through the slurry to a froth layer that forms at the top of the flotation cell. This froth layer is removed and usually becomes the concentrate. Hydrophilic particles remain in the slurry in the flotation cell.

1.1.2 Subprocesses of Flotation

For froth flotation to occur successfully (i.e. for a mineral particle to be selectively removed from the pulp and to report to the concentrate), a large number of independent subprocesses must take place. These subprocesses are represented in schematic form below, as identified by Deglon (1998).

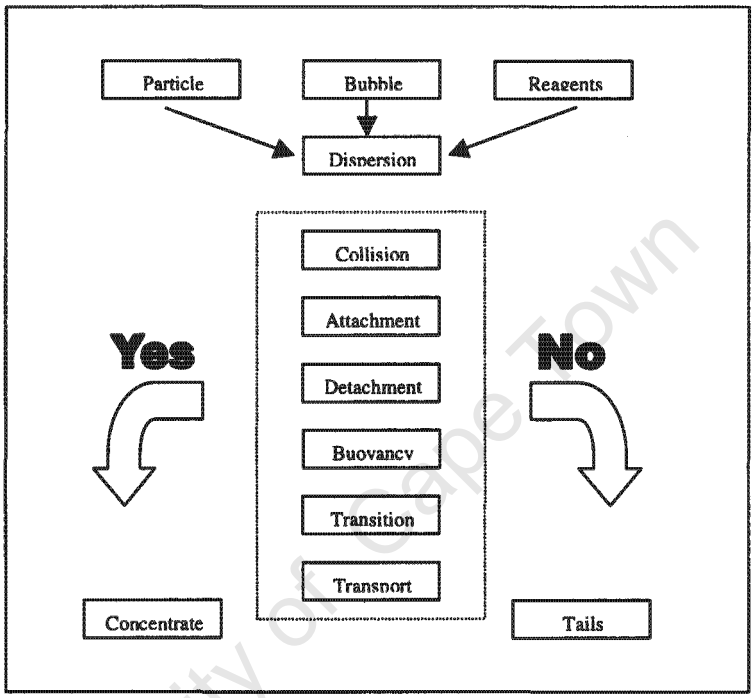

Figure 1.1 Subprocesses of flotation (after Deglon (1998)).

Schulze (1984) identified three broad areas that cover the subprocesses of froth flotation. These three areas are conditioning, particle collection and froth removal, and each of these will be discussed further.

1.1.2.1 Conditioning

The action of the impeller causes solid particles to be suspended in the pulp to form a slurry, and reagents such as collectors, frothers, activators and depressants are added to the cell. The various reagents perform different roles in the flotation process. Collectors are used to render the surface of the valuable mineral hydrophobic, and therefore amenable to collection. Frothers are used to help create a stable froth at the surface of the cell. Activators selectively activate certain mineral species

within the pulp to allow a collector to render them hydrophobic. Depressants are used to suppress the natural floatability of gangue minerals in the slurry.

1.1.2.2 Particle Collection

The three most important subprocesses in flotation are those of collision, attachment and detachment. During collision, reagentised mineral particles are contacted with gas bubbles, and in the subprocess of attachment the mineral particles adhere to the bubbles and are transported through the pulp to the froth phase. Some of the attached mineral particles detach from the bubble, for example due to the rupture of the bubble. These three subprocesses are extremely important to flotation as they determine the overall success of the process: namely, the ability to collect and remove valuable mineral particles from the slurry. General expressions for each of these subprocesses will be given in the following sections.

1.1.2.2.1 Collision

Collision is the process whereby reagentised and conditioned mineral particles are brought into contact with gas bubbles that are dispersed inside the flotation cell. The main mechanism of collision is a direct encounter between particle and bubble in suspension (Arbiter, 1984). Taggart (1945) suggested an alternative mechanism which requires saturation of pulp water by air, then localised pressure reduction to induce supersaturation. Under these conditions, hydrophobic surfaces can act as the preferred nuclei for bubble formation. There is no direct evidence that this occurs in commercial cells, however.

To collide with a bubble, a solid particle must have sufficient momentum to resist the tendency to follow the streamlines around the bubble (Ahmed and Jameson, 1989). Many expressions exist for the efficiency of collision, E_c, but one of the more common expressions is given by:

$$E_c \propto \frac{d_p^m}{d_b^n} \qquad \text{- 1.1}$$

where m and n vary between 1-2 and 2-3 respectively.

In reality, particle trajectories deviate from straight lines, so various collisions need to be defined:

- Ideal Collision, E_{id} – Approach without any change in the magnitude and direction of velocity,

- Interception Effect, E_s – Particles follow the stream lines of the bubble without any change in direction,
- Inertial Effect, E_{In} – Inertial forces of the particle result in increased collisions compared to the interception effect
- Gravitational Effect, E_G – Gravitational forces lead to partly increased collisions.

There are also a number of other effects, namely:

- Collision in the turbulent region behind the bubble
- Collision caused by diffuse or turbulent particle action
- A "cloud of bubbles", the spacing of which is smaller than that of the solids, thus holding back particles.

1.1.2.2.2 Attachment

Once a collision has occurred, there are a number of microprocesses that need to occur for the particle to become attached to the bubble. Ahmed and Jameson (1989) identified three microprocesses that occur during the attachment/adhesion of a particle to a bubble:

- Approach of a particle to a bubble.
- Thinning of the water film between particle and bubble to rupture thickness.
- Receding of the residual film to give an air-solid interface.

It is believed that the second step is the controlling mechanism in this process. Whether the particle can attach is dependent on the contact between particle and bubble, τ_{con} (Schulze, 1989). This is either the collision time (where a particle impacts on the bubble, deforming the surface strongly) or the sliding time (where the particle slides along the bubble, weakly deforming the surface).

During this contact period, the thin liquid film between the bubble and the particle must drain and rupture, giving a three-phase contact (TPC), which is large enough to stabilize the aggregate. The time required for this is the sum of the film drainage time (τ_F) and the expansion time (τ_{TPC}). It is referred to as the induction time (τ_i) and can be expressed as:

$$\tau_{con} \geq \tau_i = (\tau_F + \tau_{TPC}) \qquad \text{- 1.2}$$

The induction time is proportional to the bubble size, implying that small bubbles promote faster adhesion (Ahmed and Jameson, 1989). In turbulent flow, bubbles deform continuously. These

pulsating bubbles behave differently than those in a quiescent system, but the higher momentum of collision in a turbulent system is expected to increase the chance of thinning and rupturing the liquid film.

Laskowski (1989) postulated that the attachment of particles to bubbles has a probability that is dependent on a thermodynamic energy barrier which is the result of long range forces between particles and bubbles acting at the moment of attachment. The probability of attachment is given by:

$$E_c = 1 - \exp\left[-\left(\frac{\tau_{con} - \tau_i}{\tau_o}\right)\right] \qquad - 1.3$$

Where τ_o is the induction time when the kinetic hindrance to attachment is at a minimum. While there are a number of expressions for the probability of attachment, this particular expression predicts that an increase in the power input to a cell will increase the probability of attachment, and therefore improve the rate of flotation.

1.1.2.2.3 Detachment

Once bubble-particle attachment has occurred, the aggregate will rise to the froth-pulp interface and be transferred into the froth for collection of the mineral particle. However, if conditions in the cell make the particle-bubble aggregate unstable, then the mineral particle may become detached from the bubble and return to the pulp. For a particle-bubble aggregate to be stable, the restoring force of surface tension must balance the forces associated with the weight of the particle. The balance of these forces determines the maximum floatable particle size (Ahmed and Jameson, 1989). In a static system, the chances of retention also improve with the surface's hydrophobicity, increasing bubble size and decreasing particle size.

In a flotation cell, naturally, the static situation is not appropriate. Mika and Fuerstenau (1968) found the detachment rate to be proportional to $d_p^{7/3}$, assuming isotropic turbulence. It has also been argued that once a stable three-phase contact is formed, the particle can only be pulled away by some external factor, such as the energy of the turbulent field. A particle-bubble aggregate caught in a turbulent eddy will rotate with a frequency appropriate to the eddy size, and if the kinetic energy of the particle exceeds the work of rupture, the particle will detach (Ahmed and Jameson, 1989).

1.1.2.3 Froth Removal

To be collected, particle-bubble aggregates must be both sufficiently buoyant to rise through the pulp and sufficiently stable to endure any disturbances in the pulp (Deglon, 1998). Bubbles that reach the froth-pulp interface do not rupture immediately, but remain beneath the froth for some time while the liquid film separating the two phases drains away gradually (Egya-Mensah, 1998).

Bubble crowding occurs when new bubbles rising into the froth zone arrive behind bubbles already at the pulp-froth interface. The original bubbles are pushed further into the froth zone while still carrying the load of particles, resulting in the entrainment of some gangue particles into the froth. Composite particles (i.e. particles which comprise both valuable mineral and gangue) are also collected in the froth zone when they become attached to the bubbles. Fine slimes are also collected in this way. However, liquid film drainage and rupture of bubbles with age causes some of the particles to return to the pulp from the froth. Froth is then transported out of the flotation cell, carrying the trapped particles. The rate of froth transportation is dependent on a number of factors, most notably aeration rate, pulp chemistry and cell geometry.

1.1.3 Overview of Flotation Cells

The flotation cell has been under continuous development since the first years of the Twentieth Century (Arbiter, 1984), although an understanding of the role of the cell itself in the flotation process was slower to develop. Many types of flotation cells have been developed. Taggart (1945) makes mention of 171 different cells, although the majority of these existed only in patent descriptions. A number of authors (Wills (1988), Miller (1988) and Skillen (1993)) have discussed the types of flotation cells in use today. These cells can be divided into three broad categories: *mechanical cells, column cells* and *novel cells*. Each category will be discussed here.

Mechanical Cells

These cells are far and away the most common flotation cells in the minerals industry (Wills, 1988). Modern cells can be square or round and have volumes of up to $200m^3$. They are characterised by a mechanically driven impeller that agitates the slurry and disperses the introduced air into small bubbles. These cells produce high levels of agitation in order to maintain solids in suspension and so they are most effective for fine and medium sized particles. Coarse particles are not as effectively floated in these cells due to strong detachment effects with the high agitation. There are a number of manufacturers of these type of cell. Each manufacturer uses slight variations

on tank dimensions, impeller design, rotor/stator assembly and so on, although the basic principle of operation is the same in each case.

Column Cells

Column cells are a technology that has struggled to find acceptance in the minerals industry, although in recent times columns are becoming more widely used. A column cell is either round or square and can be up to three metres in diameter and over ten metres tall. Feed enters the cell near the top and flows downward in the cell under gravity. This runs countercurrent to the gas, which is introduced into the cell near the bottom through gas spargers. This results in better contact between the bubbles and the particles and has been shown to be a physical improvement in the flotation separation process, particularly for fine particles (Wills, 1988). Higher-grade concentrates can also be achieved through the use of wash water at the top of the cell, which helps to wash entrained gangue minerals out of the froth and back into the pulp. Therefore, column cells have become more widely used in cleaning applications (Deglon, 1998).

Novel Cells

There have been two major thrusts in the development of new flotation cells that attempt to improve the different flotation subprocesses (Deglon, 1998). These two thrusts are the improvement of gas dispersion through microbubble production and the improvement of particle-bubble contact through high agitation levels and separating the solids suspension and gas dispersion processes. These developments have been made possible through better understanding of the fundamentals of flotation, leading to an appreciation of the micro-environment required for optimum flotation. An example of this type of cell is the Jameson cell. This involves using a downcomer in which feed and gas are mixed rapidly before entering the cell itself. This technique improves the contact between particles and bubbles and also shortens the conditioning time, allowing for higher throughputs.

1.2 Mechanical Flotation Cells

As stated earlier, mechanical flotation cells are by far the most common type of froth flotation cell. Although there are a number of major flotation cell manufacturers, all mechanical flotation cells have the same basic features and fulfil the same basic function. Because of their common use in modern flotation plants, and because this thesis is based on work performed using mechanical cells, these will be discussed in greater depth in this section. A basic overview of mechanical cells will be given, along with a discussion of some of the more common differences between the different manufacturers' cells.

1.2.1 Types of Mechanical Flotation Cells

There are a number of different flotation cell manufacturers currently operating around the world. All produce mechanical flotation cells, with slight variations in impeller design, or mechanism of air introduction. However, all cells have certain features in common, and the following diagram shows the basic layout of a mechanical flotation cell.

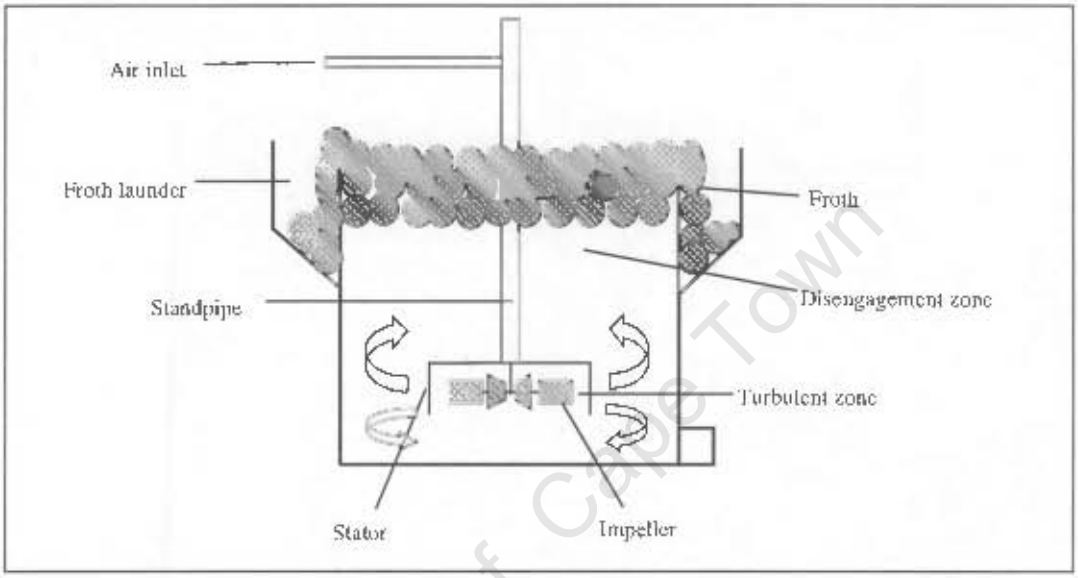

Figure 1.2 Mechanical flotation cell.

While there are a number of flotation cells manufacturers, the types of cells can be separated into two main categories: those that use induced air and those that use forced air.

1.2.1.1 Induced Air Flotation Cells

Induced air cells are those that use a Venturi effect to draw ambient air into a draft tube and then down into the cell. The amount of air is controlled by the speed of the impeller: the faster the impeller speed, the more air that is drawn into the cell.

Baker Hughes is the manufacturer of the most common induced air cells, in the form of WEMCO cells. One of the largest cells in the line of SmartCells has a volume of $4500ft^3$ (or approximately $127m^3$). The design of this cell was based on the same hydrodynamic principles as that of the WEMCO 1+1 cell. Like all modern large volume cells, WEMCO SmartCells are cylindrical rather

than square. This shape maximises the number of bubble-particle collisions and minimises short-circuiting. "Dead zones", associated with uneven air distribution, are also eliminated. WEMCO cells consist of a rotor-disperser assembly, rather than an impeller (Wills, 1988). A typical WEMCO cell has the following features:

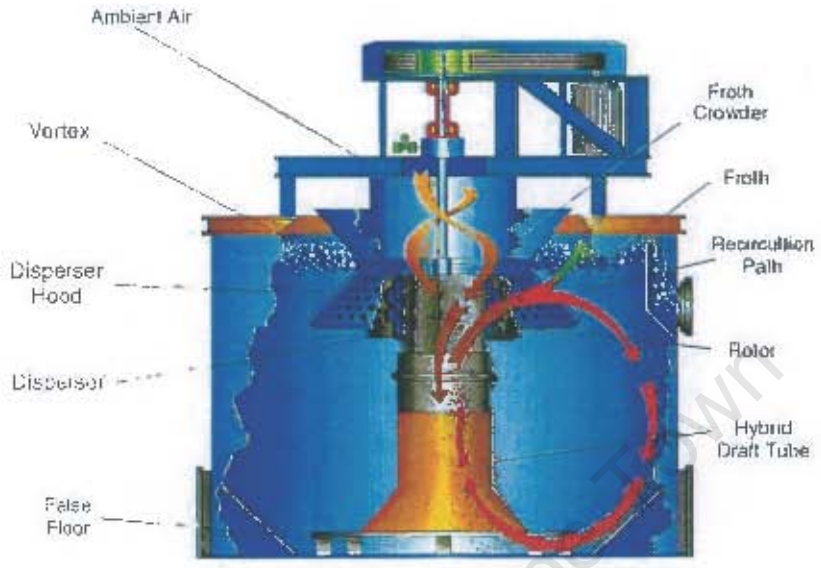

Figure 1.3 Typical WEMCO flotation cell.

As can be seen in the diagram, slurry that has been in contact with air is drawn up into the draft tube and then circulated into the cell through the disperser hood. Fresh slurry is drawn into the draft tube from beneath the false bottom, meaning the impeller acts as a pump.

1.2.1.2 Forced Air Flotation Cells

The majority of mechanical flotation cells fall into this category. Rather than introducing ambient air, forced air cells are connected to air blowers which blow fixed amounts of air directly into the cell. A number of manufacturers utilise this sort of cell, including Svedala (now Metso), Bateman and Outokumpu.

Outokumpu first developed their TankCell in the 1980s, the idea of this design being to develop a mechanical flotation cell with "virtual column" features (Jonaitis, 1999). The first 16m^3 TankCell was trialled in 1991, based on knowledge gained from the use of a cylindrical cell installed at Pyhäsalmi Concentrator in 1983, and also information produced during the development of a high-grade (HG) cell. Outokumpu TankCells are now as large as 160m^3. Outokumpu (OK) impellers vary quite markedly from those of other common flotation machines (Wills, 1988). The OK

impeller consists of a number of vertical slots that taper downwards, the top of the impeller being closed by a horizontal disc. As the impeller rotates, slurry is accelerated in the slots and forced out near the point of maximum diameter. This outward-flowing slurry is replaced by fresh slurry drawn into the impeller mechanism from the bottom of the cell. The impeller, like in WEMCO cells, acts as a pump. OK cells use air blown in from flotation blowers for their operation. The cross-section of a typical OK cell is shown in Figure 1.4.

Figure 1.4 Typical Outokumpu tank cell.

1.2.2 Subprocesses in Mechanical Flotation Cells

To design and efficiently operate a mechanical flotation cell it is essential to have knowledge of some of the subprocesses which take place inside the cell. The following section provides a brief overview of the important subprocesses of hydrodynamics, solids suspension, gas dispersion and flotation. These subprocesses are explored in more detail in Section 1.4 which focuses on the effects of the key "hydrodynamic" variables of impeller speed and air flowrate on these subprocesses.

1.2.2.1 Hydrodynamics

Hydrodynamics refers to the flow of fluid in a flotation cell. Hydrodynamics is largely driven by the action of the impeller, which establishes a flow pattern, or average path of the bulk fluid flow, in mechanically agitated flotation cells. These flow patterns influence key hydrodynamic parameters such as the pulp recirculation rate and the residence time distribution. The flow pattern created in mechanical cells is governed by vessel characteristics, such as size and shape, and impeller properties such as shape, rotational speed and submergence. A knowledge of hydrodynamics is essential for the design and efficient operation of mechanical flotation cells. The

hydrodynamic aspects of a cell's operation give insight into micro-level events such as how much time particles and bubbles remain in contact, the energy with which they contact each other, whether solids are in suspension in the pulp and how these parameters change with cell scale.

Mechanical flotation cells typically have Rushton turbine impellers located near the bottom of the cell which generate radial fluid jets. These jets strike the cell walls and split into an upper and lower wall jet (cf. Figure 1.5). The lower jet spreads over the bottom of the cell and aids in solids suspension, while the upper jet travels vertically before spreading to the surrounding fluid. The upper jet carries kinetic energy, in the form of fluid flow, into the bulk tank, where it ultimately decays into turbulence in the eddy spaces and is dissipated as heat. The fluid then either circulates back to the impeller or flows out of the cell. The upper wall jet, however, should not extend to the pulp-froth interface, so that a quiescent zone is established for particle-bubble disengagement.

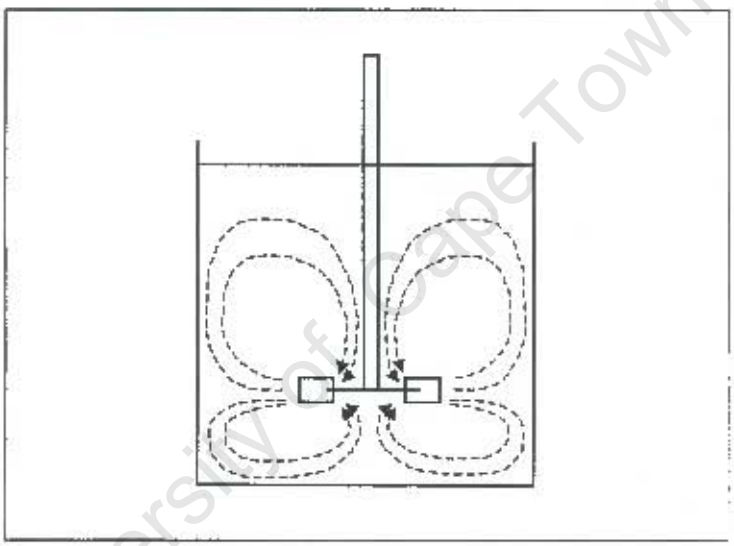

Figure 1.5 Schematic of bulk flow patterns in a mechanically agitated flotation cell.

There are a number of design and operational variables that affect the hydrodynamics in a flotation cell. The major operational variables are the impeller power consumption, impeller speed, air flowrate and pulp density, while the major design variables include the cell volume, the impeller diameter and the location of the impeller in the tank.

1.2.2.2 Solids Suspension

Solids suspension is a measure of the degree to which solid particles in a mechanical cell are kept suspended in the pulp. Solids suspension is of great importance to the flotation process, as without

adequate suspension of solids, the flotation of particles cannot take place. As mentioned in Section 1.2.2.1, the suspension of solids is achieved through the action of the lower wall jet, which spreads across the bottom of the cell. As hydrodynamics governs the action of the fluid jets inside a flotation cell, it is clear that one of the main actions of the impeller is to keep solids suspended within the cell. Therefore, high levels of agitation are required in cells to maintain the solid particles in suspension. The suspension of particles is closely related to the impeller power input. A sudden decrease in power input, caused by an increase in air flowrate to the cell, results in an increase in particle sedimentation. Therefore, solids suspension is affected by a combination of both impeller speed and air flowrate.

1.2.2.3 Gas Dispersion

Gas dispersion in a flotation cell refers to the ability to disperse gas in a manner conducive to contacting and collecting particles. Despite the obvious link between gas parameters and flotation rate, it has only been in recent times that flotation researchers have begun to design flotation cells in terms of gas dispersion performance. Gas dispersion plays a crucial role in flotation, as without adequate contact between gas bubbles and particles the efficiency of the flotation process is dramatically reduced.

In the past, bulk gas phase parameters were used to quantify the gas phase, namely the air flow number and the gas velocity into the froth. However, these parameters ignored the micro-level characteristics. It is now widely held that the principal gas phase parameters in flotation are the bubble size, superficial gas velocity and gas hold-up. These three properties are, once again, largely controlled by the impeller speed and the air flowrate. Gas hold-up, for instance, is a measure of the volume of the cell occupied by gas, and is directly related to the flowrate of gas into the cell. Air that enters the cell is affected by impeller action, as small bubbles are formed by the shearing action of the impeller. Further bubble breakage occurs in the turbulent conditions in the impeller zone and bubbles are dispersed into the cell by the bulk fluid flow caused by the pumping action of the impeller.

1.2.2.4 Flotation

The process of froth flotation and the various subprocesses affecting flotation have been discussed in Section 1.1. The flotation efficiency in mechanical flotation cells is strongly dependent on the efficiency of hydrodynamics, solids suspension and gas dispersion in the cell. Hydrodynamics is the driving force for both solids suspension and gas dispersion and is responsible for creating a suitable turbulent environment for effective particle-bubble contacting. Good solids suspension is

necessary for particles to be suspended throughout the flotation cell so as to maximise the volume available for particle-bubble contacting. Good gas dispersion is necessary to disperse air into small bubbles throughout the flotation cell so as to maximise the efficiency of particle-bubble contacting. The three fundamental micro-level sub-processes of flotation (particle-bubble collision, attachment and detachment) are strongly dependent on bubble size.

Hydrodynamics, solids suspension, gas dispersion and flotation are strongly influenced by the two key hydrodynamic variables of impeller speed and air flowrate. These two variables have an enormous effect on each of the subprocess occurring in a mechanical flotation cell and, consequently, on the mineral recovery, concentrate grade and flotation rate constant. The effect of these two important hydrodynamic variables on the flotation process will be discussed further in Section 1.4.5 and represents the central focus of this thesis.

1.3 Dimensional Analysis

Dimensional analysis is central to the hydrodynamic study of mechanical flotation cells, and is used in both design and scale-up. The basis of dimensional analysis is such that similar fluid motion for different fluids or geometrical conditions can be compared. Two of the common variables used in dimensional analysis, impeller speed and air flowrate, also appear as central hydrodynamic variables. This section serves to provide an overview of dimensional analysis, and presents concepts that will be used later in Section 1.4. The following overview of dimensional analysis and dimensionless numbers is derived from Arbiter *et al* (1968), Arbiter *et al* (1969) and Degner (1985).

1.3.1 Overview of Dimensional Analysis

As mentioned previously, the basis of dimensional analysis is such that similar fluid motion for different fluids or geometrical conditions can be compared. This is possible if all variables describing a fluid system can be expressed in terms of the three fundamental units. The number of variables in a flotation system can be restricted if only power requirements are considered. The remaining variables can be summarised into a number of main categories.

Linear Variables

Table 1.1 lists the main linear variables.

Table 1.1 Linear variables.

Variable	Meaning
T	Tank Diameter
D	Impeller Diameter
H	Liquid Depth
C	Impeller Height Above Tank Bottom
L	Length of Impeller Blade
W	Width of Impeller Blade
J	Baffle Width
d	Solid Particle Diameter

These variables are independent and arbitrarily chosen, and it is possible to use systems where all linear variables are in constant proportion to an arbitrary reference dimension. In this situation, dimensionless groups formed by the ratios of any of these variables to the reference dimension will have constant values, and this is referred to as a geometrically similar system.

Unfortunately, this complete geometrical similarity is impossible to produce due to the particle size effect represented by the d/D ratio. This means that laboratory scale tests would have to be performed with a much smaller particle size than in the plant scale cells to keep this ratio constant. In turn, this will produce different metallurgical performance due to liberation differences. Also, other forces acting on particles (gravitational forces, or surface forces) may become more significant in one system than the other, which may also have an effect on the flow pattern. Particle size must, therefore, be kept constant, so geometrical similarity is achieved if the dimensions of the impeller, tank and baffles are kept in constant linear ratios, and particle size can instead be used to define the fluid.

Variables Defining the Fluid and Kinematic and Dynamic Characteristics

Variables that fall into these categories are listed in Table 1.2. Other variables (e.g. average pulp density and viscosity, density around impeller, and bubble retention time) are all functions of the variables listed above. Chemical variables, frother concentration for example, are taken into account by their effects on independent physical variables such as Q and γ. What this means is that there are eleven variables that define a geometrically similar system: the nine listed in Table 1.2 and the impeller diameter (D) and the particle size (d) listed in Table 1.1. Of these eleven variables, the net power input, P, is the only dependent variable and is a function of the other ten.

Table 1.2 Fluid and dynamic variables.

Variable	Meaning
ρ_L	Liquid Density
μ_L	Liquid Viscosity
ρ_s	Solids Density
C	Solids Concentration
Q	Air Flowrate
γ	Surface Tension
N	Impeller Speed
P	Net Power Input – Agitation power only
G	Gravitational Forces

1.3.2 Dimensionless Numbers

A number of important dimensionless numbers can be formed with the variables mentioned in Section 1.3.1. These numbers are often used for designing and characterising the performance of mechanical flotation cells.

Table 1.3 Dimensionless groups used in characterising flotation cells.

Dimensionless Group	Formula	Range	Physical Meaning
Power Number (N_P)	$P/\rho N^3D^5$	0.5 – 5	Ratio of actual to theoretical power consumption
Air Flow Number (N_Q)	Q/ND^3	0.01 – 0.07	Ratio of airflow rate to impeller pumping rate
Froude Number (N_{Fr})	N^2D/g	0.1 – 5	Ratio of inertial to gravitational forces
Reynolds Number (N_{Re})	$\rho D^2N/\mu$	$5x10^4 – 2x10^6$	Ratio of inertial to viscous forces
Solid Phase	$\frac{\rho_S}{\rho_L}, c, \frac{d}{D}$	-	Ratio of solid to liquid denisty; Solids concentration; Ratio of particle to impeller diameter
Weber Number (N_{We})	N^2D^2/γ	-	Ratio of inertial to surface tension forces

The power number is considered to be an important scale-up criterion in the design of agitated vessels as it defines a critical ratio between the absorbed power and the theoretical power draw which should be independent of cell size. It has the same significance as the resistance coefficient ($F/\rho v^2$), which is the ratio of resistive to inertial forces. F is the resistive force per unit area and v is the velocity. The power number reflects the flow straightening effects of the vessel and the baffles on the fluid, as power is related to the net change in tangential velocity imparted to the fluid by the impeller. The air flow number is an important scale-up criterion as it defines a critical ratio between the air flowrate and the impeller pumping rate which should be independent of cell size. The air flow number is significant as the rate constant is proportional to this parameter.

The Froude number is defined as the ratio between the centrifugal or inertial forces due to the pumping action of the impeller and the gravitational forces due to hydrostatic head in the flotation cell. As a result, similar Froude numbers in different size cells imply that hydrodynamic conditions between the two cells are largely equivalent. The Reynolds number is commonly used in fluid dynamics to determine the type of flow regime (whether laminar, turbulent or in transition between the two) in a pipe, where it is defined as $\rho_L V_r/\mu_L$. In hydrodynamics, the Reynolds number is the ratio of inertial forces, due to fluid flow, to the viscous forces. The Weber number represents the ratio of the inertial forces to surface tension effects and is used in momentum transfer in general, and in bubble/droplet formation and breakage of liquid jets calculations in particular.

A number of additional hydrodynamic parameters can be formed using the variables mentioned in Section 1.3.1. These are summarised in Table 1.4

Table 1.4 Hydrodynamic properties.

Property	Formula	Range
Impeller tip speed (U_{tip}) (m/s)	πDN	5.0 – 7.0
Power Intensity (kW/m^3)	P/V	0.5 – 5.0
Tank-Turnover Time (s)	V/ND^3	10 – 30
Air Flow/Cell Volume (min^{-1})	Q/V	0.04 – 1.10
Air Flow Velocity (m/s)	Q/D^3	0.02 – 0.50

Arbiter *et al* (1976) considered the impeller tip speed to be an important scale-up parameter, as it effects the velocity at which fluid leaves the impeller, and therefore affects gas dispersion and pulp circulation. Values of impeller tip speed appear to be largely independent of cell type or size (Deglon *et al*, 2000). The power input per cell volume, or power intensity, is believed to be one of the more important parameters due to its effect on metallurgical performance and cell operating

costs. Fallenius (1987) and Arbiter (1999) reported typical ranges of industrial power intensities of 1.0 to 2.0 kW/m^3.

The tank-turnover time, or its reciprocal (the circulation intensity), is considered to be an indicator of the efficiency of mixing and of particle-bubble contacting (Weber *et al*, 1999). In order to determine tank-turnover times either the fluid velocities at the impeller tip must be measured or circulation tests using a tracer injected into the impeller region must be conducted. The air flowrate per cell volume (Q/V) is an indicator of the aeration ability of a cell and is the gas dispersion equivalent of the power input per cell volume. The air flow velocity at the impeller (Q/D^2) is regarded as an important scale-up criterion by Arbiter *et al* (1976) as it defines the ability of an impeller of a specific size to accommodate a given air flowrate.

It can be clearly seen from Tables 1.3 & 1.4 that the key "hydrodynamic" variables of impeller rotational speed (N) and air flowrate (Q) are central to many of the dimensionless numbers and hydrodynamic parameters listed in this table. The fact that at least one of these variables appears in all the numbers/parameters highlights the importance of these variables to mechanical flotation cells.

1.4 Hydrodynamic Effects in Mechanical Flotation Cells

The major subprocesses occurring in mechanical flotation cells are hydrodynamics, solids suspension, gas dispersion and flotation (cf. Section 1.2.2). These subprocesses all occur simultaneously in the flotation cell and are strongly interdependent. However, solids suspension, gas dispersion and flotation are primarily affected by cell hydrodynamics as this provides a suitable "fluid environment" for each of these subprocesses to occur. Obviously, the presence of gas and solids in the flotation cell in turn has an influence on cell hydrodynamics, but this remains the primary driving force for the other subprocesses. If the flotation cell/impeller dimensions are fixed then hydrodynamics is primarily affected by the impeller speed and the air flowrate as these strongly influence the power input to the flotation cell. The following section presents an overview of the various hydrodynamic effects in mechanical flotation cells, focusing on the influence of the two key hydrodynamic variables of impeller speed and the air flowrate. The subprocesses of solids suspension, gas dispersion and flotation are included in this overview of "hydrodynamic effects" as the section focuses primarily on the influence of the hydrodynamic parameters (N & Q) on these subprocesses.

1.4.1 Power Input

1.4.1.1 Power Input

The power input to a flotation cell defines the rate at which energy enters the cell due to the action of the impeller. As discussed in Section 1.2.2.1, as the impeller turns it creates flow patterns within the cell, where radial jets generated by the impeller strike the wall and separate into upper and lower wall jets, eventually dissipating the kinetic energy into heat. It is well known from the flotation literature that both impeller speed and air flowrate have a large effect on the power input to a mechanical flotation cell. This is because the power input reflects the rate at which energy is transferred to the fluid, which is the main driver for hydrodynamics in a flotation cell. Investigations of power consumption in mechanical flotation cells have produced the following conclusions:

- Power consumption increases with increasing impeller diameter.
- Power consumption decreases with increasing air flowrate.
- Power consumption increases, and the volume of entrained air decreases, with increasing impeller submergence.
- Power consumption increases with increasing the impeller speed. This increase ranges from impeller speed to the power 2.0 at the lower limit to impeller speed to the power 3.5 at the upper limit. The average is impeller speed to the power 2.6.
- An increase in pulp specific gravity results in a direct increase in power consumption.
- Tank dimensions have no influence on the power consumption for a given impeller profile. The clearance (the distance between the bottom of the tank and the impeller), though, has a marked effect on power consumption.

1.4.1.2 Power Numbers

The power number is defined as the ratio between the absorbed power and the theoretical power draw, which should be independent of cell size. The power number reflects the flow straightening effects of the vessel and the baffles on the fluid, as power is related to the net change in tangential velocity imparted to the fluid by the impeller. There are a number of correlations for power consumption in various systems in the literature, most of which are defined in terms of the power number, which is denoted by the symbol (K) in Table 1.5, in keeping with the nomenclature used by Arbiter and Steininger (1962).

Table 1.5 Power correlations in various systems.

Correlation	Conditions
$P_L = K\rho_L N^3 D^5$	Valid for agitation of liquids
$P_{LS} = K\rho_{LS} N^3 D^5$	Valid for agitation of solid-liquid pulps
$P_{AL} = K\rho_L N^3 D^5 \frac{aQ/ND^3 + b}{Q/ND^3 + b}$	Valid for gas-liquid agitation
$P_{ALS} = K\rho_{LS} N^3 D^5 \frac{aQ/ND^3 + b}{Q/ND^3 + b}$	Valid for a three phase system

The three-phase system relationship has been shown to be valid through the use of aerated pulps of water and glass beads (Arbiter and Steininger, 1962). A number of assumptions were required for this to hold, however, namely that systems of different sizes are geometrically similar, that the system is fully turbulent with no vortex, and that the system is under normal operating conditions, with no excessive air flow or pulp density. The correlation for the three-phase system clearly shows that both the impeller speed and the air flowrate have a large influence on the power. Increasing impeller speed results in a steep increase in power consumption while increasing air flowrate has the effect of decreasing the absorbed power. This occurs as an increased air flowrate results in increased gas hold-up in the cell, due to a greater volume of gas. This, in turn, results in a decreased pulp density.

1.4.1.3 Power Intensities

Power input into flotation cells has long been a contentious issue, with metallurgists believing that high power inputs produce improved recoveries due to increased power intensities, defined as the power input per unit volume. As changes in power input are caused primarily by changes in the impeller speed and the air flowrate, power intensities are strongly affected by these variables. In laboratory-scale flotation cells, the power intensities are necessarily high, but in plant-scale cells power intensities are much lower. In the modern high-volume cylindrical cells, power intensities are generally around 1 kW/m^3. Power intensities are of particular importance to hydrodynamic scale-up. Wemco 1+1 cells are designed with power intensities of around 1.8 kW/m^3 (Arbiter, 1999). Table 1.7 lists typical power intensities for common industrial flotation cells.

Table 1.6 Power intensities for common industrial flotation cells.

Brand	Volume (m^3)	Power Intensity (kW/m^3)
Svedala	100	1.14
Svedala	130	1.10
Svedala	160	1.00
Dorr-Oliver	50	1.12
Dorr-Oliver	100	0.75
Dorr-Oliver	150	0.75
Wemco	71	1.05
Wemco	127	1.17
Wemco	160	1.17
Outokumpu	100	0.98
Outokumpu	130	0.82
Outokumpu	160	0.80

Flotation cell capacities and power intensities are generally related, with the power intensities in smaller cells generally being higher than that in larger cells, but this is not always the case. Power consumption data for the larger tank cells is still scarce. Power intensity is regarded as having an important influence on the flotation of platinum, as increasing power input is believed to improve the recovery of platinum. However, very little work has been done regarding the influence of power on platinum flotation, and very little information, other than anecdotal evidence, is currently available.

1.4.2 Mixing

Mixing in flotation cells can be approached in two ways: either by examining the bulk mixing of solids, liquids and gases in the cell (macro-mixing), or by looking at the microphenomena caused by turbulence (micro-mixing). Both macro-mixing and micro-mixing will be discussed in more detail in the following sections.

1.4.2.1 Macro-Mixing

In flotation, particles are kept suspended through the action of an impeller located near the bottom of the flotation cell. Air is introduced into the cell, either by being blown into the impeller zone or by becoming entrained by the low pressure that develops between impeller and shroud. Therefore, the hydrodynamic model of flotation is a mixing operation that takes place in a three-phase system

using a single impeller. It is clear, therefore, that the impeller is of vital importance to mixing in a flotation cell, as it is the action of the impeller which mixes the three phases in the cell. This is done through the establishment of bulk fluid flow patterns which ensure that the fluid in the cell circulates throughout the cell and returns to the impeller zone. The impeller is responsible for solids suspension and gas dispersion, both of which rely on macro-mixing for effective dispersion of particles and gas bubbles.

The importance of the impeller speed for mixing is reflected in the equation for the impeller Reynolds number ($\rho D^2N/\mu$). Turbulent conditions (and therefore improved mixing) occur at high Reynolds number values, and this is largely brought about by increases in the impeller speed. Air flowrate is also of importance to the mixing process and can result in poor mixing at high air flowrates. However, the efficiency of mixing is also improved when small bubbles are present. Mixing impacts on the flotation process as without adequate mixing, collisions between bubbles and particles cannot take place.

1.4.2.2 Micro-Mixing

In flotation machines, very high values of the impeller Reynolds number are obtained, indicating that the flow regime in these situations is almost always fully turbulent. Microphenomena such as particle suspension, bubble breakup, particle-bubble collision, attachment and detachment are dependent on turbulence. Typically, turbulence in mechanical flotation cells has been treated at a "bulk level", through parameters such as the Reynolds number, impeller speed and power input. Turbulence is modelled in terms of the propagation of energy in a continual spectrum of turbulent eddies. Large eddies are generated from the bulk flow of the fluid caused by the impeller, and these eddies transfer kinetic energy to small eddies by turbulent shear stresses. Energy is continuously transferred to smaller eddies until the energy is dissipated as heat by the action of viscosity. The level of turbulence in a given field is normally described in terms of the turbulent velocity, which has two components: a mean velocity and a fluctuating velocity.

$$u(t) = u_{mean} + u'(t) \qquad - 1.5$$

Measurements of mean and fluctuating velocity can be carried out accurately by means of hot-wire, hot-film or Laser-Doppler anemometry. In isotropic turbulent fields the mean squared fluctuating velocity is related to the shear stress according to Equation 1.6.

$$\tau = -\rho u'^{2}_{mean} \qquad - 1.6$$

In the characterisation of turbulence another useful parameter is the specific power input (ε), also known as the rate of energy dissipation, which is similar to the power intensity. Specific power input can be expressed in terms of fluctuating velocity and impeller diameter through a semi-empirical formula.

$$\varepsilon = C\frac{u'^3}{D} \qquad \text{- 1.7}$$

It is clear from this equation that the power, and therefore impeller speed and air flowrate, have a large effect on the fluctuating velocity and, therefore, on the efficiency of micro-mixing in the flotation cell. Micro-mixing impacts on flotation as is affects the various microphenomena discussed previously. Hence, the impeller speed and air flowrate affect the power input to a flotation cell, which in turn affects the level of micro-mixing in the flotation cell, which in turn impacts on microphenomena such as particle suspension, bubble breakup and particle-bubble contacting.

1.4.3 Solids Suspension

As mentioned in Section 1.2.2.2, solids suspension is simply a measure of the degree to which solid particles in a mechanical cell are kept suspended in the pulp. Solids suspension is of great importance to the flotation process, as without adequate suspension of solids the flotation of particles cannot take place. High levels of agitation are generally required to maintain the solid particles in suspension. Two cases of solids suspension have been described in the literature, namely full suspension and full dispersion following full suspension.

Suspension and dispersion of solids are two interconnected conditions. The extent of both conditions must be known in order to define the state of the system in a particular agitation regime. The reason for this is that, for example, while suspension may be incomplete, the solids that are suspended may be fully dispersed. Solids suspension requirements are the reason for an increase in peripheral speed with system size as a scale-up criterion for solid-liquid systems i.e. the vertical pulp velocity must exceed the particle sedimentation velocity in order to prevent settling of solids in the cell. Therefore, pulp streams leaving the impeller must have sufficient velocity to provide for suspension in the furthest reaches of the cell.

The suspension of particles is closely related to power input, and also to the flow patterns established by the action of the impeller. Of the two radial fluid jets created by the action of the impeller, it is the lower wall jet that aids in solids suspension, as it strikes the wall and then spreads across the floor of the cell, lifting solid particles up into the impeller zone. Arbiter *et al* (1969) observed an increase in sedimentation of suspended particles in a flotation cell with a sudden decrease in power brought about by an increase in air flowrate into the cell.

A lot of work relating to particle suspension has concentrated on the impeller speed necessary to just completely suspend particles, referred to as N_{JS}. The empirical correlation determined by Zweitering (1958) is still considered to be the most useful expression for determining N_{JS}.

$$N_{JS} = S v^{0.1} d_p^{0.2} (g\Delta\rho / \rho_L)^{0.45} X^{0.13} D^{-0.85} \qquad - 1.8$$

The exponents in this expression have been found to be independent of impeller type, vessel size, impeller clearance and the ratio of the impeller to tank diameter, which suggests a common suspension mechanism in all cell types studies. This model includes the influence of air flowrate on solids suspension through the increase in the $\Delta\rho$ term with increasing air flowrate. This equation, however, does not provide an insight into the actual mechanism of solids suspension. Other models have been developed, including one that takes into account the effect of turbulence within a flotation cell.

It is clear from the preceding discussion that both the impeller speed and the air flowrate have a large influence on solids suspension. The bulk fluid flow patterns, established by the action of the impeller, aid in solids suspension. In addition, the action of the impeller is responsible for the dispersion of solid particles, as solids leaving the impeller zone must have an exit velocity greater than the sedimentation velocity to prevent solids from settling out in the cell. The air flowrate also has an influence on solids suspension. The main effect is through changes in air flowrate affecting the power input (increased air flowrate reduces power input for a given impeller speed), and through changes to the pulp density caused by changes to the volume of air in the cell when air flowrates are altered. Solids suspension is an important factor in flotation, as improved solids suspension leads to improved particle-bubble contacting in the impeller zone.

1.4.4 Gas Dispersion

As mentioned in Section 1.2.2.3, gas dispersion refers to the ability to disperse gas in a manner conducive to contacting and collecting particles. Gas that enters the cell accumulates in the low-

pressure regions behind the rotating impeller blades forming cavities from which bubbles are sheared off by the action of the impeller. Further bubble breakage occurs in the turbulent conditions in the region of the impeller and bubbles are then dispersed into the cell by the bulk fluid flow caused by the pumping action of the impeller. In the bulk region of the cell bubbles may collide and coalesce, recirculate back to the impeller region or rise into the froth phase. The main gas phase parameters are the bubble size, the superficial gas velocity and the gas hold-up.

The bubble size is normally expressed in terms of the arithmetic mean or Sauter mean (volume to area ratio) bubble diameter. Values of the Sauter mean bubble diameter in typical industrial cells vary between 0.5 and 2.5 mm. There is currently no model available for accurate prediction of bubble size in mechanical flotation cells, although some useful empirical models exist. Bubble size is, however, a very influential parameter on flotation kinetics. Experimental studies performed in mechanical flotation cells show that flotation rates for fine mineral particles increase with decreasing bubble size. Bischofberger and Schubert (1978) found that decreasing bubble size led to an increase in the rate of tin flotation in both laboratory and industrial flotation cells, and Ahmed and Jameson (1985) found an almost one hundred fold increase in the rate of flotation of fine quartz when the mean bubble size in their laboratory mechanical cell was reduced from 655 to 75 μm. These experimental studies show that mineral recovery rates in mechanical flotation cells can be significantly improved with the use of small bubbles.

The superficial gas velocity is the ratio of gas volumetric flowrate to cell cross-sectional area. Values of superficial gas velocities measured at different locations in industrial mechanical cells vary significantly from theoretical values due to uneven dispersion of gas and the influence of the bulk fluid flow patterns in the mechanical flotation cell. Superficial gas velocity values in industrial cells vary from 0.25 to 2.5 cm/s. Gas hold-up is defined as the fraction of the cell volume occupied by gas, and is related to both the bubble size and the superficial gas velocity. Gas hold-up values in industrial cells vary from 5 to 35%. The cell gas residence time is determined by the gas hold-up, and it also plays an important role in the rates of gas phase sub-processes such as bubble breakage and coalescence. No generally accepted model for the prediction of gas hold-up in mechanical flotation cells exists.

In the past the air flow number was used as a scale-up parameter for families of dimensionally similar mechanical flotation cells (Arbiter *et al*, 1976). The air flow number (Q/ND^3) gives the ratio of air flowrate to the impeller pumping rate and is of importance in gas dispersion, as it gives an indication of the efficiency of gas dispersion within a flotation cell. Lower air flow numbers are an indication of greater turbulence within the cell, and therefore an indication of more efficient gas dispersion through the formation of smaller bubbles.

Impeller speed and air flowrate are of vital importance to gas dispersion. When the air enters the impeller region, it is the action of the impeller that controls gas dispersion, and the consequent bubble size. Increasing the impeller speed leads to smaller bubbles, which improves the rate of flotation. The air flowrate has a large effect on the air flow number, which is an important measure of gas dispersion, as it defines the ratio of air flowrate to impeller pumping rate. The air flowrate impacts significantly on the bubble size, superficial gas velocity and gas holdup. Increasing air flowrate generally leads to an increase in all three of these parameters, but overall results in an increase in the bubble surface area flux.

1.4.5 Flotation

Flotation takes place when reagentised particles and gas bubbles are brought into contact in an agitated cell. While subprocesses such as solids suspension and gas dispersion have a significant effect on flotation, a number of researchers have studied the direct effect of impeller speed and air flowrate on flotation. As mentioned in Section 1.2.2.4, the efficiency of the flotation process is largely measured in terms of three main parameters i.e. mineral recovery, concentrate grade and flotation rate constant. In this section, the effect of impeller speed and air flowrate on these parameters will be discussed in more detail.

1.4.5.1 Flotation Recovery and Grade

The recovery of valuable mineral and the concentrate grade are two of the most important measures of the efficiency of the flotation process. They are the industrial benchmarks of the performance of a flotation circuit and are strongly affected by hydrodynamic factors. The key hydrodynamic variables of impeller speed and air flowrate are crucial in many aspects of flotation performance, including recovery and concentrate grade.

Arbiter and Harris (1969) studied the role of impeller speed and air flowrate in scaling-up flotation cells. This work concluded that both recovery and grade are functions of impeller speed and air flowrate. The best way of viewing relationships between recovery, grade, impeller speed & air flowrate was by using experimentally determined three-dimensional surfaces. It was observed that, in order to maintain the recovery and grade at an acceptable level, both impeller speed and air flowrate must lie within certain operational limits. Unfortunately, the ranges of impeller speeds and air flowrates for recovery did not correlate well with those for grade. Therefore, it was concluded that to select a single value of impeller speed and air flowrate for cell operation requires an

optimisation technique using both recovery, grade, impeller speed & air flowrate surface responses and economic factors such as mining, milling, transport and smelting costs.

In order to produce acceptable recoveries and grades the impeller speed and the air flowrate must lie within a certain range. This implies that recovery and grade are functions of the air flow number which, for a fixed impeller size, depends on the ratio of air flowrate to impeller speed. Figure 1.5 shows a typical relationship between recovery, grade and the air flow number. The graph also shows the sedimentation height in the cell which is of relevance to solids suspension (cf. Section 1.4.3). This merely demonstrates that there is an upper limit to the air flow number where poor solids suspension occurs, either due to excessive air flowrates or inadequate impeller speeds or both.

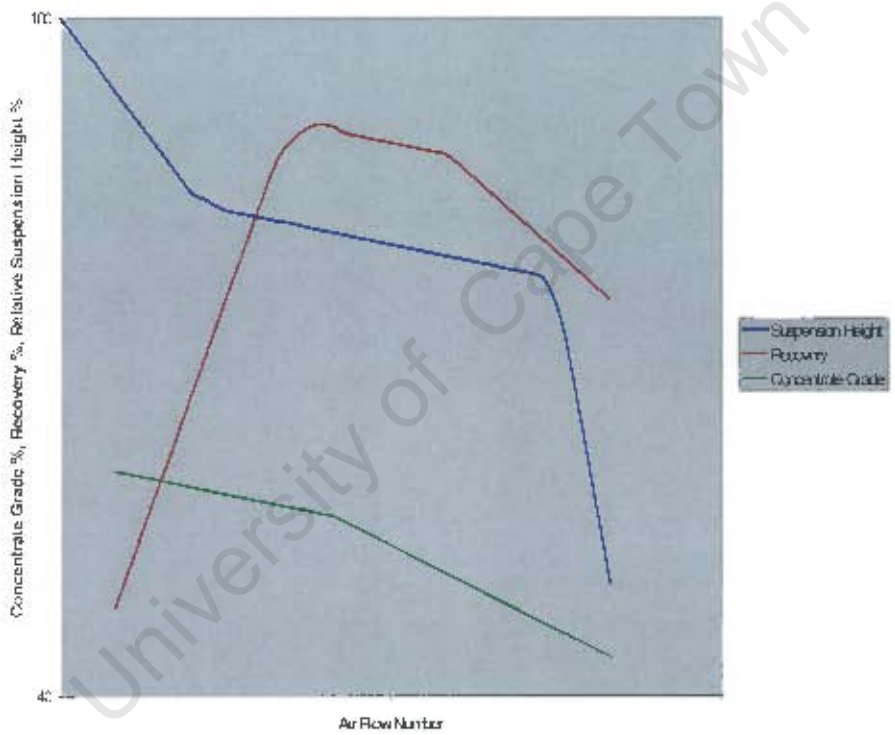

Figure 1.6 Recovery and grade as a function of airflow number (after Arbiter and Harris (1969)).

As can be seen, low air flow numbers favour grade while higher numbers favour recovery. However, both recovery and grade are reduced when the air flow number reaches certain critical values. This is particularly significant for coarse particles due to inadequate suspension. Figure 1.5 indicates that by reducing the air flowrate one may improve both recoveries and grades, up to the point at which recovery starts to be adversely affected. As coarser particles are most sensitive to

changes in impeller speed and air flowrate, it would be sensible to classify flotation feed into coarse and fine particles and float them separately under different regimes of impeller speed and air flowrate. The effect of impeller speed and air flowrate was also investigated by Darley (1998), as shown in Tables 1.8 and 1.9. Here, the "Ultimate R" value is the maximum recoverable material as derived from the Klimpel model.

Table 1.7 Effect of impeller speed on recovery (after Darley (1998)).

Constant air 4.97 l/m				
		% Recovery		
Speed rpm	**Ultimate R**	**10 min Float**	**20 min Float**	**60 min Float**
900	91.1	85.4	88.3	90.2
1000	92.5	87.5	90.0	91.7
1100	93.3	88.8	91.0	92.5
1200	93.2	88.8	90.6	92.5
1300	94.0	89.9	91.9	93.3

Table 1.8 Effect of air flowrate on recovery (after Darley (1998)).

Constant speed 1200rpm				
		% Recovery		
Air l/m	**Ultimate R**	**10 min Float**	**20 min Float**	**60 min Float**
0.65	76.6	55.8	65.9	73.0
1.32	85.1	73.8	79.5	83.2
1.98	88.8	81.7	85.3	87.6
2.98	90.0	84.8	87.4	89.1
3.97	93.0	89.0	91.0	92.3
4.97	93.2	88.8	90.6	92.5

Table 1.7 shows that an increase in impeller speed results in a clear increase in recovery. This increase in impeller speed resulted in a decrease in the air flow number which also resulted in an increase in concentrate grade. Table 1.8 shows that an increase in air flowrate also results in a clear increase in recovery. However, this increase in air flowrate resulted in an increase in the air flow number, which caused a decrease in concentrate grade, confirming the findings of Arbiter and Harris.

1.4.5.2 Flotation Rate Constant

The flotation rate constant reflects the rate at which flotation occurs and is a critical parameter in the design, modelling and simulation of flotation circuits. The flotation rate constant is a complex function of a host of variables, including particle size, bubble size, reagent concentrations, mineral surface properties and cell design (Laskowski, 1989). Flotation rate constants are generally calculated from mineral recovery versus time data from laboratory flotation experiments. Values of the flotation rate constant can be used to compare the responses of different ores to flotation in the same flotation cell, or to compare the performance of different cells with the same ore. However, because the flotation rate constant is not a true constant, but an empirical hybrid of the effects of cell and particle properties, a macroscopic rate equation can only be used to compare ore floatabilities under fixed cell conditions, or conversely, to compare cell efficiencies for fixed particle floatabilities. A number of researchers, however, have sought to bring greater physical meaning and predictive power to the macroscopic rate equation by relating the flotation rate constant to fundamental processes in the flotation cell.

Bubble size is one of the physical parameters most influential in determining the flotation performance of a mechanical flotation cell. Studies in flotation fundamentals have shown that particle-bubble collision, attachment and detachment are all strongly dependent on bubble size. It has been found that the rate of particle-bubble collision is proportional to the bubble number density and the bubble size squared, while the rate of particle-bubble attachment shows that the probability of attachment increases with decreasing bubble size. Probability of detachment increases with decreasing bubble size. These relationships, however, can't always be used to predict the effect of bubble size on the performance of a real flotation system. This is because the expressions rely on a number of simplifying assumptions which reduces their ability to be fully accurate. Also, the expressions developed for the rates of collision, attachment and detachment point to opposing effects of bubble size, which makes it difficult to determine the overall effect of bubble size on flotation rate.

In terms of experimental studies, Ahmed and Jameson (1985) found a large increase in the rate of fine particle flotation when the mean bubble size was reduced from 655 to 75 microns. This study, and a number of others, have shown that mineral recovery rates in mechanical flotation cells can be improved significantly with the use of small bubbles. The strong influence of bubble size is also apparent from the macrokinetic modelling of flotation. Gorain *et al* (1997) observed that the flotation rate constant (k) is directly proportional to the bubble surface area flux (S_b), which is inversely proportional to the Sauter mean bubble diameter.

$$k = PS_b \qquad \text{- 1.9}$$

This finding can be explained by looking at flotation theory. Jameson *et al* (1977) found that the flotation rate constant was directly proportional to ratio of the superficial gas velocity (J_g) and the mean bubble size (d_b). This is equal to the bubble surface area flux if the mean and Sauter mean bubble sizes are similar in magnitude.

$$k = \frac{3}{2}\frac{J_g P_{coll}}{d_b} \qquad \text{- 1.10}$$

Deglon (1998) defined attachment and detachment flotation rate constants and found these to be strong functions of bubble size. Deglon showed that the flotation rate constant can actually be interpreted as the net effect of two competing rates, one of attachment and the other of detachment, and proposed that the rate expression for flotation take into account both the pulp and gas phases:

$$R = \frac{k_a \tau}{1 + k_a \tau + k_d \tau_g} \qquad \text{- 1.11}$$

where R is the recovery of valuable mineral, k_a and k_d are the attachment and detachment rate constants respectively, and τ and τ_g are the pulp and gas phase residence times in the flotation cell respectively. In a series of flotation experiments performed on fine quartz particles in a well-characterised laboratory flotation cell, Deglon related k_a and k_d to micro-level properties of the system using the following general expressions:

$$k_a = \frac{{d_p}^{n_1}\left(c_1 + c_2 \varepsilon^{n_3}\right)}{{d_b}^{n_2}} \qquad \text{- 1.12}$$

$$k_d = \left(c_3 + c_4 {d_p}^{n_4}\right){d_b}^{n_5}\varepsilon^{n_6} \qquad \text{- 1.13}$$

Nonaka *et al* (1982) found a strong relationship between the flotation rate constant, the rate of energy dissipation (ε) and the air flow number (N_Q). This expression was confirmed experimentally by flotation of fine quartz in a batch flotation cell where it was assumed that the probabilities of attachment and detachment were approximately unity and zero respectively.

$$k_c \propto \varepsilon^{0.75} {N_Q}^{0.5} \qquad \text{- 1.14}$$

From this brief overview of the flotation rate constant, it should be clear that this parameter is generally indirectly related to the impeller speed and the air flowrate, through the effects of these two variables on quantities such as the bubble size, superficial gas velocity and the rate of energy dissipation. Equation 1.14 is an exception to this as here the flotation rate constant is proportional to the square root of the ratio of air flowrate to impeller speed, through the air flow number. However, there are predictable relationships between the impeller speed, air flowrate and the quantities in Equations 1.9 to 1.13. For example, the bubble size generally decreases with increasing impeller speed and air flowrate while the superficial gas velocity is directly proportional to the air flowrate. In addition, the rate of energy dissipation is proportional to the power intensity which increases with increasing impeller speed and decreasing air flowrate.

1.4.6 Scale-Up

Scale-up is not the focus of this study but needs to be discussed in some detail, for two major reasons. Firstly, hydrodynamics is central to the scale-up of mechanical flotation cells and, secondly, the main objective of the experimental rig used for generating the results for this thesis (the Floatability Characterisation Test Rig or FCTR) is to assist in scale-up.

1.4.6.1 Introduction to Scale-Up

Over the last twenty years there has been a trend towards large capacity flotation machines. The reason for this trend has been that with lower grade orebodies now being exploited, the grinding mills that are now being designed for mineral processing plants have process capacities in excess of 1500 tonnes per hour. Clearly by using larger capacity flotation cells at these tonnages, a number of important savings can be made. Degner (1979) identified the following:

- Reduced capital cost per tonne of ore processed.
- Reduced floorspace required, or increased plant capacity for an existing plant.
- Simpler flotation circuit layout.
- Reduced control complexity and therefore improved flotation section operation.
- Reduced maintenance costs.
- Possible reductions in power cost per tonne of ore processed.

The scale-up of flotation equipment has long been an issue for equipment manufacturers and flotation plant operators. The necessity for flotation cell scale-up arises from the fact that it is expensive and extremely impractical to perform preliminary tests for the evaluation of an ore body on full-size flotation cells. This, however, causes problems in that the extrapolation of results for

full-plant performance from laboratory or pilot-scale cells is not a simple process, as achieving certain metallurgical results in a laboratory cell is no guarantee that the same results will be achieved in a flotation plant. There are any number of parameters that can affect the scale-up of flotation cells, from simple things, such as feed particle size distribution, and flotation cell mechanism, to more complex issues such as power input, bubble size and gas flowrate. A number of authors have covered the topic of scale-up for a variety of flotation cells. Several, including Amelunxen (1990) and Luttrell *et al* (1993), have covered the topic of scale-up in column cells. This area will not be touched upon here, and this discussion is limited to the scale-up of mechanical flotation cells.

1.4.6.2 General Scale-Up Criteria

Arbiter and Harris (1969) refer to the most appropriate variables for dealing with a family of flotation machines as impeller peripheral speed (πND) and air velocity (Q/D^2). In order to maintain similar metallurgical performance with similar pulps in machines of different size but of the same design, these two parameters must increase slightly with cell size. An approximate relationship for this is given by:

$$(\pi ND) \propto D^{1/3} \qquad - 1.15$$

The ratio of the impeller peripheral speed and air velocity is proportional to the air flow number. For a given machine size, high grades are obtained at lower impeller speed, air flowrates and air flow numbers. On the other hand, high recovery is favoured by higher impeller speeds, air flowrates and air flow numbers. As the size of the cell increases, there is an upward shift in both impeller peripheral speeds and air velocities with the value of the air flow number remaining more consistent, as it is defined within its upper and lower limits for a family of flotation machines. As the flotation products from different size machines get closer in terms of recovery and grade, the limits of the range of values of the air flow number narrows. An approximately constant air flow number is a major scale-up factor for mechanical flotation cells.

1.4.6.3 Techniques for Scale-Up

There are a number of techniques in existence for the scaling-up of mechanical flotation cells. Some of these, such as geometrical scale-up, are based purely on maintaining dimensional similarity between two different sized cells. However, as this study is focused on hydrodynamic factors, only techniques that make use of hydrodynamics will be discussed here.

1.4.6.3.1 Hydrodynamic Scale-Up

The 1960s saw the development of a number of new types of flotation machines (Arbiter *et al*, 1969). Manufacturers began to develop machines with an emphasis on pulp flow characteristics due to new impeller-stator designs. These new designs required a departure from accepted impeller speed/air rate values. Hydrodynamic scale-up, therefore, developed out of a need to understand the mechanical part of the flotation process in hydrodynamic terms. The starting point of hydrodynamic scale-up is geometrical scale-up. For hydrodynamic scale-up to apply, geometrical similarity between laboratory and full-scale cells should apply. Hydrodynamic scale-up takes this further, however, by attempting to reproduce the hydrodynamic conditions that exist within the laboratory flotation cell in the industrial size version. This rests on the premise that, if certain hydrodynamic conditions produce a certain metallurgical result in a laboratory test, then those same conditions will produce the same metallurgical result in a full-scale cell.

Hydrodynamic scale-up is still the manner in which most modern cell manufacturers go about scaling-up their cells, although their techniques vary slightly. Hydrodynamic scale-up makes use of a number of dimensionless groups. The most important of these groups, as determined by Degner (1979) and Arbiter (1999), are the power number and the air flow number. These two groups are able to help define the five relationships that best quantify the hydrodynamic design objectives. These five relationships are worth mentioning briefly here:

- Air velocity into the froth surface – the upper limit of air transfer to prevent the onset of geysering.
- Specific pulp circulation intensity – ratio of pulp circulation to pulp feed rate.
- Air/pulp residence time – contact residence time within the disperser envelope.
- Mechanism power number – a measure of the degree of mixing in the rotor/disperser region.
- Pulp circulation – gives mechanism solids suspension characteristics.

The power number and the air flow number are used in all these expressions and as such are the most important hydrodynamic factors for scaling-up flotation cells. It is clear then that hydrodynamic scale-up is largely based on ensuring good mixing, solids suspension and gas dispersion in the flotation cell and not on the actual process of froth flotation itself.

1.4.6.3.2 Kinetic Scale-Up

Kinetic scale-up is a relatively new method of scaling-up flotation cells, which uses the principle that flotation performance will be the same in different size cells if parameters in the flotation micro-environment are the same. The technique generally uses equivalence of the flotation rate constant between cells of different size as a basis for scaling-up the flotation cell. Here, the flotation rate constant is link to parameters such as bubble size or gas holdup in the flotation microenvironment through the types of relationships explored in Section 1.4.5.2. A good example of this is the k-S_b relationship which suggests that flotation cells of different size or type will have similar flotation rate constants provided the bubble surface area flux in the cells is equivalent. An example of the relationship between the flotation rate constant and the bubble surface area flux is given in Figure 1.7. Here, it can be seen that the flotation rate constant is approximately linearly related to the bubble surface area flux and that this is largely independent of the cell mechanism.

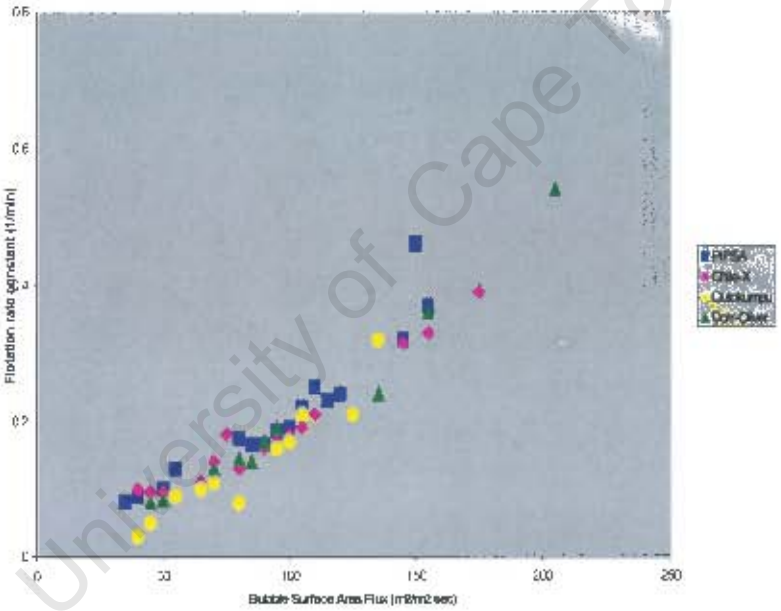

Figure 1.7 Typical k-Sb relationship (after Gorain *et al* (1997)).

1.5 Scope of Thesis

This section serves to provide an overview of both platinum and platinum flotation, as well as providing details of the aims and objectives of this study in terms of the effect of hydrodynamic variables on platinum flotation.

1.5.1 Platinum

While ancient civilisations may not have recognised platinum as a separate element, platinum has been found in a number of Egyptian artifacts. There is also evidence that platinum was known to the inhabitants of Ecuador prior to the arrival of the Spanish (Hochreiter *et al*, 1985). While platinum was known in Europe in the Middle Ages, it was not widely used until the Twentieth Century.

Platinum was first discovered in South Africa in 1923 in the then Transvaal (Hochreiter *et al*, 1985). In 1924, near the site of the original discovery, Dr Hans Merensky discovered the largest known repository of platinum group metals (PGMs) in the world. The main two platinum-bearing seams in South Africa are the Merensky and UG-2 reefs (Corrans *et al*, 1982). The Merensky Reef has been exploited since the early days of South African platinum processing, but it has only been more recently that the UG-2 Reef has been processed economically. This change has come about due to both the difficulties in deeper development of the Merensky Reef and also because of an improved ability to process the more mineralogically difficult UG-2 ore. A comparison of the mineralogy of the two seams is given in Table 1.9.

Table 1.9 Mineralogy of South African platinum reefs.

Reef	PGM (g/t)	Cu (%)	Ni (%)	Cr_2O_3 (%)
Merensky	4 – 8	0.10 – 0.16	0.16 – 0.20	0.1
UG-2	4.6 – 7.3	0.004 – 0.012	0.010 – 0.029	27 - 34

1.5.2 Platinum Flotation

As mining of the South African platinum ores progressed in depth, the proportion of oxide ore decreased and the proportion of sulphide ore began to increase. This change meant that an increasing proportion of platinum could be recovered by flotation, instead of gravity concentration processes. As a result, most producers now rely solely on flotation for the primary recovery of liberated minerals (Hochreiter *et al*, 1985). Flotation circuits are designed, basically, for the flotation of base metal sulphides, with PGMs recovered as a consequence. Base metal head grades, however, are well below the tailings values for many base metal flotation plants. The presence of the PGMs makes the process economical. There is an added consideration when designing a

flotation circuit in that fine sulphides have a slow flotation rate in the UG-2 ore, so the cleaner circuit must have a large volume to ensure a sufficient residence time for these particles.

Flotation of platinum usually involves roughing, scavenging and multistage cleaning to produce a concentrate of the required grade. Flotation reagents usually consist of copper sulphate as an activator, xanthate as a collector, a frother and a depressant such as dextrin or guar to prevent gangue minerals like talc from entering the concentrate. Flotation is usually performed at natural pH of between 7.5 and 9 (Vermaak, 1995), and flotation concentrates are thickened and sometimes filtered prior to smelting. The major gangue mineral in UG-2 ore is chromite, and a production constraint that Cr_2O_3 levels not exceed 3% is usually in place. Concentrate chromite levels are controlled by using three stages of cleaning and by using a frother which produces a brittle froth, reducing the amount of physically-entrained chromite (Vermaak, 1995).

1.5.3 Hydrodynamic Effects in Platinum Flotation

There appears to be no rigorous investigation of hydrodynamic effects on the flotation of platinum ores in the published literature. However, a number of studies have been conducted to determine the effects of impeller speed and air flowrate on flotation as part of the AMIRA P9 project (c.f. Chapter 2) for Anglo Platinum, Lonmin and Northam Platinum. These studies were not published in the open literature but suggested that increasing the power input, by increasing the impeller speed, leads to an increase in the rate of platinum flotation in certain instances. These studies were conducted on industrial flotation cells in concentrators where it was difficult to change parameters, take samples and control the cells, which is why there is a need for the controlled testwork presented in this thesis.

Stronger than the available experimental evidence is the general belief in the platinum industry that increasing power input increases the rate of flotation, especially for fine particles (Knopjes (2000), Manlapig (2000)). This has led mill operators to install flotation cells with power intensities of up to 10 kW/m^3. It should be clear from this chapter that impeller speed and air flowrate are two central hydrodynamic variables and that these have a profound effect on the power input to a flotation cell. Power input is important to the platinum industry due to its (hypothesized) beneficial effects on particle-bubble contacting.

1.5.4 Scope of Thesis

From the reviews presented in this chapter it should be clear that cell hydrodynamics, driven by the central hydrodynamic variables of impeller speed and air flowrate, has a profound effect on flotation in mechanical flotation cells. However, comparatively little work has been performed on quantifying the effect of these variables in the flotation of platinum ores. This is despite the fact that, due to the effect of impeller speed and air flowrate on the power input, platinum producers regard hydrodynamic effects as having a large impact on the recovery of platinum in their flotation circuits. It is believed, therefore, that it is important to obtain a better understanding of the way in which power input, as influenced by impeller speed and air flowrate, affects platinum flotation.

The aim of this thesis is to determine the effect of impeller speed and air flowrate on the flotation of platinum in mechanical flotation cells. The thesis firstly explores the effects of impeller speed and air flowrate on hydrodynamics, solids suspension and gas dispersion. The thesis then investigates the effects of impeller speed and air flowrate on mineral recovery and concentrate grade, after which the effects of power input and bubble surface area flux on the flotation rate constant are explored. The study was carried out using a flotation pilot plant, the Baker Process Floatability Characterisation Test Rig (FCTR), on a Lonmin platinum concentrator.

Chapter 2 Flotation Pilot Plant

The work for this thesis was performed on the Baker Process Floatability Characterisation Test Rig (FCTR) pilot plant, under the auspices of the AMIRA P9 project. The FCTR represents a major step forward in flotation research, in that it provided the first portable, fully instrumented pilot flotation plant. Because the FCTR is central to the work presented in this thesis, this chapter will provide an overview of the pilot plant and the P9 project which led to its creation.

2.1 AMIRA P9 Project

The Australian Minerals Industry Research Association (AMIRA) P9 project is the world's largest and longest-running mineral processing research programme. Begun in 1962 as a collaborative research project between AMIRA and the Julius Kruttschnitt Mineral Research Centre (JKMRC), P9 had the initial aim of optimising mineral processing operations by modelling and simulation. The project relies on minerals companies and equipment suppliers to sponsor the ongoing research. In return, sponsors are able to have research projects conducted on their plants. Sponsors currently number thirty-seven, and are based in Australia, South Africa, North America and South-East Asia. Extensions to the project have occurred every three to four years. The current extension is P9M, set to run from 2000 to 2003.

P9 covers most aspects of minerals processing, and the following areas are being actively studied:

- Milling
- Classification
- Mineral Liberation
- Dense Medium Separation
- Flotation

The flotation module has two general aims:

- An improved mathematical model of flotation cell performance for circuit optimisation and enhanced cell technology, and
- Accurate procedures for sizing industrial flotation plants from laboratory-scale tests, using simulation.

Within the flotation module, there are a number of areas being researched:

- Cell hydrodynamics
- Froth performance
- Determination of stream floatability
- Entrainment modelling
- Development of total flotation model
- Circuit modelling and simulation

The work performed for this thesis falls under the flotation module of the P9M project.

2.2 Floatability Characterisation Test Rig (FCTR)

In the past there has been no way of accurately predicting full plant performance from laboratory flotation data. As the applicability of laboratory flotation data has been a major shortcoming in flotation research (particularly in the study of flotation cell scale-up), it became necessary to construct a flexible, portable flotation pilot plant that could be used to validate flotation models and to predict accurately the effect of changes in process conditions on full-plant performance. The FCTR was the result of this, in that it provided a means of simulating full-plant conditions through the continuous operation of banks of flotation cells. This section will serve to present both the background to the design of the pilot plant and details of its operation.

2.2.1 FCTR Design

The FCTR consists of two banks of six cells: one rougher bank and one cleaner bank. Rougher cells (cf. Figure 2.1) have a total volume of 150 litres (active volume of 127.5 litres) and cleaner cells have a total volume of 50 litres (active volume of 42.5 litres). The design of both banks of cells was based on the existing mechanisms used in early versions of the WEMCO 1+1 machine (Rahal, 1999). These cells, however, were not fitted with draft tubes or false bottoms. The design for these on the FCTR cells was based on the design used in the SmartCell machines. The FCTR is self-contained and fully instrumented, fitting into a twelve metre shipping container. The pilot plant can be slid in and out of the container along rails. FCTR cells are mounted on a set of stairs that are inclined at a 30° angle to provide adequate static head along both banks of cells (cf. Figure 2.2). In the figure, the rougher cells are on the left and the cleaner cells are on the right.

Figure 2.1 FCTR rougher cell.

Figure 2.2 Rougher and cleaner bank layout.

Feed slurry for the FCTR was diverted from within the concentrator and pumped to a 750 litre stirred conditioning tank. From this tank, situated at ground level, the slurry was pumped vertically upwards to the first rougher cell by a Bredel peristaltic pump. The pump was fitted with a variable speed drive (VSD) such that the slurry flow could be adjusted between 40 and 80 litres per minute. The former was chosen as the minimum flow required to maintain pulp levels in the rougher cells of the FCTR. Concentrates were collected from each cell, and these concentrates flowed under gravity to Watson-Marlowe twin-head pumps located directly under the banks of cells. Each cell concentrate flowed to a separate pump head, ensuring that concentrates were never mixed. From the pumps, concentrates were run in standard hoses to wherever in the circuit they were required. For example, rougher concentrates could be run either to the head of the cleaner bank or to the final tails sump depending on the configuration of the circuit.

Each cell had an alternate feed port, located next to the feed port from the previous cell, which could be used to add reagents or to recycle streams from various places in the circuit. Each cell was fitted with a three-way valve on the tails line, allowing for full-stream sampling or for diverting the stream to an alternative place in the circuit. The PLC and control computer were located in the control room within the container. When fully set up (cf. Figure 2.3), the FCTR is roughly twenty metres long (including the container) and seven metres high.

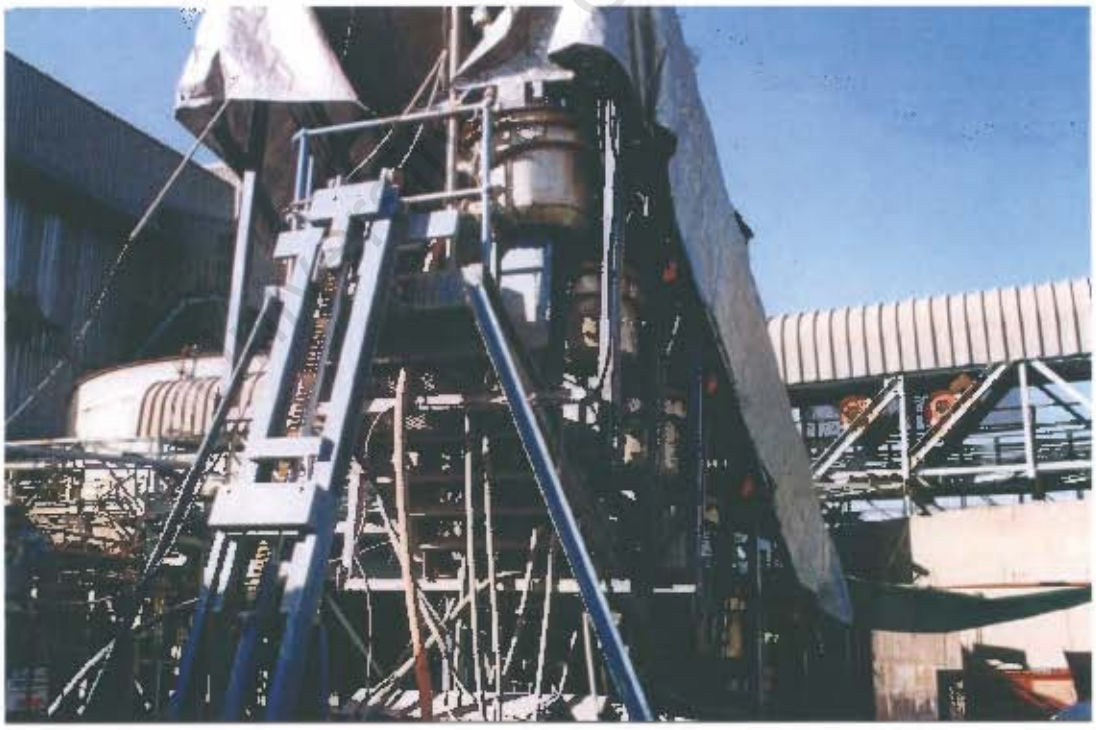

Figure 2.3 FCTR in operational position.

2.2.1.1 Feed Control

Feed from inside the plant was delivered to a baffled 750 litre mixing tank equipped with a 0.55kW Lightnin mixer. An SPX-40 Bredel pump was used to transfer the slurry from the mixing tank to the first rougher cell, and the flow from this pump was accurate to ±0.41 l/min. The determination of the accuracy of the measurement of feed flowrate will be discussed later in Section 3.3.1.

2.2.1.2 Level Control

The pulp level in the FCTR cells was controlled by the Mintek Float Star control system. Float Star is a computer-based control system similar to many industrial Distributive Control Systems. This system allowed the setting of a number of variables (such as level control and impeller speed) through a computer located in the FCTR control room. Once conditions were set, Float Star automatically controlled the variables at or around the setpoint through the automatic adjustment of tailings dart valves located in each cell. Endress + Hauser Prosonic T ultrasonic level probes (cf. Figure 2.4) were used to monitor the slurry level in the cells. Information from these probes was sent to Float Star, which chose an appropriate control action and sent a signal to Biman actuators controlling the dart valve on the tailing port of each cell. Actuator air was controlled by a Wilkerson pressure regulator, which maintained air pressure constant at 4 bar. Control system accuracy was ±2.0mm, and the determination of this accuracy will be discussed in Section 3.3.2.

Figure 2.4 Endress + Hauser ultrasonic level probe.

The Biman actuators were initially connected to plant instrument air lines, but, due to pressure drops in the instrument air, were changed to being supplied with air by a compressor to ensure constant operating pressure. Water traps were fitted on the compressor air line prior to each actuator. Each cell also had a number of attachable concentrate lip extensions, ranging in height from 20mm to 80mm, which allowed a number of froth depths to be used in each cell while maintaining a constant pulp volume.

2.2.1.3 Air Control

Wemco cells use self-induced air for their operation. Despite this, the FCTR cells' air inlets were connected to plant instrument air, and air was blown into the cells. This was done to ensure that the volume of air entering the cell could be accurately measured. Air fed to each cell first passes through a Wilkerson pressure regulator which was set at a pressure of 2 bar (Rahal, 1999). King air rotameters (cf. Figure 2.5) were used on both rougher and cleaner cells, and the rougher air rotameters had an operating range of 40 - 450 l/min, while those on the cleaners had a range of 30 – 280 l/min. In this testwork, however, only the rougher cells were used and the range of operating air flowrates used was 90 – 200 l/min.

Figure 2.5 King air rotameter.

Pressure gauges were mounted on the outlet of the air rotameters to allow for an accurate flowrate reading. The stated accuracy of air control was ±9 l/min for the roughers and ±6 l/min for the cleaners. However, this was simply the manufacturer tolerance at the highest end of the rotameter

scale, translating to a 2% error in rotameter readings. Aside from this, no measurements of the accuracy of the rotameters were made during this testwork.

2.2.1.4 Launder Water Control

Two water lines were connected to the FCTR to provide launder water, one for the roughers and one for the cleaners. Each cell was fitted with its own launder water control system to improve the accuracy of the water balance in the circuit. Launder water was controlled by a Cole Parmer water rotameter with a range of 1 – 10 l/min, with a stated accuracy of ±0.2 l/min. However, during the FCTR campaign it was found that the accuracy of these rotameters varied by much more than this amount. The determination of the accuracy of the water flow will be discussed later in Section 3.3.3.

2.2.1.5 Impeller Speed Control

Each cell was fitted with a polyurethane Wemco impeller and disperser mechanism, and impeller shafts were connected via a bearing directly to Alstom inductively-coupled motors. 2.2 kV motors (cf. Figure 2.6(a)) were fitted to the rougher cells and 0.75 kV motors to the cleaner cells. The rougher motors were controlled by 2.2 kW Yaskawa VS-606V7 single phase 200V variable speed drives, while the cleaners were controlled by 0.75 kW Omron SYSDRIVE 3G3EV single phase 200V variable speed drives (cf. Figure 2.6(b)), with the VSD output being controlled from Float Star. The specifications for the motors are given in Table 2.1. The accuracy of the impeller speed measurements will be discussed later in Section 3.3.4.

Table 2.1 FCTR impeller motor specifications.

Cells	Volts	Hz	RPM	kW	Cos φ	Amps
Rougher	230	50	1425	2.20	0.80	8.5
Cleaner	230	50	1400	0.75	0.78	3.4

Throughout this study, impeller speed is represented as a percentage of maximum speed rather than in RPM. This is due to the way in which Float Star operated: impeller speed was changed in this program by entering it as a percentage of maximum speed, where the maximum speed was 1425 RPM. For convenience, percentages were used throughout the testwork to represent impeller speed.

Figure 2.6 (a) Alstom 2.2kV motor, (b) Yaskawa and Omron variable speed drives.

2.2.1.6 Sampling Points

The FCTR allows full stream sampling around every cell in the system. Feed and tails discharge on each cell are fitted with two-inch three way valves and each concentrate launder was connected to flexible hosing that allowed the entire stream to be sampled, and for a flow rate to be calculated. The availability of the entire stream for sampling on every stream within the FCTR greatly increases the accuracy of mass balancing and modelling.

2.2.1.7 Configuration Flexibility

The FCTR was equipped with a number of pumps that makes changing the configuration of the circuit simple. Concentrate streams were pumped to their destination using Watson-Marlowe 704 U/R twin channel peristaltic pumps. The cleaner tails stream was also pumped to the same type of Watson-Marlowe pump, allowing the stream to be recycled to any point in the FCTR circuit. Rougher tails flowed into a sump that was connected to a Bredel SPX-40 peristaltic pump and from here, the slurry was pumped to a bunded area within the plant to be returned to the flotation process via a spillage pump.

2.2.2 FCTR Commissioning

The FCTR was delivered to Lonmin's Karee concentrator in January 1999, where it remained until January 2000, undergoing a number of major design and equipment modifications. Section 2.2.1 outlined the results of these modifications in terms of the equipment now used in the FCTR. After leaving Karee, the FCTR was moved to Lonmin's Eastern Platinum concentrator in January 2000. Eastern Platinum concentrator is located near Brits in the North-West Province of South Africa and handles about 300 000 tonnes per annum of UG2 ore. A more complete description of the ore and concentrator is given in Sections 3.1 and 3.2, respectively, in the following chapter.

2.2.2.1 Equipment Modifications

A further few modifications were made after the unit arrived at Eastern Platinum. The main modification was replacing mild steel impeller shafts with stainless steel to prevent bending and warping of the shafts, which helped to reduce the amount of vibration in the rig and enabled the ultrasonic level probes to operate more effectively. Each impeller stand was strengthened, and the mechanism for changing the impeller engagement was altered, by lengthening the thread on each stand and changing the handle to a bicycle handlebar style that made raising or lowering the motor and impeller much easier. In addition, the reservoir of oil for the hydraulic jack that raises the FCTR into position was replaced with a larger reservoir at the start of the Eastern Platinum campaign.

The level indicators for the ultrasonic probes were also altered. Large Perspex discs were attached to the top of a thin stainless steel shaft with a polystyrene ball at the other end of the shaft. The polystyrene ball would float at the pulp/froth interface, changing the height of the Perspex disc as it did so. The ultrasonic beam would reflect off the disc, controlling the pulp level in the cell. Other changes were made to the three-way sampling valves by replacing the handles of these valves, which had proved to be difficult to use, with larger valve handles that were easier to move and also less likely to snap off.

Operating the Biman valve actuators on air from a compressor provided some commissioning difficulties. Water from the compressor was entering the actuators and hindering their operation, despite the water traps attached to the air lines. The actuators all required servicing by Biman, and it was discovered that the water traps on the air lines as well as the drain valve on the compressor needed to be released twice daily to prevent water build-up.

The dart valve shafts were lengthened during the Eastern Platinum campaign. An extra piece had been added to the cell at Karee, making the outer edge of the cell higher, but when the Biman actuators were connected at this new height the original shafts for the dart valves were no longer the right length to get a perfect seal when the valve was closed. The shafts were all lengthened, making the dart valves the correct size.

Concentrate lines were also altered. At Karee, concentrate had flowed from the launder into a plastic cup connected via plastic hose to the concentrate pump. At Eastern Platinum, however, the concentrate froth began to overflow the plastic cup so a single hose from the launder to the concentrate pump was used to replace the plastic cup. At Karee, the concentrate pumps (located directly under the cells) were not covered, meaning that any slurry spillage would fall onto the pumps, with the potential to damage the pump mechanism. Metal covers were built to protect the pumps from any slurry spill at Eastern Platinum.

The settings for the variable speed drives on the rougher cells were altered for this testwork. When the impellers were run without slurry in the cells, it was discovered that the motor current was higher than when there was a load in the cell, due to the VS drive adding its own load to protect the motor. This setting on the VS drive was switched off to allow an accurate measurement of no load current. In addition, it was found that the VS drives were set to 220V, at the upper limit of their operating range, so this setting was reduced to 200V. This had the two-fold effect of protecting the drives and also increasing the motor trip current, which was of particular use during the testwork on power.

2.2.2.2 Operational Commissioning

At Eastern Platinum, the FCTR was initially commissioned on the plant's primary cleaner tail stream. The first section of testwork was conducted on this stream with a Svedala Stirred Media Detritor (SMD) for fine grinding installed prior to the FCTR, and this period of commissioning represented the first time that both banks of cells on the FCTR had been run at the same time. Start up of the cleaners, especially, proved to be much easier than anticipated, and no major difficulties were encountered.

Commissioning on the primary cleaner tail stream, in general, was straightforward. There were no problems encountered with solids suspension and launder water was not required, as the fine, low-chrome stream flowed from the launders by itself. Commissioning the rougher feed stream, however, was more difficult. The initial choice of sampling point was from an agitated conditioning tank at the head of the rougher bank, but this sampling point was abandoned after a

number of attempts to take feed to the FCTR. The reason for this was that the impeller blades inside the tank were worn and solids were not being suspended. As a result, the sampling point was taking a sample with a slurry density of 2.6, rather than the 1.4 it was supposed to be. Not only was this sample point producing an unrepresentative sample of feed, but it also proved impossible to pump slurry of this density from the sample point to the FCTR, some fifty metres away. Following this discovery, the sample point was moved to the slurry inlet inside the first cell in the rougher bank. This produced a slurry density that was much more representative of the plant feed. It was only discovered later, however, that this sample was actually not representative of the plant feed: assays for this sample point were all in the range of 2–2.5 g/t platinum, as opposed to plant feed platinum grades of 4–4.5 g/t. Despite this discrepancy between plant feed grade and FCTR feed grade, this proved not to be a major issue in this testwork. Although the FCTR feed grade was lower than plant feed grade, it was relatively consistent and provided the FCTR with a suitable feed for the test campaign.

Solids suspension in the FCTR cells was also an issue on the rougher feed stream. With coarse particles, and containing 26% chrome, optimising the air flowrate and impeller speeds took some time. It was found that air flowrates needed to be maintained at significantly lower values than for the rougher feed work in order to keep solids suspended. If the FCTR cells sanded-up when running rougher feed, the only course of action was to dump the contents of the cells and the head tank onto the ground, as stopping the Bredel feed pump would choke the line inside the pump, so it was necessary to keep the feed pump running and simply let the cells overflow. If it was noticed early enough, however, the cells could be prevented from overflowing by reducing the air flowrate into the cells to below 100 l/min, which would re-suspend solids. This problem was not encountered during the testwork, however, as during commissioning it was possible to determine the conditions of impeller speed and air flow at which solids were just suspended. Once this was determined, any solids suspension problems were avoided by not running tests below the minimum conditions for solids suspension.

2.2.3 FCTR Operation

2.2.3.1 Operational Staff

The FCTR campaign at Eastern Platinum ran from January to June 2000. The initial phase of the campaign involved the setting up of equipment and commissioning of the cells, followed by a period of intense sampling beginning in late April. During this sampling, the FCTR was operated continuously in two twelve-hour shifts. This was done to minimise the time taken to start up and

shut down the rig (each of these procedures taking approximately ninety minutes), and also to maximise the amount of work that could be completed in the allotted time.

FCTR operational staff were drawn from the University of Cape Town (Rob Coleman and Jonathan Lewis) and the University of British Columbia (Tad Crowie and Cameron Lilley), as well as a total of ten laboratory staff supplied by Lonmin for sample preparation. Each of the shift crews comprised one University of Cape Town (UCT) staff member, one University of British Columbia (UBC) staff member and five Lonmin laboratory staff.

On each shift, laboratory staff were responsible for the preparation of wet samples for assay (filtering, drying, splitting and correct labelling of each sample). UCT and UBC staff were responsible for the installation of pipework leading from the sampling points to the FCTR and the changeover of pipework when changing from rougher feed to cleaner tails slurry streams. During the sampling campaign itself, UCT and UBC staff were responsible for setting FCTR operating conditions and ensuring these conditions were maintained, as well as providing any running repairs to the FCTR as required. These staff were also responsible for collecting reagent from inside the plant and adding this via a dosing pump to the pilot rig. The largest task was the sampling itself, which was conducted continuously during each shift, conditions permitting. If feed to the FCTR was consistent throughout the shift, then a sample would be taken every fifteen minutes during the twelve-hour period, with slightly longer delays between tests when operating conditions were changed.

2.2.3.2 FCTR Start-Up

To begin with, the conditioning tank at the head of the FCTR needed to be filled. It was usual to run water through the FCTR before introducing slurry to the system to allow the pulp levels in the cells to stabilise fully. In addition, if slurry was added to empty cells it would be some time before the slurry level reached the impeller, meaning that solids in the slurry may have settled out in the cell, blocking the tails line. When slurry was added to the head tank, it was essential to make sure the agitator was running in the tank. Without this there was the potential to sand-up the conditioning tank.

Once cell levels had stabilised on water, slurry could be introduced to the system. This was done by switching on the pump at the head of the rougher bank inside the plant, for rougher feed, or by opening a pressure pipe sampler valve on the primary cleaner tails line. The level of slurry in the FCTR conditioning tank was controlled by level probes inside the tank. When the slurry level reached the shortest probe (i.e. highest slurry level) a signal was sent to cut off the feed and then

when the level dropped to the second shortest probe another signal was sent to start feeding to the FCTR again.

Rougher cell levels were set at around 300mm, but this could vary by 10-15mm depending on the cell. This setpoint was chosen to provide the shallowest froth depth possible without pulping the cells. Pulp levels were set on the Float Star system in the FCTR control room. Care had to be taken when operating the cells for this campaign. Because the cells were not utilising self-induced air, but rather had plant air blown in, it was essential to remember to introduce air to the cells prior to starting the motors. If this was not done, the motor current would be high, running the risk of damaging the motors.

2.2.3.3 Continuous Operation

An FCTR cell in operation at Eastern Platinum is shown in Figure 2.7.

Figure 2.7 Operating FCTR cell.

Once the cells were full of slurry, it then took some time for the system to equilibrate. Pulp levels would often cycle around the setpoint before finally stabilising close to the setpoint. At times, the levels would take longer than usual to stabilise. At these times, controller gain could be changed on the Float Star system to attempt to change the controller's reaction time to changes in the system. When the impellers were being run at high speeds, there would often be a certain amount of vibration in the rig, and this vibration would also often cause the level control to cycle around the

setpoint without stabilising. Level control could also be affected if the ball and float arrangement became stuck in the cell. Occasionally, an error would occur with the ultrasonic probes, and they would give a false reading of zero level, and in this instance, the tails dart valve would close to try and raise the level, even though quite often the cell would already be full. If this occurred, the Perspex disc would need to be manually lifted to change the signal being sent to the Float Star system, and the error corresponding to that level probe would need to be acknowledged and cancelled on Float Star.

One problem that occurred from time to time was the loss of feed from the concentrator to the FCTR. This would happen particularly in the primary cleaner tails section of work when plastic or wood chips would block the pressure pipe sampler feeding slurry to the FCTR. It was necessary to keep a virtually constant watch on the slurry level in the FCTR conditioning tank to ensure that slurry was feeding into the tank. If slurry feed was stopped, the volume of the conditioning tank meant that there was some time to react before the tank ran dry. Usually, restoring feed was a matter of stroking the valve to the pressure pipe sampler to clear the blockage. If noticed early enough, this loss of feed did not disturb the process, but if not picked up, any test in progress would need to be abandoned if the tank ran dry while sampling.

It was also necessary to keep a close watch on the concentrate pumps as over time, the flexible hoses inside the pump heads would wear and eventually rupture. This was a particular problem for two reasons. Firstly, a ruptured hose meant that not all slurry would be delivered to the sampling point, making for an unrepresentative sample, and, secondly, The Watson-Marlowe twin-head pumps were very sensitive to slurry in the mechanism. If solid particles got into the pump head mechanism, the head would wear and become inoperable. Maintenance of these Watson-Marlowe pumps proved to be a major problem, and at one stage the pumps were replaced by a new model Watson-Marlowe pump, on temporary loan from Lonmin. These pumps also suffered from wear to the hoses, but, unlike the model used on the FCTR, the new pumps were not sensitive to slurry leakage. The mechanism was, sensibly, kept separate from the hose, so any leakage of slurry did not result in damage to the pump head.

Once started up and stabilised, sampling on the FCTR could begin. Between sampling runs it was necessary to check and re-set both launder water and air flow rotameters as these instruments would drift over time, and small adjustments needed to be made between samples to ensure that the correct air and water flowrate was being delivered.

A number of problems were encountered with the impellers themselves. Apart from the change from mild to stainless steel shafts, as mentioned earlier, there were also problems encountered with

shafts slipping out of the coupling with the motor. In these instances, the impeller engagement would be changed by the shaft slipping further down into the cell. With this would come an associated increase in motor current, sometimes to a point dangerously close to the trip current of the motor. If a shaft slipped it was necessary to remove that impeller from the circuit for repair and this required the entire motor and impeller assembly to be physically lifted out of the cell. If the impeller could be refitted and tightened in place in a satisfactory manner, it could be put back into the circuit but if not, it would be necessary to replace it with a spare motor/impeller assembly. While the impeller was out of the cell it was necessary to drain that cell and, obviously, abandon any sampling that had been in progress at the time.

Most process variables could be adjusted through the Float Star system. Impeller speed, pulp level, and - if required - manual operation of dart valves was all set through Float Star faceplates. The quality of the control of the pulp levels could also be assessed through Float Star, as the package kept a six-minute trend of the process variable for pulp level for each cell, and it became quickly apparent if the pulp level for a particular cell was varying from the setpoint. If it was, there were a number of things that could be done, such as manually opening and closing the dart valve, which would often improve the control if the cycling of the level was out of control. Reducing impeller speed was also another way to improve the control. Often at higher impeller speeds the vibration would cause the ultrasonic probe to provide inferior level control, so reducing the amount of vibration would help to rectify this.

2.2.3.4 Reagent Addition

Reagents could easily be added to the FCTR. Dosing pumps were set up next to the conditioning tank to allow reagents to be added. Buckets of reagents were collected from inside the plant and diluted as necessary in a 200 litre drum and the drum was topped up as required. For most of the power input testwork at Eastern Platinum, no reagents were added to the FCTR, as the FCTR sample was taken after reagent addition in the concentrator. For the cleaner tails section of work, the sample from the concentrator was taken prior to the addition of depressant so in this case, a dosing pump was set up next to the FCTR to run 300 g/t of CMC depressant to the FCTR conditioning tank.

2.2.3.5 FCTR Shut Down

Shutting down the FCTR involved cutting off the slurry feed to the conditioning tank and lowering the level in the tank. Once the level was low, water could be added, either directly into the head tank, or inside the plant to flush out any sumps. Water was run through the FCTR cells until there

was clear water running into the tails sump. Often this would take between an hour and ninety minutes, but once clear water was running through the FCTR, the cells could be drained one by one, taking care not to overflow cells further down the bank. As the cells drained, motors could be shut off, along with the air to each cell. Once the cells were drained, the compressor that supplied air to the actuators could be shut off, along with the feed pump and agitator in the head tank.

2.2.4 FCTR Summary

There were a number of problems encountered during the commissioning of the FCTR, such as the difficulties with solids suspension, problems with obtaining a representative feed from inside the concentrator, initial difficulties with motor trip currents and mechanical problems with the impellers themselves. As a result of these problems, the commissioning period prior to the commencement of the testwork was significantly longer than expected. However, due to the length of the commissioning period, it was possible to identify and rectify a number of operational issues, both minor and major, that may otherwise have gone unnoticed and adversely affected the quality of the testwork. As a result of this, by the time the study began, the FCTR was operating as fully functioning pilot plant and no unexpected operational problems were encountered during the actual testwork.

Chapter 3 Experimental

This chapter presents details of the experimental program conducted on the FCTR at Lonmin's Eastern Platinum concentrator. Sections 3.1 and 3.2 describe the ore and the concentrator, respectively, while Section 3.3 outlines the experimental measurements used in the study. Sections 3.4 and 3.5 cover the background to the statistical design of the experimental program as well as details of the program itself. Section 3.6 outlines the sampling program on the FCTR. The chapter concludes with a description of the mass balancing and data reconciliation in Section 3.7.

3.1 Ore Details

The Merensky Reef and the UG2 chromitite layer occur as distinct layers within the gigantic intrusive referred to as the Bushveld Complex. This occupies an area of about 40 000 km^2 in the central Transvaal (Hochreiter *et al*, 1985). The Bushveld Complex is the world's largest layered complex, and accounts for about 80% of the world's platinum reserves, with proven reserves of 1360 million ounces of platinum. The UG2 layer is located between 20 and 370 metres below the Merensky Reef.

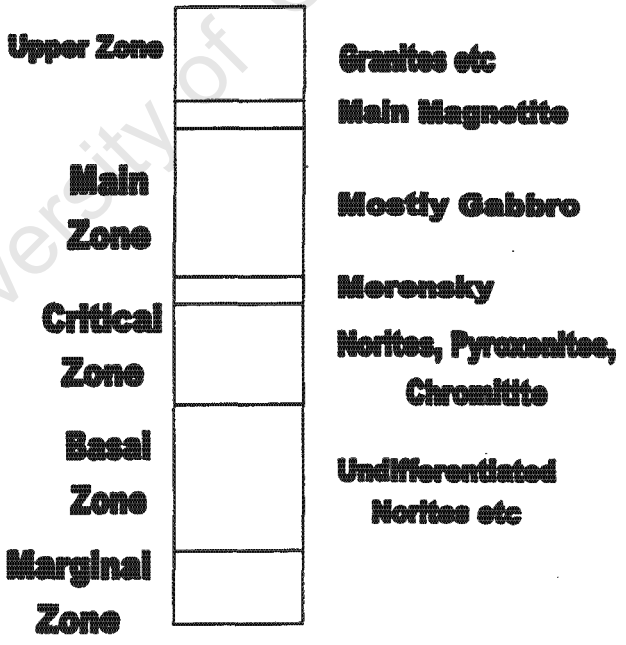

Figure 3.1 Cross-section of the Bushveld Complex (after Hochreiter *et al* (1985)).

It is believed that the formation of the Bushveld Complex was the result of a magmatic event in which large volumes of molten rock from the Earth's mantle were injected into the crustal rocks of the Transvaal millions of years ago. This injection took place in pulses of magma, each of which was subtly different from the previous one. Some differentiation of the layers may have taken place as different minerals crystallised out at different temperatures, leading to the distinct, stratified compositional layers of the Bushveld Complex (cf. Figure 3.1). A general trend is observed in the Bushveld Complex of magnesium-rich, high temperature rocks in the lower zones, to low temperature siliceous and iron-rich rocks in the upper regions.

In terms of the PGM content, the Critical Zone forms the most important region. This zone consists of a series of chromitite layers within pyroxenite in the lower portion, and a series of cyclically repetitive sections of chromitite, pyroxenite and norite in the upper regions. The Critical Zone is divided, according to chromitite layer, into Lower, Middle and Upper Groups. These are further subdivided into classifications such as LG1, LG2 (Lower Group chromitites), MG1, MG2 (Middle Group chromitites), and UG1 and UG2 (Upper Group chromitites) (cf. Figure 3.2).

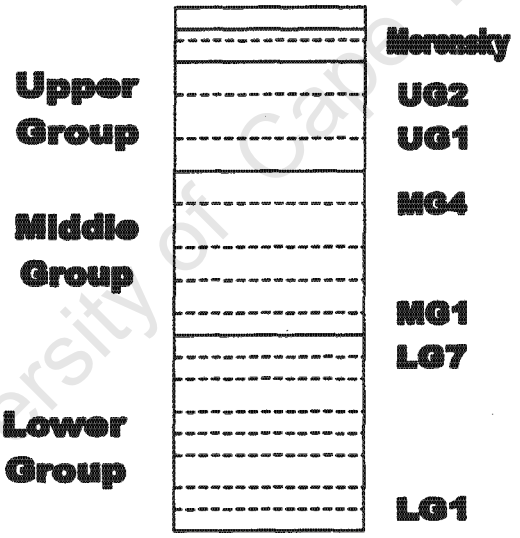

Figure 3.2 Cross-section of the Critical Zone (after Egya-Mensah (1998)).

There are thirteen chromitite units in the Critical Zone, although only one of these – UG2 – bears significant platinum values. At the top of the Critical Zone, there is evidence to suggest that conditions leading to the formation of another chromitite-pyroxenite-norite triplet occurred. The pyroxenite is prominent, but the chromitite is poorly developed. This section is known as the Merensky Reef.

The final chromitite-pyroxenite layer is known as the Bastard Reef, and is located above the Merensky Reef. Its chromitite is poorly developed or even absent in some places, and the reef is virtually non-platiniferous. Above this Bastard Reed, the Critical Zone's norites give way to gabbrous members of the Main Zone, which represent a new and compositionally different infusion of magma into the ore mineralogy of the Bushveld Complex. The gabbrous layer has been found to play an important role in the flotation characterisation of the floatable particles.

The characteristics of both the Merensky and UG2 ores are very different (cf. Table 3.1), and from the different characteristics of each ore it is clear that they will require different processing conditions. For instance, the UG2 ore (the ore used in the testwork for this thesis) requires a fine grind to allow sufficient mineral liberation, whereas coarse grinding is generally acceptable for Merensky ores.

Table 3.1 Comparison of Merensky and UG2 ores.

Merensky	UG2
Less than 1% chromite	Around 26% chromite
Found in pyroxenite layer	Found in chromite layer
Up to 20% talc	Less than 5% talc
Large sulphide grain size	Small sulphide grain size
High sulphide grade	Low sulphide grade
SG 3.0-3.2	SG 3.6-4.0
Bond Work Index 19kWh/t	Bond Work Index 13 kWh/t

3.2 Description of Concentrator

Lonmin operates Eastern Platinum Ltd, a PGM plant located between Rustenburg and Brits in the North West Province of South Africa. UG2 ore is treated in this concentrator. The concentrator consists of primary and regrind mills and four stages of flotation (cf. Figure 3.3). This is known as the MF2 circuit (mill-float, mill-float). Regrinding of the primary rougher tailings is required since a large proportion of the metal sulphides and PGM in UG2 ore is locked in fine silicate grains.

The primary and secondary rougher flotation banks consist of WEMCO 144 cells, while primary and secondary cleaner banks are WEMCO 84 cells. First and second cleaner concentrates are fed to the final cleaners, while the final cleaner tailings are fed to the first cleaners, for both primary and secondary circuits. Final cleaner concentrate is thickened and transported by road to the smelter.

The Eastern Platinum concentrator has two similar process streams with identical flowsheets, known as A and B stream. The major difference between the two streams is that B stream utilises OK 16 cells for roughing purposes. In the testwork for this thesis, only slurry taken from A stream was used.

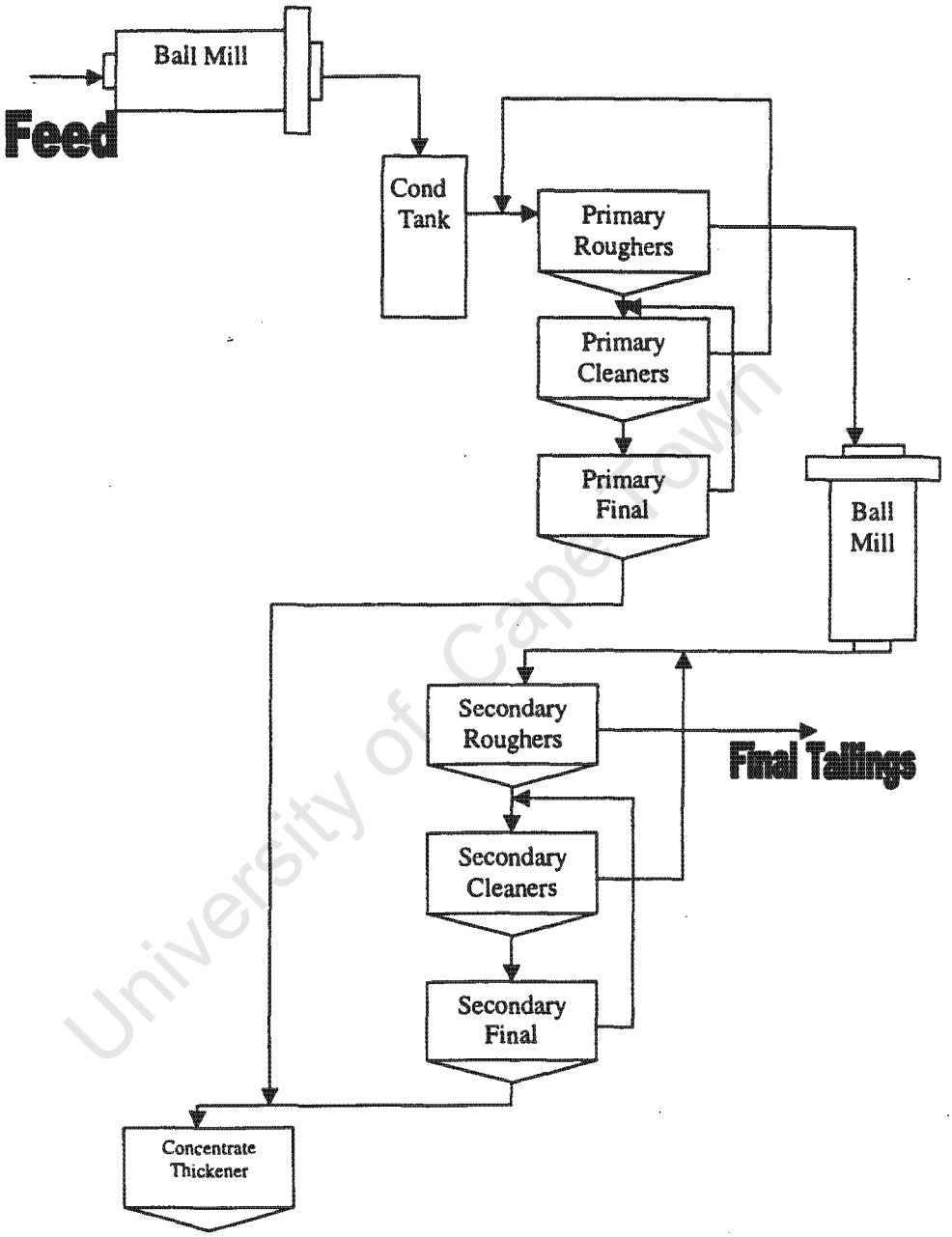

Figure 3.3 The milling and flotation circuit at Eastern Platinum concentrator.

3.3 Experimental Measurements

There were a number of variables measured during this testwork. Most of the measurements made were taken directly from instrumentation on the FCTR itself. The FCTR is a fully instrumented pilot plant, and so most process variables are measured and controlled through the Float Star program.

3.3.1 Feed Flowrate

One of the major variables measured was the feed flowrate (calibrated to 40 l/min of slurry). This was done by running water through the Bredel peristaltic feed pump into four twenty-litre buckets. The time taken to fill these buckets was recorded, and from this the feed pump settings for certain flows were able to be determined. The process of pumping water into the buckets was repeated in order to ensure accuracy of measurement, and in each case, the original and repeated measurements varied by an average of 1.5 l/min (3.75%). Given that this method of measurement had an element of subjectivity to it (determining when each twenty-litre bucket was full), this error is not particularly significant.

3.3.2 Pulp Level

The pulp level was manually calibrated at the beginning of the testwork. This was done by holding the ultrasonic level probe at the "full" (recorded as approximately 380 mm) and "empty" (recorded as 0 mm) positions for each cell when the cells were empty. Once each cell had been calibrated in this way, mid-point probe positions could be checked to ensure that the Float Star calibration was correct (e.g. holding the probe at a level of 100 mm above the empty level and checking the position that Float Star gave). Once each probe had been checked in this way, the pulp levels were controlled by the Float Star programme during the actual sampling campaign. During the period in which the feed was changed from primary rougher feed to cleaner tails, the calibration was checked again.

The accuracy of the pulp level readings was checked in two ways. The first has already been outlined, where probes were held at a known level and the probe position was checked on Float Star. This was done over a range of probe positions between the full and empty positions. In addition to this, while the cells were operating, the "live" Float Star position reading was checked by measuring the probe position against the side of the cell. Using these methods, the pulp level was found to vary within ±2 mm of the Float Star reading.

3.3.3 Launder Water Flowrate

Launder water was controlled by the use of rotameters attached to the water lines. Prior to sampling, and again during the changeover period from rougher feed to cleaner tails, the rotameters were manually checked to make sure that a known volume of water was passing through them. This involved setting the rotameter to a particular value and then timing the flow of water into a measuring cylinder.

It was found that the rotameter settings did not accurately reflect the volume of water passing through, with an average difference of 5.1% between the rotameter setting and the actual flow of water. To compensate for this, actual flows were determined on the various settings for each rotameter so that a known volume of water was passing into the cell for a given setting. These flow tests were repeated a number of times and found to have an average error of 0.8%. Launder water was used during the rougher feed section of work, but was not required for the cleaner tails section.

3.3.4 Power Readings

A number of variables relating to the impellers and motors were also recorded. These were the impeller speed (recorded as both a percentage and RPM value) and motor current. Both impeller rotational speed readings were taken from the Float Star control panel, whereas the motor current could be read either from Float Star, or directly from the variable speed drive.

Motor power, read directly from Float Star, was taken in two situations. The first of these was as a no load measurement (i.e. the motor was run when the cell was empty), and then measurements were taken under all test conditions used. The purpose of the no load current was to test the amount of power that was used to simply operate the motor and, therefore, how much power was absorbed by the slurry under each test condition.

The accuracy of the Float Star impeller speed was not tested during this campaign. However, the RPM of each impeller shaft was checked using an optical tachometer while the FCTR was installed at Karee concentrator, and the average difference between this measurement and the Float Star measurement was found to be 3% for all rougher cells.

Power draw was calculated by determining the no load current on each motor; that is, the power draw when the motor is run in an empty cell. This value was subtracted from the power draw under

load recorded during the testwork to give an absorbed power value. Power itself was calculated by Float Star using the motor currents and voltages, and while this can be regarded as something of an estimate, it is a reliable estimate. The motor currents were checked by a plant electrician when problems with the motor trip current were experienced and found to be accurate within around 5%.

3.3.5 Sample Percent Solids

During sampling, wet and dry masses of sample were recorded for percent solids calculation. All buckets had tare weights written on them, meaning that a wet weight of sample could be easily determined by recording both this tare weight and the total bucket weight, including the slurry sample.

Once this was done, samples were filtered and dried under heat lamps. The dried samples were then weighed prior to preparation for assay. Percent solids could be calculated using the dry sample weight and the wet slurry weight. For the rougher feed work there was the extra complication of the concentrate launder water. For these samples, the flow of launder water was subtracted from the wet mass of the slurry sample and the percent solids was calculated based on that wet mass.

3.3.6 Sample Mass Flow

Each slurry sample taken from the FCTR was a timed sample, enabling the calculation of mass flows for each stream. Despite the fact that all the cell tailings streams were pumped to the final tailings sump, each stream was pumped there separately. This meant that each tails stream could be sampled individually, without contamination from the other tails streams.

The taking of the wet samples was very accurate: a stopwatch was started when the sample line was directed into a sample collection bucket, and stopped again when the hose was removed from the bucket. Using this method, errors in timing the sample would be measured in tenths of a second, which is fairly insignificant when sample times could be a minute or more.

Inevitably, some sample would have been lost during the sample preparation process. However, every care was taken to minimise this error. Sample buckets had lids fitted to prevent accidental spillage of the wet sample and the inside of filter presses were scraped to remove any wet filter cake that had stuck to the press. In addition, a balance was installed next to the drying lamps to ensure that dry filter cakes did not have to be carried any distance, minimising the risk of dropping the dry sample.

The mass balancing (discussed in more detail in Section 3.7) showed that on average there was a 8.8% error between experimental and mass balanced rougher feed mass flows, and an average error of 5.2% between experimental and mass balanced cleaner tails mass flows. The rougher feed error can be largely attributed to larger discrepancies between experimental and calculated tails flows, and will be discussed further in Section 3.7.

3.3.7 Sample Assay

Dry samples were split (if they were large samples) before being bagged and labelled and sent to Lonmin's laboratory for assaying. Samples were analysed by fire assay, and the PGM and chromium assays were reported. The detection limit for the fire assay of PGMs (and therefore the accuracy of PGM fire assay results) is 0.01ppm, which translates to a maximum 1% error in the lowest assay streams (the rougher feed tails assays), which were generally between 1.1 g/t and 1.5 g/t platinum. Overall, however, when all streams are considered, the assaying error is negligible.

3.3.8 Slurry Density

Slurry densities were recorded on the feed stream to the FCTR every half an hour during sampling to confirm that the slurry being received by the FCTR was similar to that in the plant. In the absence of on-stream analysis facilities for assaying, slurry density was a good measurement of the representativity of the sample. Slurry density was measured using a Marcy scale. While not completely accurate, using this device allowed for a rough, instantaneous estimate of slurry density. This rough estimate was good enough to tell whether slurry density was operating in the right region, which was all that was required of this measurement.

3.3.9 Reagent Dosing Rate

The reagent dosage to the FCTR head tank was measured when reagents were being added. While most reagents were added in the plant, depressant was added at the head tank for the primary cleaner tail section of work, due to a reagent line within the concentrator that couldn't be moved to a point in the circuit before the FCTR sampling point.

CMC depressant was collected in buckets from within the plant, and these were added to a drum at the head of the FCTR. These were diluted to allow fewer trips into the plant to collect depressant,

and also to allow a large enough volume of diluted depressant to be added to the FCTR to be accurately read on a dosing pump.

Slurry density and depressant flowrate were used to maintain a depressant addition rate of 300 g/t. The depressant was added via a peristaltic dosing pump placed at the depressant drum at the head of the FCTR. The dosage was corrected every half-hour as a new slurry density sample was taken. Depressant volumes were altered by changing the stroke on the pump, and by measuring the volume of depressant into a measuring cylinder for each new pump setting. It is clear that this method would not give an exact dosage of 300 g/t, but this figure itself was just a plant estimate of the dosage of depressant added to the cleaner bank. For the purposes of the testwork, the accuracy of the dosages was adequate.

3.3.10 Superficial Gas Velocity

Superficial gas velocity (Jg) was measured using the UCT superficial gas velocity device. This testwork was performed only on the first cell in the FCTR circuit, at all test conditions. A tube filled with water was lowered into the cell, and then a pinch valve was opened to allow gas from the cell to enter the tube. The time taken for the water level to drop fifteen centimetres in the tube was measured. Superficial gas velocity could then be calculated from this, and the test was repeated at each condition until four or five similar results were obtained. This procedure was identical for both primary float feed and primary cleaner tail work. The average error in the measurements of superficial gas velocity was only small, at 1.45%. The superficial gas velocity could be calculated using the following formula:

$$Jg = 2.77 \times \frac{Height}{Time} \qquad -3.1$$

In this equation "Height" refers to the fifteen centimetres the water level was allowed to drop in the plastic tube. 2.77 is a factor derived from the ratio of the cross-sectional areas of the pinch valve and the plastic tube.

3.3.11 Bubble Size

Bubble size, like the superficial gas velocity, was only measured on the first cell of the FCTR. Bubble size was measured using the UCT Bubble Size Analyser, details of which have been described extensively in the literature. A total of approximately eight readings were taken at each

setting. From these, perhaps five or six of the data points were accurate enough to be used. The procedure was identical for both rougher feed and primary cleaner tails. In terms of the accuracy of these measurements, the two most varied measurements differed by 19.4%, but for the majority of the power settings, the measurements varied by less than 10%. The Sauter mean bubble diameter (d_{32}) was calculated from this, using the following formula:

$$d_{32} = 6000 \times \frac{Volume}{SurfaceArea} \qquad - 3.2$$

Using this value and the superficial gas velocity, the bubble surface area flux was calculated using Equation 3.3.

$$Sb = \frac{6Jg}{d_{32}} \qquad - 3.3$$

3.4 Experimental Design

The experimental design for this testwork took the form of a central composite rotatable design (CCRD). This was used with a view to developing an efficient regression model for use in optimisation, and to determine which variables were significant (Napier-Munn, 2000a). The other motivation for using a CCRD design was to extract as much information as possible from a limited data set. The reason for this limited data set was that the Lonmin assay laboratory could only handle a limited number of samples for assay each day, thus limiting the number of possible combinations of impeller speed and air flowrate.

CCRD experimental design is also referred to as Box-Wilson design after the two authors who, in 1951, first described the central composite design. Rotatability was introduced in 1957 by Box and Hunter (Napier-Munn, 2000b). CCRD experimental design can be used when the object of a program of experiments is to study the relationships between variables, and to obtain an empirical model to optimise or predict a response over a particular range of conditions. Using the model to predict the response, a visualisation of the relationship can be by a three-dimensional graph. This is referred to as a response surface (cf. Figure 3.4).

The form of the model is not important, provided it accurately reflects the relationship between the factors and the response over the region of interest. It does, however, need to include linear, quadratic and interaction terms to accommodate most trends likely to be encountered, including

curvature. A typical model for a response surface in two factors would be the second order function:

$$y = a_0 + a_1x_1 + a_2x_2 + a_{11}x_1^2 + a_{22}x_2^2 + a_{11}x_1x_2 + \varepsilon_u \qquad -3.4$$

In this equation y is the response, and x_1 and x_2 are the factors. The coefficients a_i are estimated from the data, and ε is the error which cannot be explained by the model. In Figure 3.4, the dependency of nickel recovery on frother concentration and air flow is shown. The optimum region (where recovery is maximised) is easily identified.

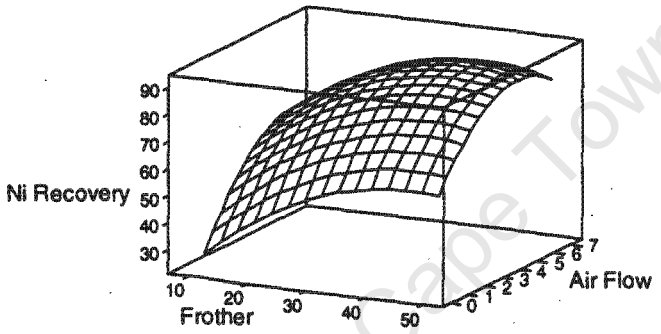

Figure 3.4 Example of a response surface (after Napier-Munn (2000b)).

The test programme was designed to eliminate the effect of time from the experiments. This was done to ensure that when it came to analysing the effect of each variable, that the only variables that would influence the results of the tests would be the air flowrate and the impeller speed.

A factorial design experimental program could be used to estimate the coefficients in the above equation. However, Napier-Munn (2000b) identified two problems with factorials:

1. At least three levels per factor would be needed to estimate the model's quadratic terms, which requires large numbers of experiments (3^k = 27 for three factors and 81 for four factors, etc.)
2. It was shown by Box and Wilson (1951) that a 3^k factorial gives low precision estimates of the squared term coefficients.

When the separate determination of high order interactions can be sacrificed, fractional factorials are an alternative. A better solution, however, is central composite designs, which use fewer tests than full factorial designs and also have desirable properties for fitting polynomial models for seeking optimum points, or for sequential experimentation.

Central Composite Designs are based on a two-level factorial with its origin at the centre, and with additional points added axially a fixed distance, α, from the centre to provide the quadratic terms, plus at least one test at the centre itself. Extra replicates at the centre are desirable as they provide an independent estimate of experimental error.

The basic design of this sort of test requires $2^k + 2k + 1$ tests (i.e. fifteen tests for a three factor investigation). Any appropriate practical value could be used for the distance of the axial points from the centre, α, but it is usually chosen to achieve a desirable property of the design, rotatability, a concept introduced by Box and Hunter (1957). This rotatability improves the quality of the model prediction by ensuring that the variance of the prediction of the model is constant at all points equidistant from the design centre. The value of α for rotatability is given by:

$$\alpha_{rot} = 2^{k/4} \qquad \text{- 3.5}$$

The whole experiment is then called a central composite rotatable design.

The choice of the number of centre point runs (CPs) is based on other desirable features of the design, such as better estimates of experimental error and the value of the constant a_0. The number of CPs controls the distribution of the precision of the predicted response in the vicinity of the design. It was shown by Box and Hunter (1957) that the number of CPs should be chosen so as to satisfy the following:

$$\lambda = \frac{N_{TOT}}{n_c + 4\left(1 + n_c^{1/2}\right)} \qquad \text{- 3.6}$$

where $N_{TOT} = n_c + n_a + n_0$ = total number of experiments

n_c = number of factorial runs

n_a = number of axial runs

n_0 = number of centre point runs

λ = parameter

λ is usually chosen to give equal precision of the predicted response within a circle of radius 1, in which case λ<1, and takes the particular values shown in Table 3.2.

Table 3.2 Values of λ for various numbers of factors.

No. of factors, k	2	3	4	5	6
λ	0.7844	0.8385	0.8704	0.8918	0.9070

When λ = 1, the design is said to be orthogonal. This means that variation in the regression coefficients can be minimised, as the model terms are estimated independently of one another without confusion between them. An orthogonal CCRD requires more centre point runs.

The benefit of this type of test programme is that not only does it significantly reduce the number of tests that need to be conducted, but, as mentioned previously, it also allows for the effect of the studied variables to be independently assessed.

3.4.1 Two Factor CCRD

Although this testwork used three factor CCRD, it is worth mentioning the two factor CCRD as an introduction to the technique used for this study. The principle of the CCRD is best appreciated in two or three dimensions. The design for k = 2 factors is easily drawn in 2-D (cf. Figure 3.5).

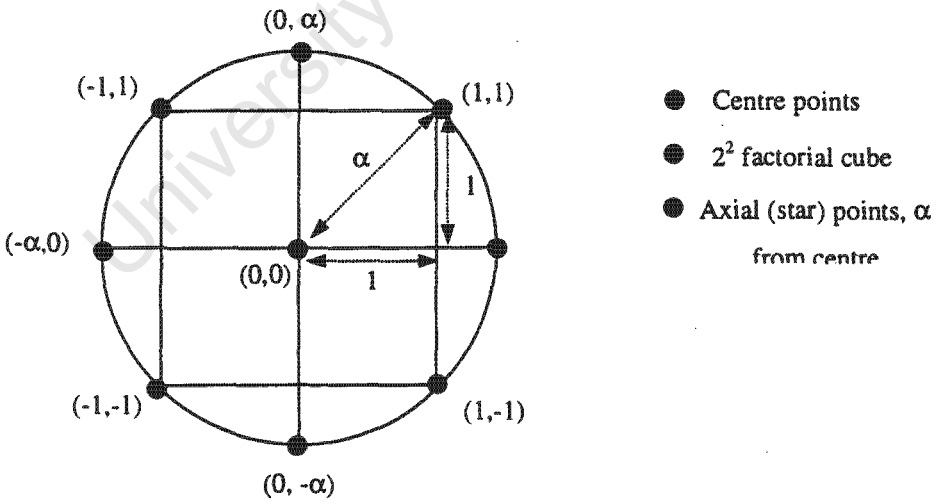

Figure 3.5 Two factor CCRD design (after Napier-Munn (2000b)).

This design comprises a standard 2^k factorial, plus 2k = 4 axial points equally spaced on a circle of radius α circumscribing the factorial points, plus one or more centre point tests. For rotatability, $\alpha^2 = 1^2 + 1^2$ or $\alpha = \sqrt{2} = 1.414$, which is the value of $2^{k/4}$. The codes indicated in the figure (0, 1 and α) define standardised coordinates for the position of each test in the chosen experimental space, with (0,0) marking the centre of the design. Therefore, the three components of the design are:

1. The four points on the square, which constitute a normal 2^2 factorial.
2. The four axial ("star") points.
3. Five centre points are required to satisfy the centre point run equation.

This makes a total of 13 tests, which is the same as a 3^2 factorial with four centre points, but this design has a number of mathematical advantages stated earlier, which make it superior. Data are collected at all points, and the model is fitted by multiple linear regression analysis in the usual way.

3.4.2 Three Factor CCRD

The same principle can be extended to any number of factors. The diagram overleaf shows the CCRD design and coordinates for k = 3 factors, which can be visualised in 3-D (cf. Figure 3.6), with coded factor levels for each test shown. Actual experimental factor levels are chosen from practical maximum and minimum values of interest. Other levels are then calculated. In the example given (cf. Table 3.3), the investigator assessed the response over a large range of values from 10 to 100 units ($\alpha = 2^{k/4} = 1.682$ for k = 3).

The polynomial model for this design is given in Equation 3.7.

$$y = a_0 + a_1x_1 + a_2x_2 + a_3x_3 + a_{11}x_1^2 + a_{22}x_2^2 + a_{33}x_3^2 + a_{12}x_1x_2 + a_{13}x_1x_3 + a_{23}x_2x_3 + \varepsilon \quad \text{- 3.7}$$

The high order interaction term $x_1x_2x_3$ is usually omitted from the model. In general there are (k+1)(k+2)/2 terms to be fitted for k factors. Box and Hunter (1957) summarised the number of tests and the appropriate values of α for various values of k (cf. Table 3.4).

Factor Levels			
	x_1	x_2	x_3
2^3 factorial	-1	-1	-1
	1	-1	-1
	-1	1	-1
	1	1	-1
	-1	-1	1
	1	-1	1
	-1	1	1
	1	1	1
Axial points	-α	0	0
	α	0	0
	0	-α	0
	0	α	0
	0	0	-α
	0	0	α
6 Centre-points	0	0	0
	---	---	---

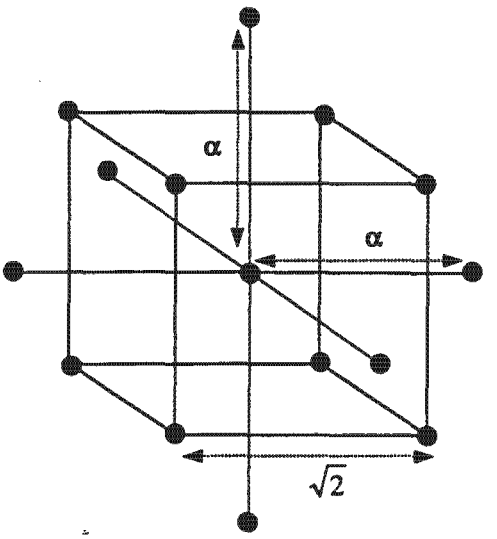

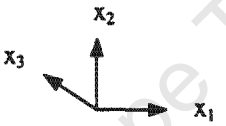

- Centre points
- 2^3 factorial cube
- Axial (star) points, α from centre

Figure 3.6 Three factor CCRD design (After Napier-Munn (2000b)).

Table 3.3 Calculations of experimental factor levels.

Code	Actual Value of Factor	Example
- α	x_{min}	10.00
- 1	$\frac{(x_{max} + x_{min})}{2} - \frac{(x_{max} - x_{min})}{2\alpha}$	28.25
0	$\frac{(x_{max} + x_{min})}{2}$	55.00
+ 1	$\frac{(x_{max} + x_{min})}{2} + \frac{(x_{max} - x_{min})}{2\alpha}$	81.75
+ α	x_{max}	100.00

Table 3.4 Number of tests for various numbers of factors.

No. of factors, k	2	3	4	5	5 (1/2 rep.)*	6	6 (1/2 rep.)*
Factorial points	4	8	16	32	16	64	32
Axial points	4	6	8	10	10	12	12
Centre points	5	6	7	10	6	15	9
Total tests	13	20	31	52	32	91	53
α_{rot}	1.414	1.682	2.000	2.378	2.000	2.828	2.378
CPs for orthogonality	8	9	12	17	10	24	15

* Half replicates

3.5 Experimental Program

The FCTR test program was a three-factor CCRD design, where the effects of both impeller speed and air flowrate on the recovery of platinum and the concentrate grade were measured. The CCRD was a blocked design to remove the effect of an unwanted variable, namely time.

The test program for the FCTR was made up of only fourteen tests in a full set. Of these fourteen sets of conditions, six were replicates of the statistical midpoint of the experimental conditions, in terms of both impeller speed and air flowrate. One test was conducted at each of the upper and lower limits of impeller speeds, using the midpoint value of air flowrate for both. Two further tests were conducted at the midpoint value for impeller speed, using upper and lower limit values of air flowrate. Other tests were conducted at values of both air flowrate and impeller speed at equal values each side of the midpoint. For example, in the rougher feed work, the midpoint was 65% impeller speed. Tests were conducted at 72.1% and at 57.9%.

The upper and lower values of both impeller speed and air flowrate were determined by experimental trial and error. As there were difficulties in the rougher feed testwork with maintaining solids suspension in the FCTR cells, a lower level of impeller speed and an upper level of air flowrate was determined at the point where all solids were just suspended. In addition to the solids suspension problems, there were also problems encountered at higher power inputs with motor trips when the motor load current got too high due to the density of the solids. As a result of this, the upper impeller speed and lower air flowrate were chosen at a point where the motor load current was high enough to provide as broad a range of power input values as possible, but was not so high that the testwork would be interrupted by motor overload trips. Therefore, the rougher feed range of power inputs was chosen for operational reasons. The cleaner tails upper and lower power

set-point values were not as influenced by operational factors (due to the ease of suspending solids) but were chosen to give a similar range of power input values as those used in the rougher feed section of work. This allowed the two sections of work to be more easily compared.

In this test campaign, two slurry streams were tested: the rougher feed stream and the primary cleaner tails stream. For each of these streams, the CCRD test programme was performed. Each set of fourteen tests was repeated once, making a total of 28 tests for each of the two streams (cf. Tables 3.5 and 3.6). The letter codes for each set of test conditions were the means to identify the assay results of the samples generated during each test, and these codes will be used in later chapters to identify the individual tests.

Table 3.5 Rougher feed test conditions.

Test Name	Air Rate (l/min)	Impeller Speed (%)	Test Name	Air Rate (l/min)	Impeller Speed (%)
A	99	57.9	O	99	57.9
B	120	65.0	P	120	65.0
C	141	57.9	Q	141	57.9
D	120	65.0	R	120	65.0
E	141	72.1	S	141	72.1
F	99	72.1	T	99	72.1
G	120	65.0	U	120	65.0
H	150	65.0	V	150	65.0
I	120	65.0	W	120	65.0
J	120	65.0	X	120	65.0
K	120	65.0	Y	120	65.0
L	90	65.0	Z	90	65.0
M	120	75.0	AA	120	75.0
N	120	55.0	AB	120	55.0

Table 3.6 Cleaner tail test conditions.

TEST NAME	Air Rate (l/min)	Impeller Speed (%)	Test Name	Air Rate (l/min)	Impeller Speed (%)
AC	149	52.9	AQ	149	52.9
AD	170	60.0	AR	170	60.0
AE	191	52.9	AS	191	52.9
AF	170	60.0	AT	170	60.0
AG	191	67.1	AU	191	67.1
AH	149	67.1	AV	149	67.1
AI	170	60.0	AW	170	60.0
AJ	200	60.0	AX	200	60.0
AK	170	60.0	AY	170	60.0
AL	170	60.0	AZ	170	60.0
AM	170	60.0	BA	170	60.0
AN	140	60.0	BB	140	60.0
AO	170	70.0	BC	170	70.0
AP	170	50.0	BD	170	50.0

3.6 Sampling Campaign

This section gives information on the FCTR campaign itself: the way the sampling was performed for each stream, and the FCTR circuit used during the campaign.

3.6.1 FCTR Circuit

The FCTR circuit was modified for this testwork. Only four of the rougher cells were used, and the cleaner circuit not being used at all (cf. Figure 3.7). Studying hydrodynamic effects in one rougher cell would have provided suitable results for this study. However, the FCTR provided an opportunity to study four cells in a bank and, consequently, to improve the scope and accuracy of results. Using all six cells in the rougher bank was unnecessary, as the last two cells in the bank would, in effect, be scavenging cells, and would not provide any extra information.

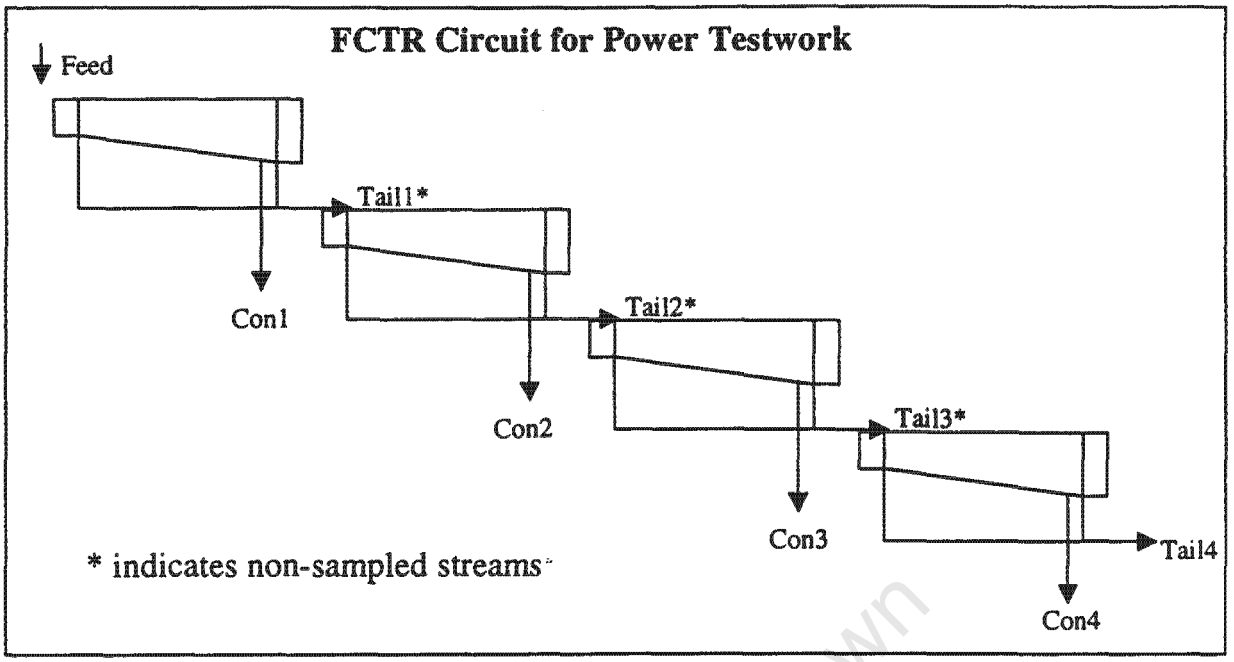

Figure 3.7 Modified FCTR circuit for power testwork.

3.6.2 FCTR Feed Slurry

The feed slurry to the FCTR was from streams diverted from inside the concentrator. Rougher feed was initially to be sampled from one of two conditioning tanks at the head of the plant's rougher bank. However, on inspection it was discovered that the impeller blades inside the conditioning tank were so badly worn that the sampling point would deliver slurry with a density far above that which could be successfully pumped from the plant to the FCTR. There was no spare impeller in stock, and so an alternative sampling point was sought. As an alternative, a hose was inserted into the first rougher cell as close to the slurry inlet as possible. The hose was attached to a positive displacement pump, and this set-up was used to feed rougher feed slurry to the FCTR. A piston was attached to the head tank and when the level rose in the tank, level probes would indicate high level. The piston would change position and slurry would run into a drum next to the head tank. Slurry in this drum was pumped back into the plant.

For the primary cleaner tails, a pressure pipe sampler was installed on the primary cleaner tail line inside the concentrator. The stream diverted by the pressure pipe sampler was fed into an unused sump on the ground floor of the concentrator. That line was connected to a piston that was controlled by level probes inside the FCTR head tank. As the level in the head tank dropped, the piston would move to allow slurry to be pumped to the FCTR. At other times slurry would run continuously into the sump to be returned to the flotation circuit.

3.6.3 Sampling

3.6.3.1 Set-up

Conditions for each test were set (impeller speed changed on the Mintek Float Star control system, air flowrate changed manually on the rotameter attached to each cell) and then sampling began forty-five minutes to an hour later, depending on the stability of the circuit. If no change had been made to the impeller speed and air flow rate (such as where three mid-point runs were made in a row, for example tests I, J and K in the rougher feed testwork) then the minimum time between finishing one test and starting the next was 20 minutes. This corresponded to the same time as between samples during a test, but was naturally dependent on any operational repairs that needed to be made, or any logistical considerations, such as ensuring that the buckets of sample from the previous test were correctly labelled and ready for sample preparation. Where a change had been made to the hydrodynamic variables, the time taken for the circuit to become stable was more variable, and was determined by the pulp level trends on the Float Star system. When hydrodynamic variables were changed, the levels in each of the cells in the bank would fluctuate for a time as the tails dart valves adjusted to the new conditions. This manifested itself as a wave-like trend in the pulp level graph on the Float Star package. Generally, it would take about half an hour for the wave-like trend to become steady, and then the circuit was allowed to run at this stable condition for twenty minutes before sampling started, hence the forty-five minute to one hour between tests.

3.6.3.2 Sample Collection

Sampling consisted of three cuts of each sample stream. Each cut was twenty minutes apart and the duration of the cut was timed in all instances to determine the mass flow of the stream. Samples were collected in pre-weighed buckets, which were weighed again to determine wet mass of sample. This procedure was identical for both primary float feed and primary cleaner tail work. In the rougher feed work, however, the high density of the solids meant that there was a significant build-up of solids in the concentrate launders between samples. Launder water was not able to prevent this build-up, and, as a result, each cell launder was cleaned by hand prior to sampling.

Sampling of the streams was a two-person process. While one person could have been capable of doing the sampling alone, it would not be as efficient a process. Indeed, the disturbance to the

system in the event of one person sampling would be such that it would take extra time for the circuit to restabilise after each sampling run.

The first sample taken each time was tails. This sample was taken first as diverting this stream did not affect the rest of the FCTR circuit. Initially, tails slurry from the fourth cell of the FCTR was run through the last two, unused cells into the tails sump. In this case, the tails sample was taken by using the three-way valve on the tails line between cells four and five of the FCTR. When the three-way valve was turned, slurry would be diverted away from flowing through the next cell, and would instead pass down a plastic hose to the ground next to the FCTR. One operator would turn the three-way valve while the second would take a timed sample. Once sampling was completed, the three-way valve would be turned back to allow the slurry to again flow through the two lower cells. Later, however, the circuit was changed so that the tails from cell four would flow directly to the tails sump. This was done by attaching a length of plastic pipe to the tails line of the fourth cell and running that pipe directly to the tails sump. Once this system was in place sampling this stream was a simple matter of taking the pipe out of the sump and into a bucket placed next to the sump. Concentrate lines were also run from the concentrate pumps to the tails sump. Each concentrate had its own pump head, and therefore its own line, ensuring that concentrates were never mixed. To sample these streams, the plastic hose corresponding to each cell concentrate was taken out of the tails sump and placed into a bucket for sampling.

Sampling the feed was the final step in the sampling process. This was done last as sampling the feed stream diverted slurry away from the FCTR. This, therefore, affected cell pulp levels, and, as a result, concentrate flow rates. Sampling the feed required one operator to turn the three-way valve on the line where feed from the FCTR head tank was pumped into the first cell. The three-way valve was located next to the first rougher cell, at the top of the stairs on the FCTR. A second operator would stand on the ground below the FCTR, where a plastic hose connected to the three-way valve was run down to ground level. The second operator would take a timed sample of the stream and signal the first operator to turn the three-way valve back to allow slurry to flow into the FCTR again.

If this process had been performed by only one operator, the time taken between turning the three-way valve and taking the sample, and also completing the sample and turning the three-way valve back would have been much increased. In turn, it would have taken more time for the circuit to restabilise after sampling. As it was, with two operators, it could take up to ten minutes for the circuit to restabilise. The reason for this is that when feed was cut off, there was a certain amount of dead time between the flow of slurry being cut off and the Float Star system reacting to the resulting drop in the pulp level of the first cell. Similarly, once the flow of slurry was restarted, it

would take some time for the system to react to the sudden increase in pulp level. Especially when the cells were being run at higher impeller speeds, the pulp level would often cycle around the setpoint due to the excessive vibration in the rig.

3.6.3.3 Sample Preparation

After the conclusion of each test, the sample buckets were sealed to prevent sample spillage and then the samples were prepared for assay by the Lonmin laboratory staff working on the FCTR project. The first stage in this involved weighing each of the full sample buckets to determine a wet sample weight (the weight of the bucket and lid was already known). Once this had been done, samples were filtered in a filter press, and the wet filter cake was placed under drying lamps to dry.

Feed, concentrate and tails samples were filtered in separate filter presses to avoid sample contamination, and concentrate samples were dried under red heat lamps (as opposed to white heat lamps) to prevent the sample from burning. Once the filter cake was dry, the sample was weighed again to get a dry sample mass. This could be used in conjunction with the wet sample mass to determine a percent solids value. The dry sample was rolled to break up lumps in the sample, before being split in a riffle, bagged, labelled and sent to the assay laboratory for analysis.

3.7 Data Reconciliation

Once samples were taken and prepared for assay they were sent to Lonmin's assay laboratory for analysis by fire assay. Assays were determined for platinum and chrome, and a specific gravity was also determined. These assays, along with the experimental and recalculated mass flows were inputted into JKSimMet for mass balancing purposes. Mass balanced data was then used for further analysis.

Two major problems were discovered in the analysis of this data. The first is that, in both sections of work, one of the midpoint repeat runs was run at an incorrect setting of air flowrate. To counter this, a synthesised replicate was created using a random value of the same mean and standard deviation of the other replicates. This synthesised replicate replaced the incorrect run in all cases. The second problem was that regressions for platinum recovery were not good. Examination of the data suggested that the problem lay in the fact that feed grade varied sufficiently during the testwork to influence the results (Napier-Munn, 2000a).

The solution to this was to run regressions using feed grade as a factor. As feed grade was not included in the experimental design, it could not be included in the complete CCRD analysis. However, multiple regressions were performed to analyse the data with feed grade, and its associated terms included, by using stepwise regression to include only significant terms.

Along with the CCRD analysis of the mass balanced data, it was also necessary to determine the quality of the mass balancing. This was done by plotting the mass balanced data obtained from JKSimMet against the experimentally obtained data to determine the degree to which the data had been altered during the mass balancing process.

3.7.1 Mass Balancing

Parity charts for the rougher feed and cleaner tails mass flows were produced for all tests (cf. Figures 3.8 and 3.9).

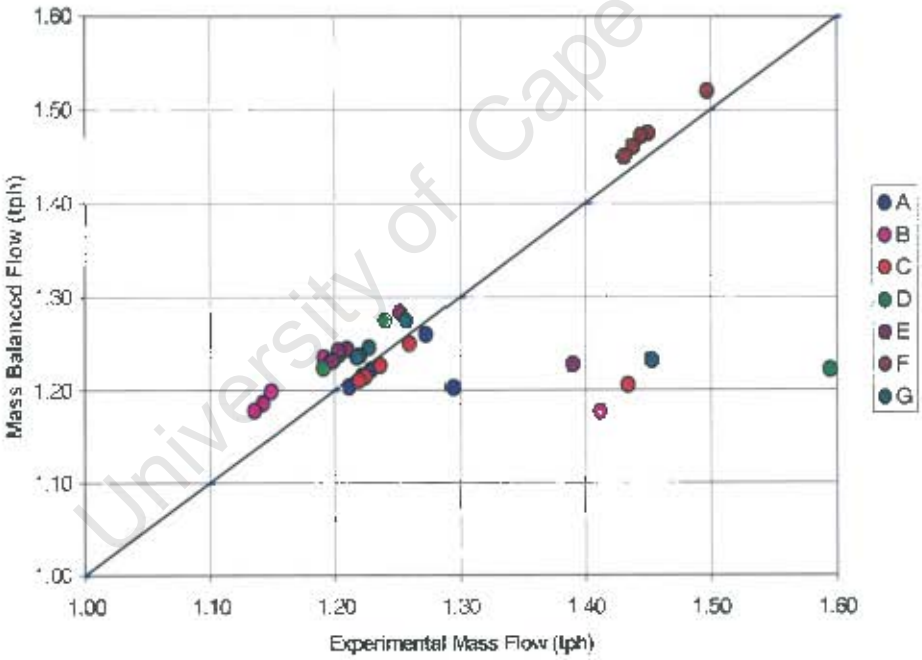

Figure 3.8 Rougher feed mass flow parity chart: tests A-G

As mentioned previously, there was an 8.8% error between the experimental and mass balanced rougher feed mass flows. As can be seen from Figure 3.8, the majority of this can be attributed to discrepancies between the experimental and mass balanced tails mass flows (the outlying points to

the right of the parity line). In some cases the tails mass flows were reported as being higher than the feed mass flow for the same test. The reason for this was clear: the final tails dart valve operation was dependent on the slurry level in Cell 4, and Cell 4 tended to cycle slightly above its level set point. As a result, changes in dart valve action would result in small surges of slurry into the final tails sample. However, it was possible to overcome this problem, as the feed and concentrate mass flows were considered to be much more reliable. Feed mass flow samples were taken directly from the feed pump, and so were not affected by any cell operation problems, and could therefore be considered to be very accurate. Concentrate sample mass flows were, apart from Cell 4, not affected by cycling of pulp levels, so could also be considered to be good quality data. Consequently, when the raw data was used in JKSimMet, a higher level of error was attributed to the tails mass flow values, enabling the program to produce a good quality mass balance.

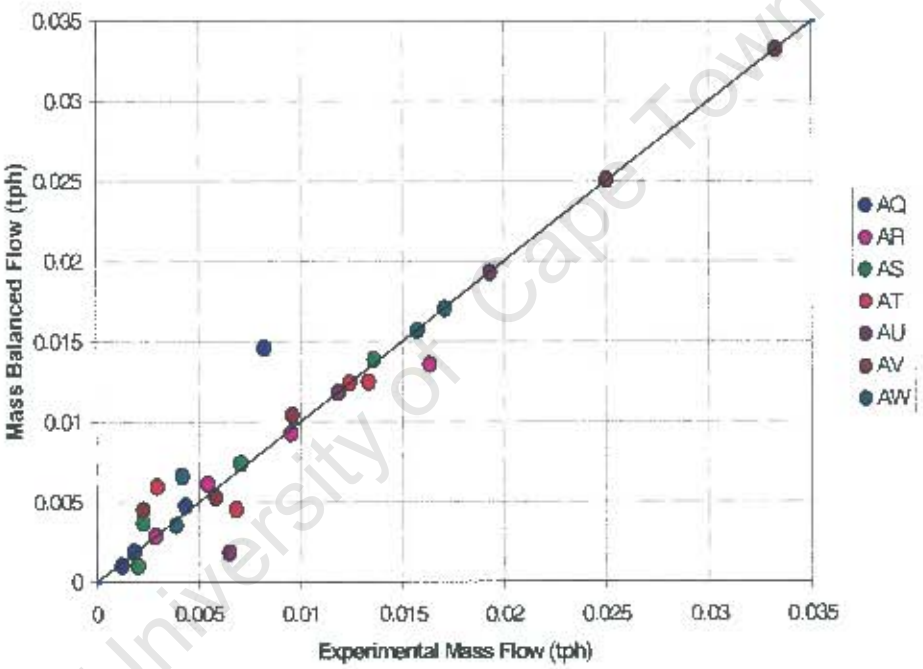

Figure 3.9 Cleaner tail mass flow parity chart: tests AQ-AW.

Figure 3.9 shows that the quality of the cleaner tail mass flow data was an improvement over that for the rougher feed, but that overall there was still a 5.2% error between experimental and mass balanced mass flows. Again, much of this was attributed to large tails mass flows caused by cycling of the Cell 4 pulp level. However, the effect was much less pronounced in this section of the work, as the finer feed material made pulp level control significantly better in the cleaner tails section of the work than in the rougher feed section. Again, when the raw data was mass balanced using

JKSimMet, a higher error value was attributed to the tails mass flow, allowing the program to produce good mass balanced data.

Parity charts for the rougher feed and cleaner tails sample grades were produced for all tests (cf. Figures 3.10 and 3.11).

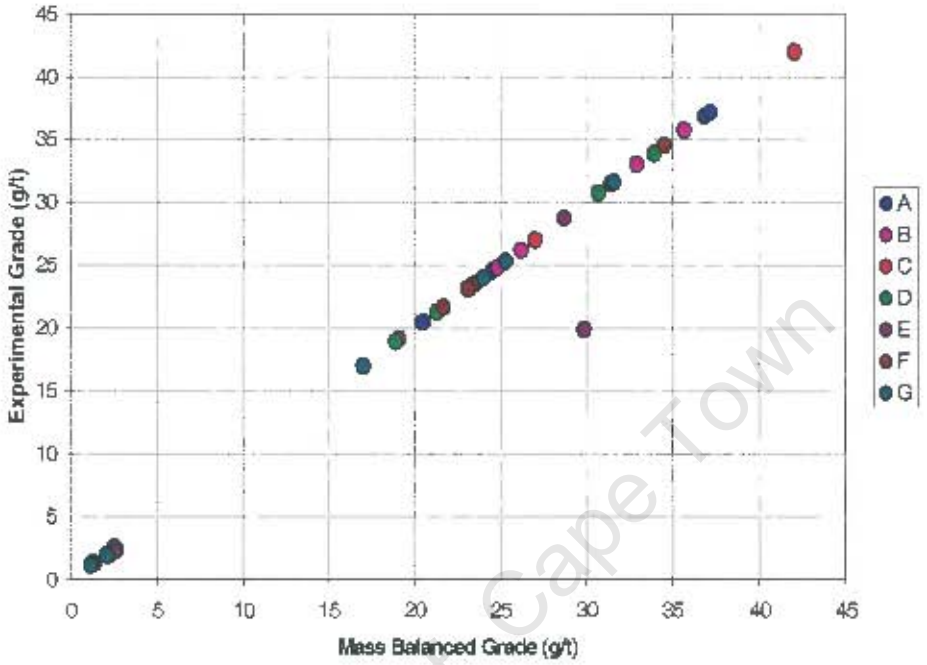

Figure 3.10 Rougher feed PGM grade parity chart: tests A-G.

This figure clearly shows that the quality of the assay data obtained during the sampling campaign was very good. Most of the points sit along the parity line, meaning that the mass balancing had little effect on the experimental assay results. An average error of 3.1% was obtained for the rougher feed section of the work, and most of this error was attributed to the feed and tails grades. As the tails mass flows needed to be altered by the mass balancing to produce reasonable quality data, the PGM grade of the streams also had to be altered to maintain the mass balance. However, as can be seen from the figure, the adjustments made during the mass balancing were only minor, and most data sits on or near the parity line.

A similar trend was discovered for the cleaner tails sample grade mass balancing. As less adjustment of the data was required during mass balancing, due to improved process control during the sampling campaign, there was little adjustment to the sample grades. Most assays fell on or very close to the parity line, and the average error across all tests was only 2.2%, indicating that the quality of this data was very good.

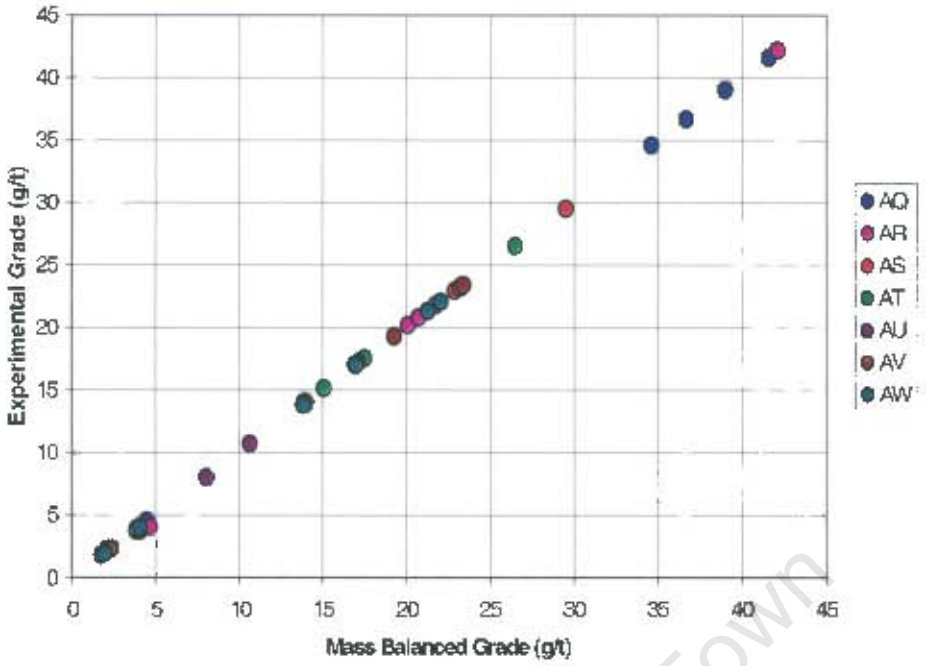

Figure 3.11 Cleaner tail PGM grade parity chart: tests AQ-AW.

3.7.2 CCRD Analysis

A statistical evaluation of the mass balanced data was also obtained during the CCRD analysis. The analysis showed that the data obtained from the rougher feed section of the work was inferior to that for the cleaner tails, as barely half of the data variation could be accounted for by the regression (R^2 = 44-54%). There was also some evidence of bias in the rougher feed model, suggesting that there may have been a term missing in the model. The cleaner tails data is, however, much better, with good fits (R^2 = 75-87%) and no evidence of bias.

The degree of bias is reflected in the way the points cluster around the line for both the observed versus predicted recovery graphs and the observed versus predicted concentrate grade graphs. In the rougher feed graphs, the points are spread, whereas for cleaner tails the points are clustered more uniformly around the line (cf. Figure 3.12).

ROUGHER FEED

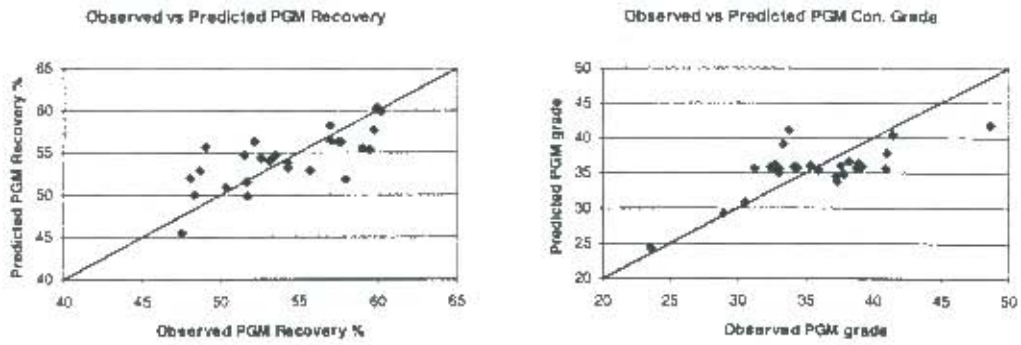

CLEANER TAILS

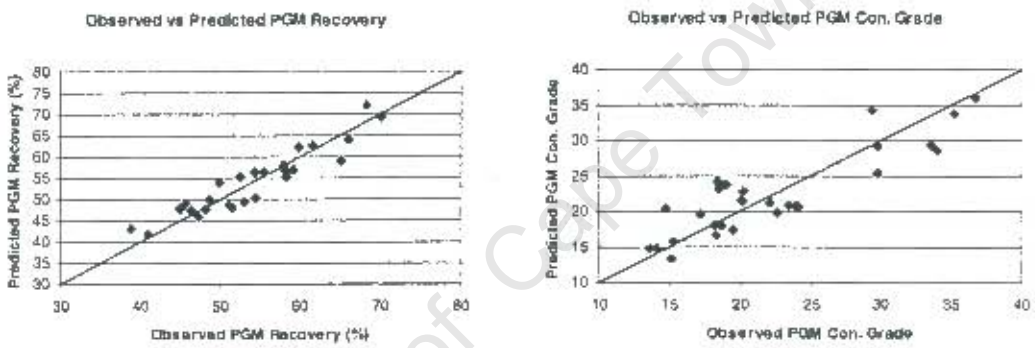

Figure 3.12 Observed versus predicted PGM grades and recoveries.

It is unlikely that errors in the rougher feed results were experimental in nature as the basic experimental error (the variance left after model effects have been removed) is the same for both the rougher feed and the cleaner tails. It is more likely that there was an additional variable which was not monitored or controlled or that an alternative model term was missing. It is also possible that the dependencies were simply not sufficiently strong for the rougher feed. Residual standard errors are given in Table 3.7.

Table 3.7 Residual standard errors.

Residual Standard Errors		
Variable	**Rougher Feed**	**Cleaner Tails**
PGM Recovery	3.14	2.91
PGM Concentrate Grade	3.55	3.42

Chapter 4 Results and Discussion

The results presented in this chapter are derived from and are applicable to the experimental program outlined in Chapter 3. Hydrodynamic and gas dispersion results are presented in Sections 4.1 and 4.2 respectively. The various dimensionless groups and numbers outlined in Chapter 1 are incorporated into the analysis of hydrodynamic and gas dispersion results where appropriate (c.f. Tables 1.4 and 1.5). Flotation results are presented in Section 4.2 with rougher and cleaner results being discussed in Sections 4.2.1 and 4.2.2 respectively. Mass flowrate, grade and recovery data for all the flotation tests are presented in Appendix A. In this chapter, emphasis is placed on the interpretation of the results when compared to the flotation literature, particularly the results of testwork performed on industrial flotation cells.

4.1 Hydrodynamic Results

The power numbers observed during this study were between 4.6 and 7.8 for the rougher feed and 3.4 and 6.2 for the cleaner tails sections of the testwork. These values, particularly in the rougher feed section, are quite high when compared to the flotation literature. Deglon *et al* (2000) observed a range of 3.4 to 6.6, although the majority of power numbers in this survey lay around 5.0. Mavros (1992) listed a typical range of power numbers in industrial flotation cells as being between 0.5 and 5.0. Power numbers greater than 5.0 are considered to be unusually high for flotation cells (Deglon *et al*, 2000). The power draw, and therefore the power number, is strongly influenced by the air flowrate. The power numbers were found to decrease steeply with increasing air flowrate, which is consistent with the literature.

The Froude numbers observed during this study ranged between 0.54 and 0.80 for the rougher feed and 0.43 and 0.71 for the cleaner tails sections of the testwork. Mavros (1992) suggested that Froude numbers can vary between 0.1 and 5.0, although Deglon *et al* (2000) observed typical Froude numbers of between 0.5 and 1.0. These results were largely independent of cell type or size. It is clear that the Froude numbers observed in this study are identical in range to those observed in the flotation literature. The Froude number is the ratio between the centrifugal forces due to the pumping action of the impeller and the gravitational forces due to the hydrostatic head in the flotation cell (c.f. Section 1.3.2). Therefore, similar Froude numbers in different cells indicate that hydrodynamic conditions in the cells are largely equivalent.

4.1.1 Power Draw

The power input per cell volume (P/V), generally termed the power intensity, is considered to be an important parameter due to its influence on metallurgical performance and cell operating costs. High power intensities are thought to improve flotation performance through improved aeration and particle-bubble contacting (Schubert and Bischofberger, 1978). According to a number of authors (Fallenius, 1987; Arbiter, 1999) the usual range of power intensities for industrial cells is between 1 and 2 kW/m^3. Figure 4.1 is a graph of power intensity versus impeller speed for the rougher feed section of the testwork. This graph shows the relationship between power intensity and impeller speed at various constant air flowrates.

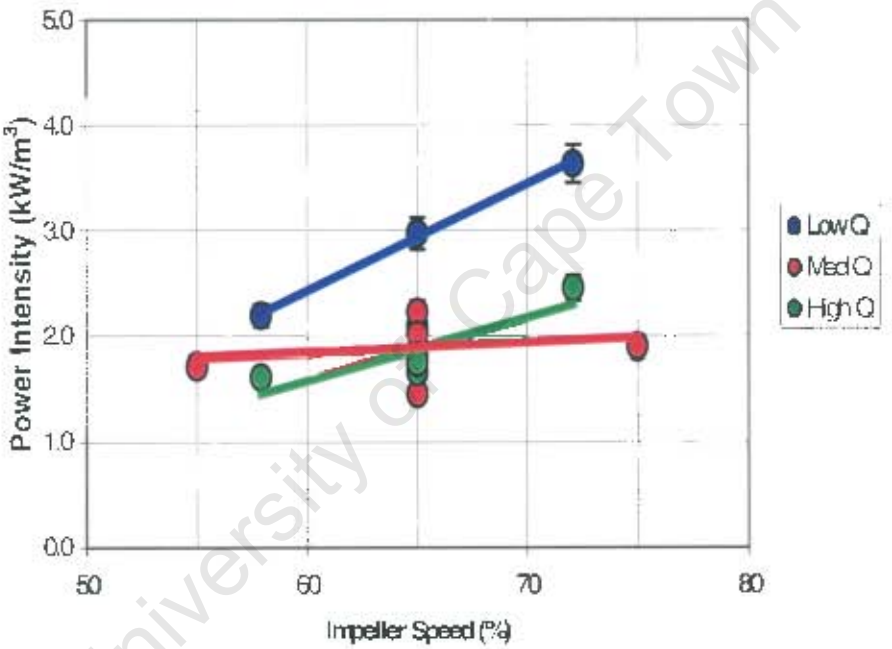

Figure 4.1 Power intensity versus impeller speed – rougher feed.

Figure 4.1 shows that there is an increase in the power intensity with increasing impeller speed across all air flowrates used in this study. Both Read (1933) and Arbiter and Steininger (1962) observed this relationship. This effect was most noticeable at low air flowrates, where the power intensity almost doubled across the range of impeller speeds used. The power intensities range between 1 and 4 kW/m^3 which is slightly above the power intensities found in typical industrial cells. However, these results are not unreasonable when compared to those found by Deglon *et al* (2000). This study found that cells used in South African platinum concentrators have power

intensities of up to 9.5 kW/m^3, although most results were between 1 and 3 kW/m^3. In light of this, the power intensities encountered during this study are within a reasonable range for industrial cells on platinum concentrators. While it would have been preferable to obtain power intensities of up to 10 kW/m^3 in this study, this was not possible in the FCTR as impeller motors began to overload above 4 kW/m^3.

Figure 4.2 is a graph of power intensity versus air flowrate for the rougher feed section of the testwork. This graph shows the relationship between power intensity and air flowrate for a number of constant impeller speeds.

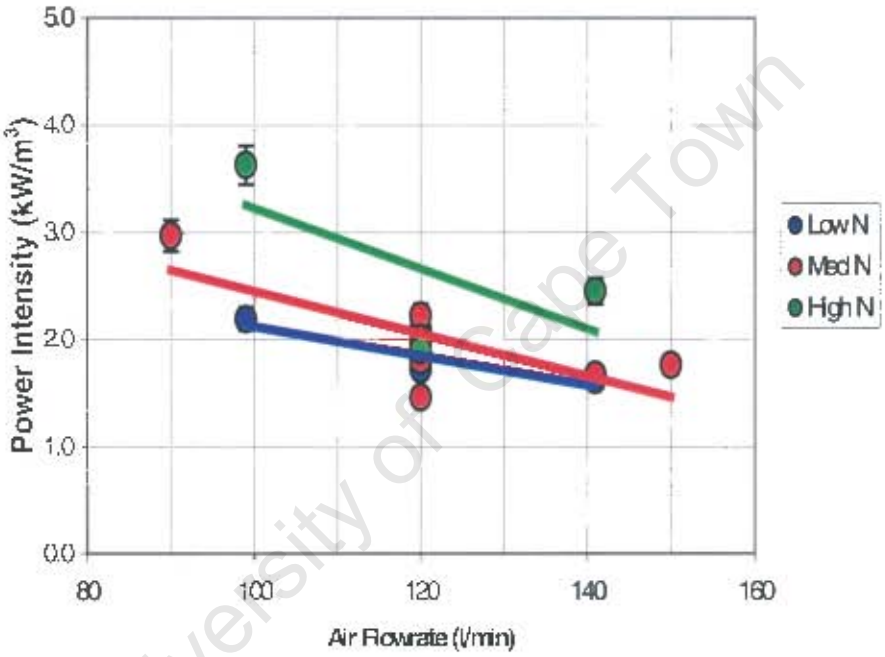

Figure 4.2 Power intensity versus air flowrate – rougher feed.

Figure 4.2 shows clearly that the power intensity decreases with increasing air flowrate across all impeller speeds used in this study. The effect is most noticeable in the high impeller speed tests where the power intensity almost halves across the range of air flowrates used. This trend is in keeping with the literature (Read, 1933; Arbiter and Steininger, 1962) and is due to decreases in both impeller pumping rates and slurry density with increasing air flowrate.

4.1.2 Mixing

The mixing characteristics of the FCTR were determined during the commissioning phase at Karee concentrator (Rahal, 2000). The results of residence time distribution tests performed during commissioning found that the FCTR behaved as a series of well-mixed tanks (Constant Stirred Tank Reactors). It is expected that the FCTR cells should be well mixed. Power intensities in the FCTR were between 1 and 4 kW/m^3 which is higher than the usual range of power intensities for industrial cells (1 to 2 kW/m^3). The power intensity is an indicator of the level of turbulence in the flotation cell and high power intensities suggest strongly turbulent conditions i.e. good micromixing. The range of impeller tip speeds observed during this study was 5.1 to 7.2 m/s for the rougher feed and 4.7 to 6.8 m/s for the cleaner tails. These values are in keeping with the typical range of 5.0 to 7.0 m/s in the literature (Fallenius, 1987; Arbiter, 1999; Deglon *et al*, 2000). The impeller tip speed is an indicator of the velocity at which pulp leaves the impeller in the radial fluid jets which cause bulk flow in the flotation cell i.e. good macromixing (Degner, 1979).

The range of (estimated) tank-turnover times observed in this study was between 13 and 19 s for the rougher feed and 11 and 15 s for the cleaner tails. As tests for the tank-turnover time were not performed, the tank-turnover times were approximated using V/ND^3 (c.f. Table 1.5). Here, the velocity with which fluid leaves the impeller is considered to be proportional to the impeller tip speed and the area available for fluid to leave the impeller is considered to be proportional to the square of the impeller diameter. These values are towards the lower end of the range of between 7 and 29 s determined by Deglon *et al* (2000). The tank-turnover time is an indicator of the efficiency of mixing within a flotation cell. Low tank turnover times suggest that mixing is good as the entire volume of pulp within the flotation cell is being circulated (turned-over) rapidly.

4.1.3 Solids Suspension

Solids suspension was not measured in the FCTR as it was not possible to use an in-pulp sampler for taking samples due to froth crowders on the cells. Consequently, size-by-size concentration profiles could not be determined. However, solids were considered to be well suspended in the FCTR cells due to the good residence time distributions, high power intensities, low tank turnover times and correct impeller tip speeds i.e. indicators of good macro and micromixing. In addition, the range of impeller speeds used in the study were found to be above the critical impeller speed for solids suspension (cf. Section 1.4.3). Observations made during the FCTR campaign also indicated that no sanding was taking place in the cells at any of the experimental conditions used. This was

particularly applicable to the cleaner tails section of the testwork, where a dilute stream of very fine solids was used. Arbiter *et al* (1969) noted that high power intensities result in less sedimentation/sanding in flotation cells.

4.1.4 Gas Dispersion

The air flow numbers observed during this study were between 0.11 and 0.19 for the rougher feed and 0.14 and 0.20 for the cleaner tails. These are consistent with the range of air flow numbers reported by both Mavros (1992) and Deglon *et al* (2000). The results from this study, therefore, lie exactly within this range. The air flow number is strongly affected by both the impeller speed and the air flowrate. In general, low air flow numbers favour grade and high air flow numbers favour recovery (Arbiter and Harris, 1969), although both grade and recovery may be optimised at lower values of air flow number. Lower air flow numbers are an indication of greater turbulence in the cell, leading to improved mixing, solids suspension and gas dispersion.

The air flowrate per cell volume observed during this study was between 0.60 and 1.00 min^{-1} for the rougher feed and between 0.93 and 1.33 min^{-1} for the cleaner tails tests. Both Deglon *et al* (2000) and Schubert and Bischofberger (1978) reported wide ranges of air flowrate per cell volume. The former observed a range of 0.04 to 1.06 min^{-1}. While the rougher feed tests fall within this range, the cleaner tails tests are generally just outside the upper end of this range. The air flow per cell volume is a measure of the aeration ability of a flotation cell, and is the gas dispersion equivalent of the power intensity. In the cleaner tails section of the testwork, the higher air flowrate per cell volume values indicate superior aeration to the rougher feed tests. This was observed to be mostly the case, except at tests conducted at very high air flowrates, where the cells appeared to be operating beyond their limits, therefore leading to a reduction in the ability of the cell to disperse gas.

The air flow velocities observed during this study were between 0.11 and 0.19 m/s for the rougher feed and between 0.18 and 0.25 m/s for the cleaner tails. These ranges lie within those identified by Deglon *et al* (2000) and Arbiter *et al* (1976), although they lie at the lower end of the range of between 0.05 and 0.50 m/s observed by Deglon *et al* (2000). The air flow velocity defines the ability of the impeller to accommodate a given air flowrate. This is an important factor for the gas dispersion in the cell. Higher air flow velocities indicate that the gas dispersion is likely to be poorer due to the greater volume of gas which has to be dispersed by the impeller. The fact that the air flow velocities observed in this study are towards the lower end of those observed by other researchers indicates that the FCTR should have been able to disperse gas effectively.

Bubble size, superficial gas velocity and bubble surface area flux results are presented in Sections 4.1.4.1 to 4.1.4.3. Key trends for each of these parameters are illustrated using the results from the cleaner tails tests as a broader range of gas dispersion parameters was observed during this section of the testwork. A summary of the bubble size, superficial gas velocity and bubble surface area flux results measured in both the rougher feed and cleaner tails is given in Table 4.1. Gas hold-up is a common parameter used to describe gas dispersion in flotation cells but was not measured in this study for the same reasons as for solids suspension i.e. a sample of aerated pulp could not be taken out of the FCTR cells.

Table 4.1 FCTR bubble size, superficial gas velocity and bubble surface area flux results.

Parameter	Rougher Feed	Cleaner Tails
Bubble size (d_{32}, mm)	1.71 – 1.87	1.51 – 1.71
Superficial gas velocity (Jg, cm/s)	0.92 – 1.14	0.95 – 1.15
Bubble surface area flux (Sb, s^{-1})	29.8 – 39.1	36.4 – 42.8

Despite the fact that broad ranges of both impeller speeds and air flowrates were used in this study, the range of the parameters listed in Table 4.1 is relatively narrow. However, the ranges observed in the FCTR testwork are generally within those listed by Deglon *et al* (2000) as being typical for industrial flotation cells. The variation of these parameters with impeller speed, air flowrate and power intensity are discussed further in the following sections. It should be noted that, due to the narrow ranges of gas dispersion parameters, many of the trends illustrated in these sections are slight and sometimes cannot be considered meaningful due to experimental error (see error bars). However, most of the trends are predictable and are discussed accordingly.

4.1.4.1 Bubble Size

A bubble size range of 1.51 to 1.71 mm was observed during the cleaner tails section of the testwork. While this range is quite narrow, it falls within or close to the range of bubble sizes quoted as typical of industrial flotation cells in the literature. Ahmed and Jameson (1985), for instance, suggested that the bubble size in industrial cells varies between 0.5 and 2.5 mm. Deglon *et al* (2000) found that bubble sizes varied from 1.2 to 2.7 mm in flotation cells on South African platinum concentrators, with an average size of 1.6 mm. The results from this study correspond to that average value exactly.

Figure 4.3 is a graph of the Sauter mean bubble size versus impeller speed. This graph shows the relationship between bubble size and impeller speed for a number of fixed air flowrates.

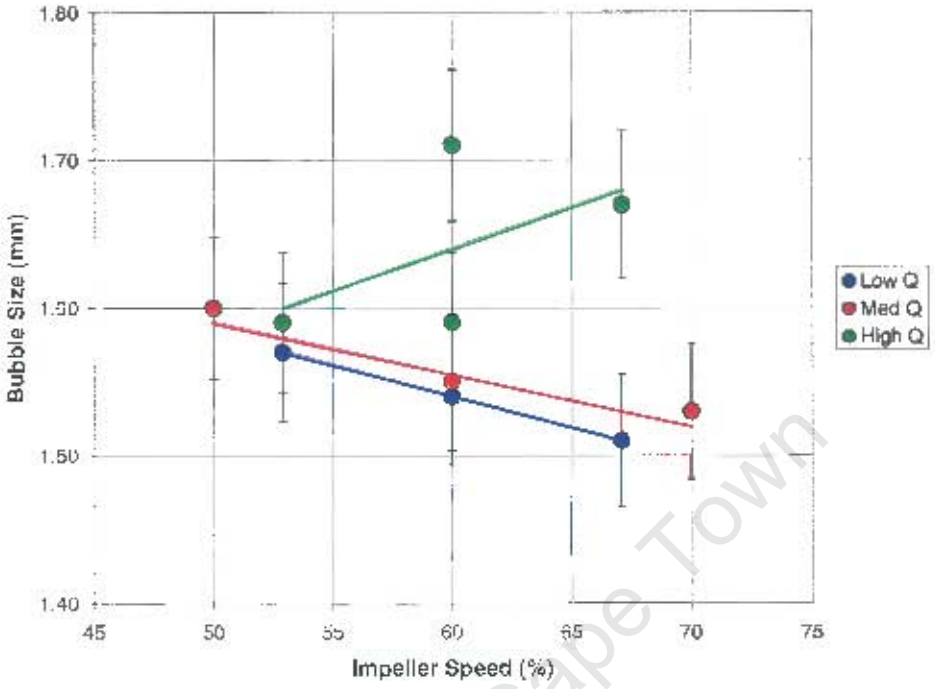

Figure 4.3 Sauter mean bubble diameter versus impeller speed.

Figure 4.3 shows that the bubble size decreases with increasing impeller speed for low and medium air flowrates and increases with high air flowrates. The trends in the low and medium air flowrate tests are as expected from the flotation literature. As the impeller speed increases, there is an increase in both shear and power intensity in the impeller zone. This in turn leads to an increase in bubble breakup which results in a decrease in the bubble size. The high air flowrate tests are not in keeping with this, however, although it is likely that at higher air flowrates the cell was operating beyond its ability to disperse gas properly.

Figure 4.4 is a graph of Sauter mean bubble size versus air flowrate. This graph shows the relationship between bubble size and air flowrate for a number of fixed impeller speeds.

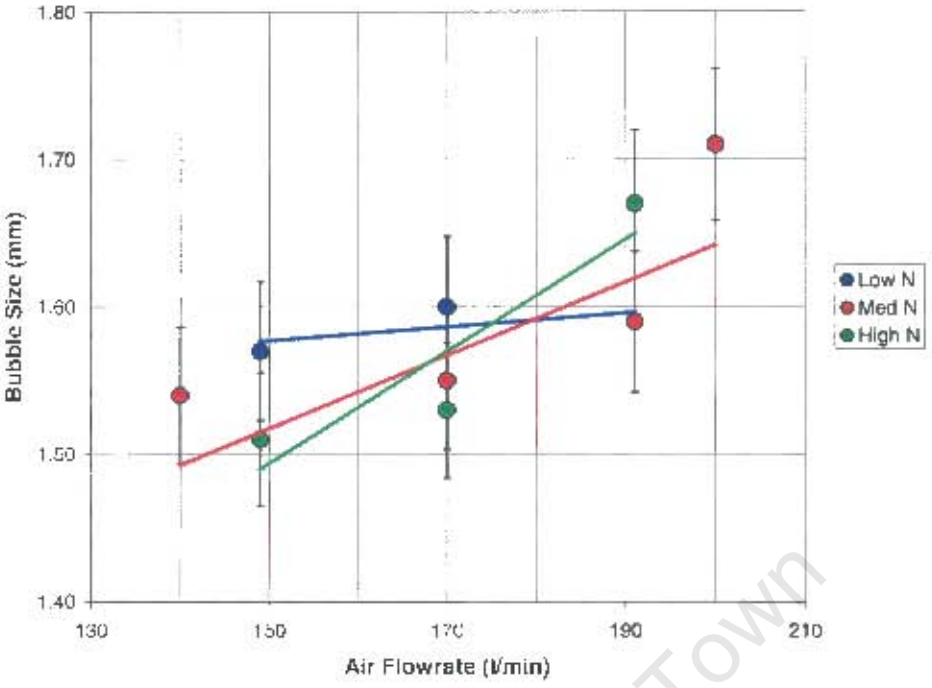

Figure 4.4 Sauter mean bubble diameter versus air flowrate.

Figure 4.4 shows that bubble size increases with increasing air flowrate across all impeller speeds. The effect is most pronounced at high and medium impeller speeds. At low impeller speeds there is only a small increase in bubble size and this cannot be considered meaningful due to experimental error. These trends are to be expected from the flotation literature. When the air flowrate is increased, the resulting increase in gas holdup in the impeller zone reduces both the shear and power intensity in the cell. This leads to a reduction in bubble breakup and an increase in the bubble size. This increase in gas holdup can also lead to increased bubble coalescence and, in extreme cases, can cause flooding of the impeller.

Figure 4.5 is a graph of Sauter mean bubble size versus power intensity. This graph shows the relationship between bubble size and power intensity for various fixed values of air flowrate.

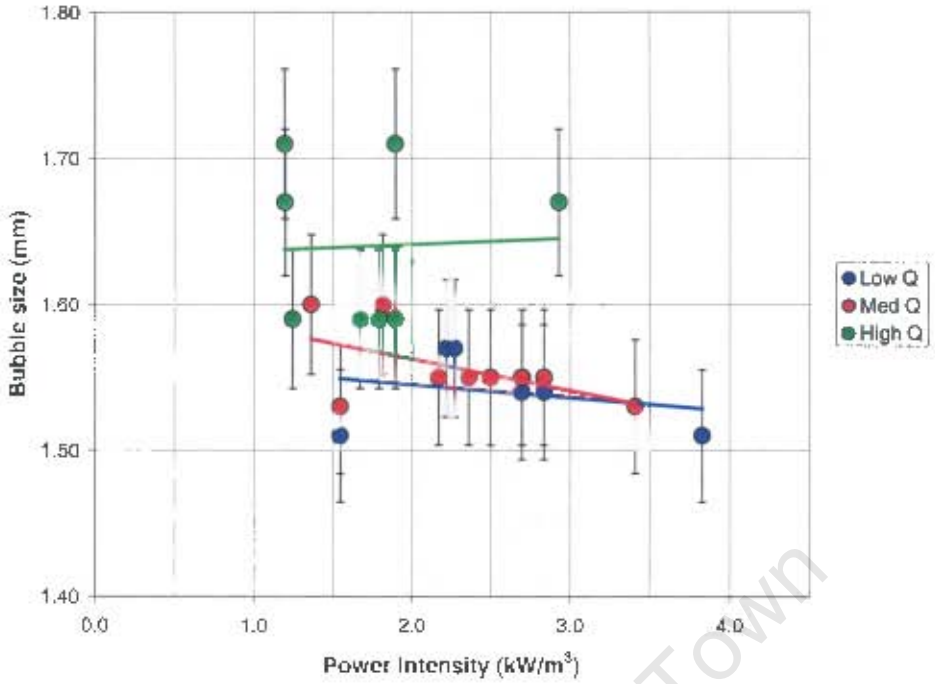

Figure 4.5 Sauter mean bubble diameter versus power intensity.

It is impossible to deduce anything from the trends in Figure 4.5 as these are very slight and cannot be considered meaningful due to error/scatter in the data. However, a reduction in bubble size with increasing power intensity is predicted by flotation theory. Here, the maximum stable bubble size is proportional to the power intensity to the power of 0.40. Hence an increase in power intensity should lead to a reduction in the maximum stable bubble size which will result in increased bubble breakup. However, an increase in power intensity can also lead to increased bubble coalescence, especially at high air flowrates and low frother concentrations, which will results in an increase in the bubble size.

4.1.4.2 Superficial Gas Velocity

A superficial gas velocity range of 0.95 cm/s to 1.15 cm/s was observed during the cleaner tails section of the testwork. This is a narrow range of values and is towards the lower end of the range of between about 1.0 and 3.0 cm/s typically observed in industrial flotation cells. For example, Deglon *et al* (2000) reported superficial gas velocities ranging between 0.7 and 2.7 cm/s, although the majority of measurements fell between 1.3 and 1.8 cm/s. This was considered within the acceptable range of values quoted by Degner (1980).

Figure 4.6 is a graph of superficial gas velocity versus impeller speed. This graph shows the relationship between these two parameters at various fixed values of air flowrate.

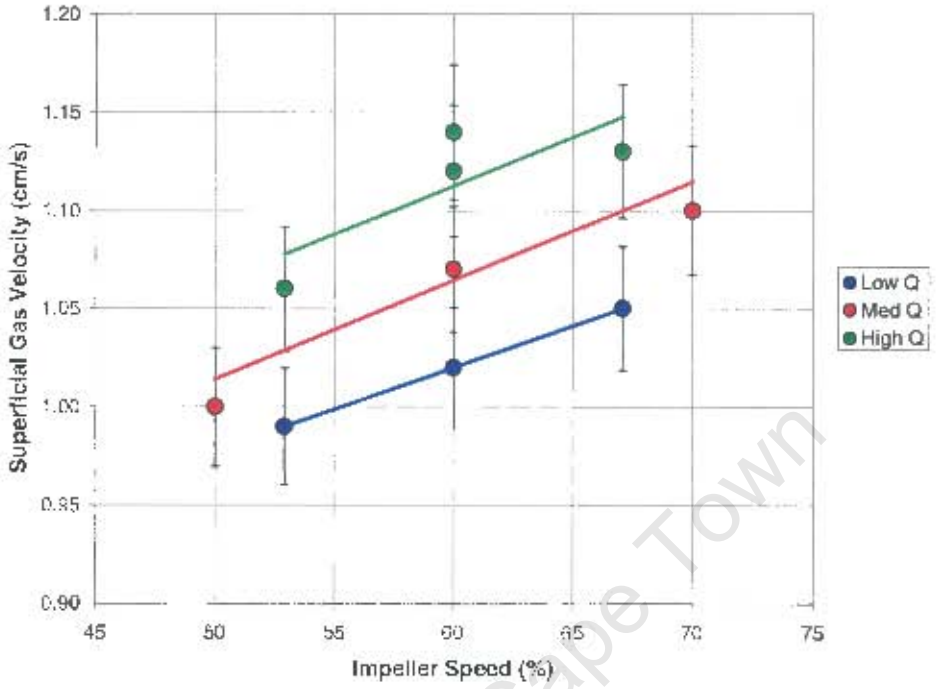

Figure 4.6 Superficial gas velocity versus impeller speed.

Figure 4.6 shows an increase in superficial gas velocity with increasing impeller speed across all air flowrates. The overall increase in superficial gas velocity of around 10% is relatively small given the range of air flowrates used. However, it is clear that there is an increase in superficial gas velocity with increasing impeller speed which should not occur if gas dispersion within the cell was good. Impeller speed should have no effect on the superficial gas velocity, at a constant air flowrate. However, if gas dispersion is poor, then increasing the impeller speed will increase the superficial gas velocity through an increase in both shear and power intensity in the cell (i.e. improved gas dispersion). This has been noted previously by Deglon *et al* (2000), particularly at high air flowrates.

Figure 4.7 is a graph of superficial gas velocity versus air flowrate. This graph shows the relationship between these two parameters for a number of fixed impeller speeds.

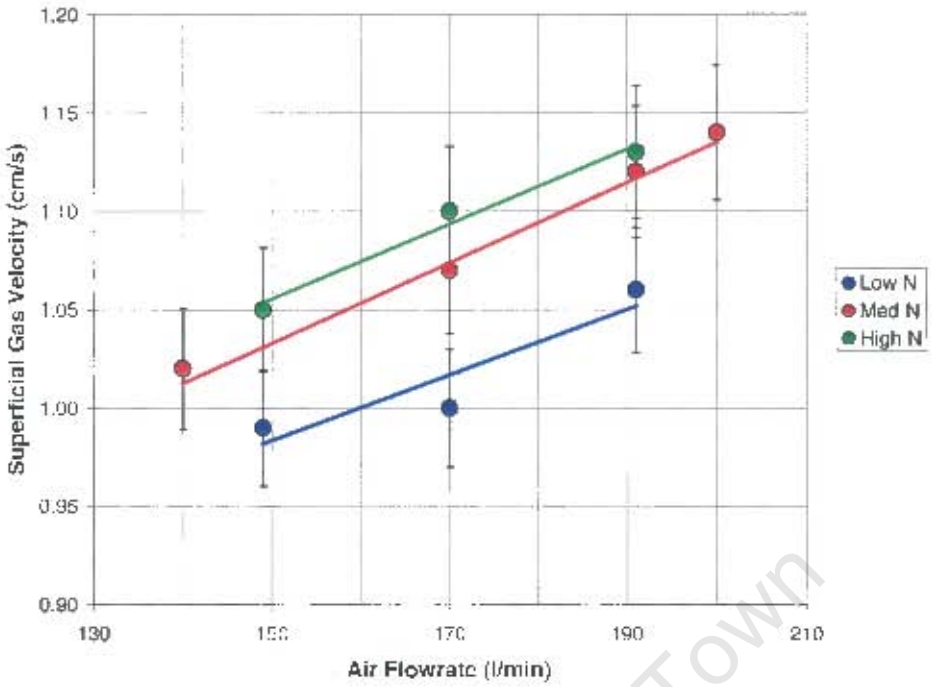

Figure 4.7 Superficial gas velocity versus air flowrate.

Figure 4.7 shows that the superficial gas velocity increases with increasing air flowrate across all ranges of impeller speeds. The effect is most noticeable at the medium and high impeller speed, with a maximum increase in superficial gas velocity of 12%. This trend is predictable as the superficial gas velocity is proportional to the air flowrate i.e. there is a direct relationship between these two parameters. However, the superficial gas velocity only increases by about 10% with a 25% increase in air flowrate which suggest that gas dispersion was less than ideal. However, as discussed previously, it is clear that gas dispersion improves with increasing impeller speed as the relative increase in the superficial gas velocity is higher at the higher impeller speeds.

Figure 4.8 is a graph of superficial gas velocity versus power intensity. This graph shows the relationship between these two parameters at a number of fixed values of air flowrate.

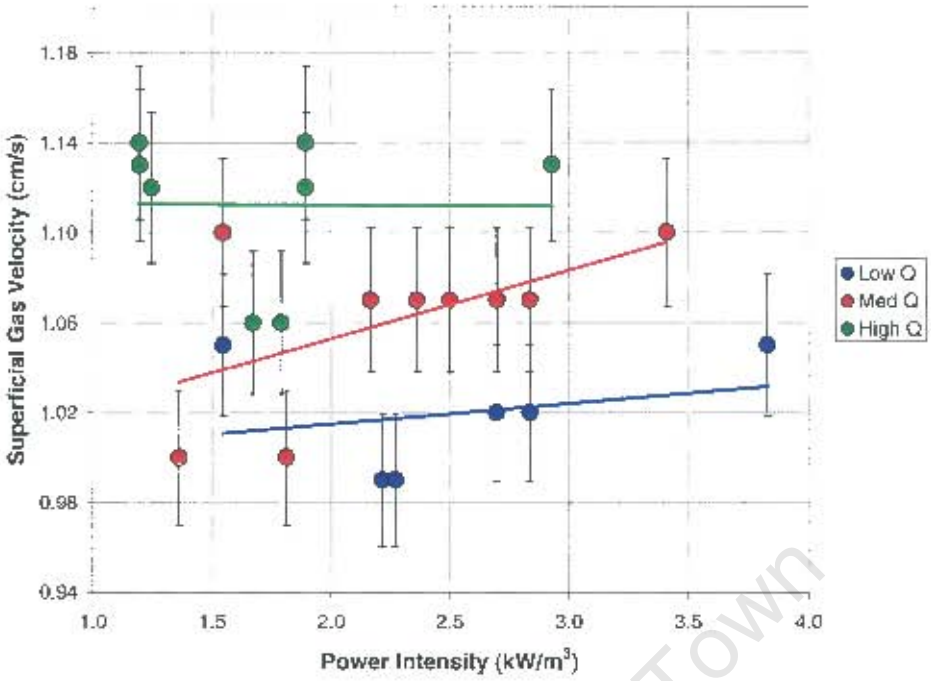

Figure 4.8 Superficial gas velocity versus power intensity.

It is impossible to deduce anything from the trends in Figure 4.8 as these are very slight and cannot be considered meaningful due to error/scatter in the data. However, as discussed previously, increasing power intensity should have no effect on the superficial gas velocity if gas dispersion is good but should lead to slight increases in the superficial gas velocity if gas dispersion is less than ideal.

4.1.4.3 Bubble Surface Area Flux

During the cleaner tails section of the testwork, a range of bubble surface area fluxes of between 36.4 and 42.8 s^{-1} was observed. This range is narrow when compared to other studies. Deglon *et al* (2000) noted that the bubble surface area flux varied between 32 and 97 s^{-1} in a number of industrial flotation cells. However, the same study also noted that the majority of bubble surface area fluxes fell between 50 and 70 s^{-1} which is well above the range encountered in this testwork. Gorain *et al* (1997) observed bubble surface area flux ranges of between 40 and 200 s^{-1}, with the majority falling between 60 and 100 s^{-1}. Clearly, not only is the range of bubble surface area fluxes narrower than those observed by other researchers, but the range encountered here is also much lower than that observed in other studies. It has been noted previously, however, that bubble surface area fluxes for mechanical flotation cells often lie within a narrow range, indicating some

sort of intrinsic limitation in the production of bubble surface area due to the method of gas dispersion.

Figure 4.9 is a graph of bubble surface area flux versus impeller speed. This graph plots the relationship between these two parameters for a number of fixed values of air flowrate.

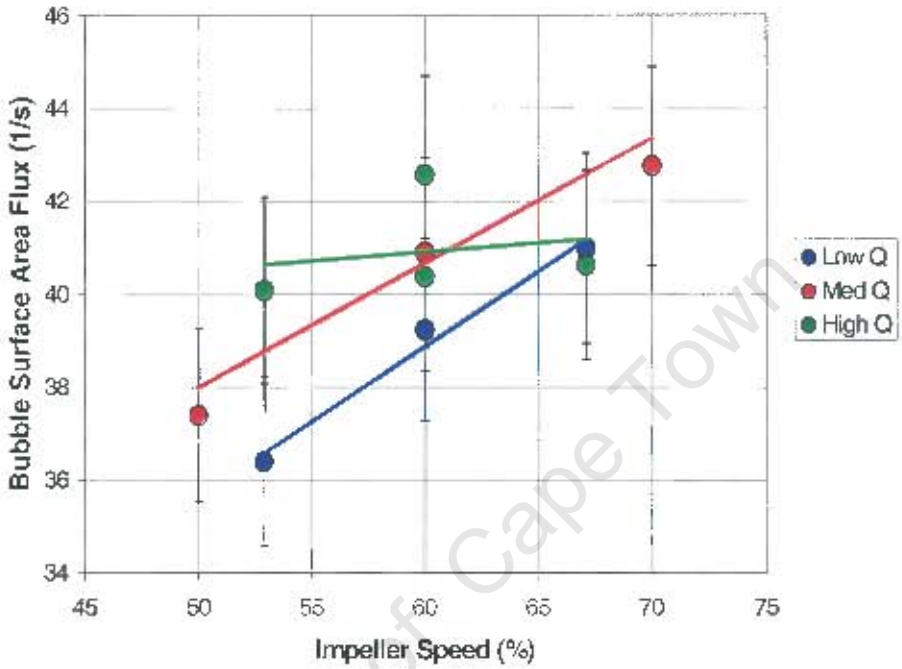

Figure 4.9 Bubble surface area flux versus impeller speed.

Figure 4.9 shows that the bubble surface area flux increases with increasing impeller speed for low and medium air flowrates but no trend is observed at the high air flowrate. This is because increasing impeller speed results in slight decreases in the bubble size and slight increases in the superficial gas velocity for the low and medium impeller speeds, as discussed previously (c.f. Figures 4.3 and 4.6). However, increasing impeller speed has no effect on the bubble size for the high air flowrate tests as the cell is operating beyond its ability to disperse gas properly.

Figure 4.10 is a graph of bubble surface area flux versus air flowrate. This graph shows the relationship between these two parameters at various constant impeller speeds.

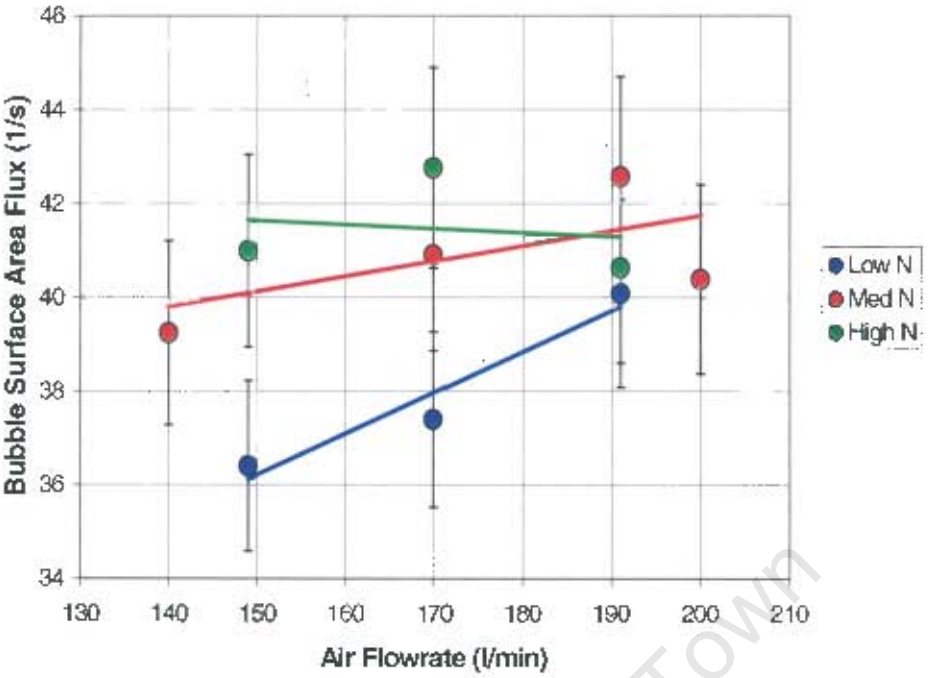

Figure 4.10 Bubble surface area flux versus air flowrate.

Figure 4.10 suggest that there are small increases in the bubble surface area flux with increasing air flowrate for low and medium air flowrates but no trend is observed at high air flowrates. These trends are less pronounced than those observed in Figure 4.9 because increasing air flowrate results in both increases in the bubble size and the superficial gas velocity, as discussed previously (c.f. Figures 4.4 and 4.7). The bubble surface area flux is obtained from the ratio of these two quantities and, consequently, is less affected by increases in air flowrate than impeller speed. The bubble surface area flux may remain constant or even decrease with increasing air flowrate.

Figure 4.11 is a graph of bubble surface area flux versus power intensity. This graph plots the relationship between these two parameters for a number of fixed values of air flowrate.

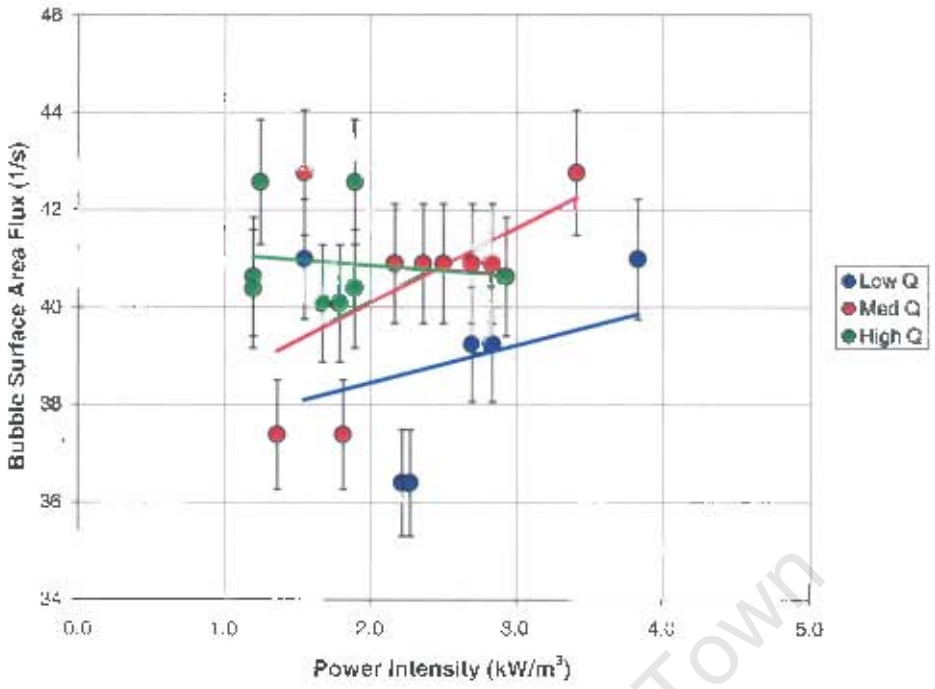

Figure 4.11 Bubble surface area flux versus power intensity.

It is impossible to deduce anything from the trends in Figure 4.11 as these are very slight and cannot be considered meaningful due to error/scatter in the data. However, the figure suggest that there are slight increases in the bubble surface area flux with increasing power intensity at low and medium air flowrates. This would seem sensible as increasing power intensity should lead to a reduction in the bubble size which should result in an increase in the bubble surface area flux. However, this will not occur as high air flowrates if the cell is operating beyond it ability to disperse gas effectively.

4.2 Flotation Results

This section presents results of the testwork performed in terms of the flotation parameters of recovery, concentrate grade and flotation rate constant. Rougher feed and cleaner tails results are presented in Sections 4.3.1 and 4.3.2 respectively. Graphs depicting trends in recovery and grade are derived from the CCRD regression analysis (cf. Section 3.7.2) of the overall FCTR performance i.e. individual cells are not analysed. It should be noted that there was significant error in the CCRD regression analysis of the rougher feed but that the cleaner tails results were generally good. Hence the analysis of the rougher feed results should be regarded with some circumspection whereas the analysis of the cleaner tails results can be accepted with reasonable confidence.

It should also be noted that the CCRD analysis found both platinum recovery and concentrate grade to be a function of impeller speed, air flowrate and feed grade i.e. 3 variables. However, 3D response curves are not plotted in this section, but rather 2D curves depicting contours at low, medium and high values of the relevant variables e.g. recovery versus impeller speed at a low, medium and high feed grade. In plotting these graphs it was necessary to hold one variable constant at some average (representative) value - air flowrate would be held constant in the previous example. The variable to be held constant was chosen as that which had the least influence on the results. For recovery, this was either impeller speed or air flowrate, depending on the graph, as feed grade had a significant influence. For concentrate grade, this was feed grade for the cleaner tails results as impeller speed and air flowrate both had a significant influence. For the rougher feed results, concentrate grade was found to be a function of only impeller speed and air flowrate i.e. 2 variables. The choice of the average (representative) value for the constant variable was generally immaterial as most response curves were fairly uniform in this variable i.e. the same trends occurred at all values.

4.2.1 Rougher Feed

This section presents the results of the tests performed on the rougher feed stream. It concerns itself primarily with the effect of the various hydrodynamic parameters on recovery, concentrate grade and flotation rate constants. It should be noted that the "Low", "Medium" and "High" contours depicted in the figures in this section refer to impeller speeds of 55, 65 & 75%, to air flowrates of 90, 120 & 150 l/min and to feed grades of 2, 2.5 & 3 g/ton.

4.2.1.1 Recovery

Figure 4.12 is a graph of recovery versus feed grade. This graph shows the relationship between recovery and feed grade at various constant air flowrates and at an impeller speed of 65%. The same general trends observed in this figure occurred at all impeller speeds used in the study.

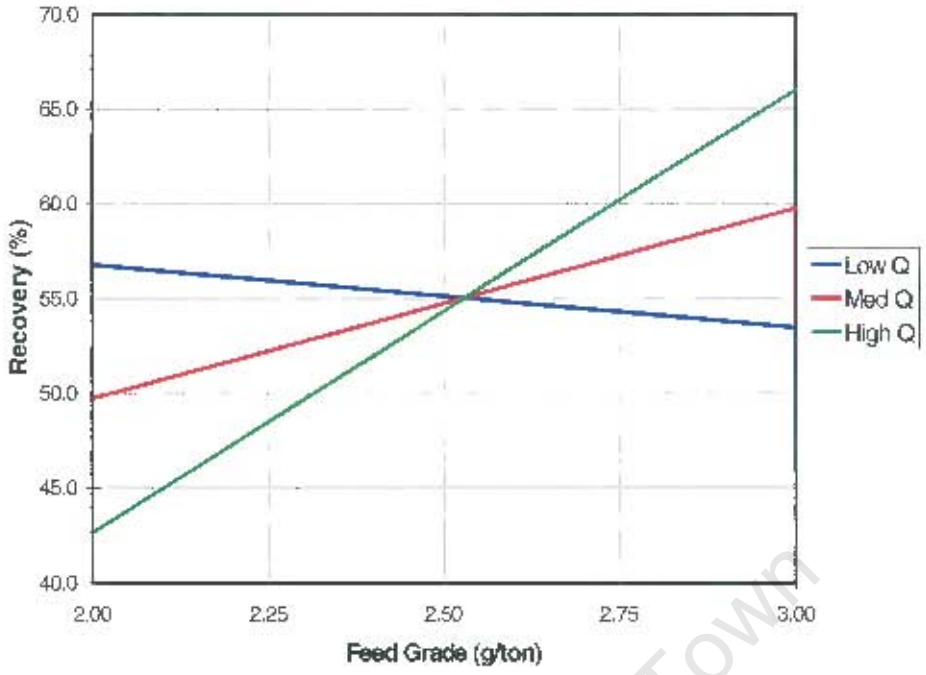

Figure 4.12 Recovery versus feed grade - rougher feed.

This figure shows that recovery generally increases with increasing feed grade but that this is dependent on the air flowrate. This is most noticeable for the high air flowrate tests, as recovery increases by around 20% over the range of feed grades. The trend is less noticeable for the intermediate air flowrates and a slight decrease is observed at the low air flowrates. The general increase in recovery with increasing feed grade is a common finding in the flotation literature, and has been noted previously in a number of studies, including Strohmayr *et al* (1998).

Figure 4.13 is a graph of recovery versus impeller speed. This figure shows the relationship between recovery and impeller speed at various constant feed grades and at an air flowrate of 120 l/min. The same general trends observed in this figure occurred at all air flowrates used in the study.

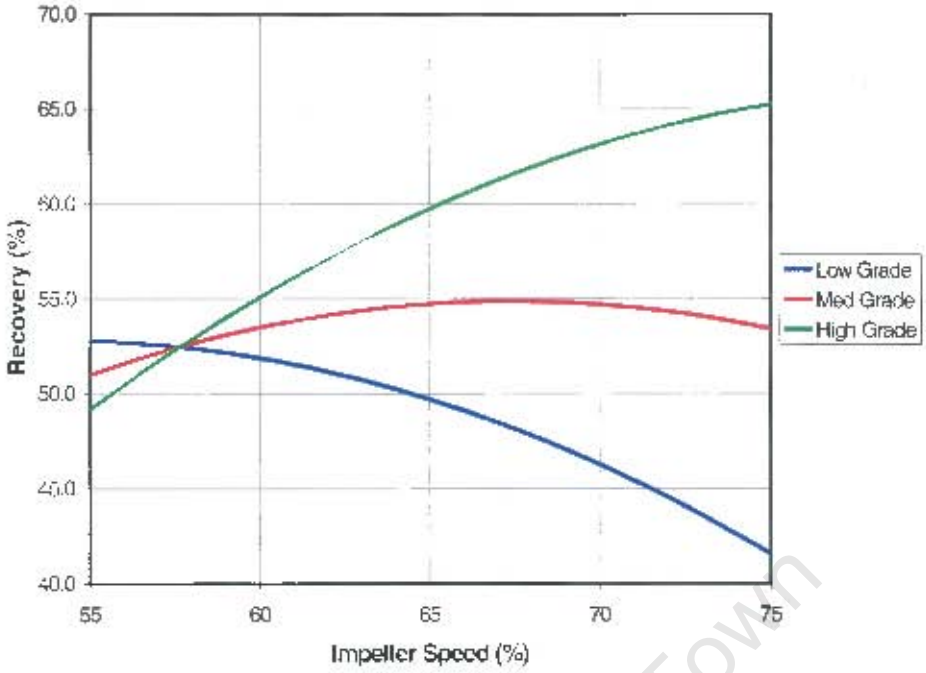

Figure 4.13 Recovery versus impeller speed – rougher feed.

This figure shows that recovery generally increases with increasing impeller speed but that this is strongly dependent on the feed grade. The recovery increases by almost 15% over the range of impeller speeds at high feed grades but decreases significantly at low feed grades. In terms of the air flow number (cf. Section 1.3.2) one would expect recovery to increase with increasing impeller speed. An increase in impeller speed, with constant air flowrate and impeller diameter, will lead to a decrease in the air flow number which will result an increase in recovery (up to a point). This was demonstrated by Arbiter and Harris (1969) and is in keeping with Darley (1998). Increasing the impeller speed results in increased turbulence in the flotation cell which improves particle-bubble contacting. However, at high impeller speeds this can also lead to substantial increases in particle-bubble detachment in the pulp zone and to instability in the froth zone. Consequently, there will always be an optimum in recovery as a function of impeller speed and this will be strongly dependent on the nature of the feed. A high grade feed, containing strongly floatable particles, is likely to respond favourably to increasing impeller speed as particle-bubble detachment is less likely.

Figure 4.14 is a graph of recovery versus air flowrate. This figure shows the relationship between recovery and air flowrate at various constant feed grades and at an impeller speed of 65%. The same general trends observed in this figure occurred at all impeller speeds used in the study.

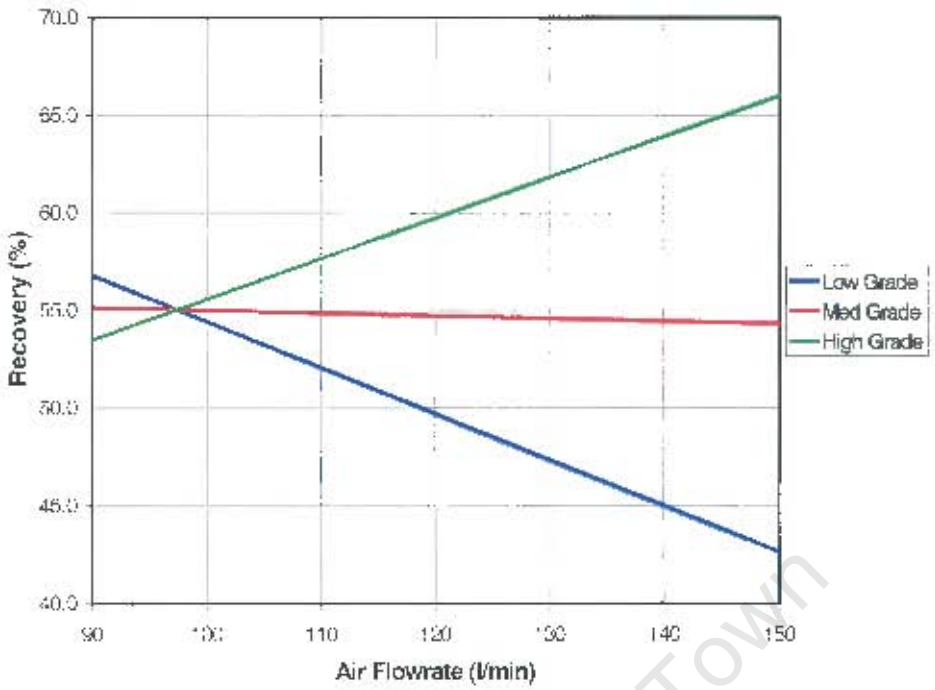

Figure 4.14 Recovery versus air flowrate – rougher feed.

This figure shows that recovery increases with increasing air flowrate at high feed grades but decreases at low feed grades. This is a bit surprising as one would generally expect recovery to increase with increasing air flowrate due to a increases in the number of bubbles in the flotation cell, which will improve particle-bubble contacting. This should occur up to the point at which ability of the cell to effectively disperse gas is exceeded i.e. the impeller starts flooding. However, high air flowrates can also lead to instability in the froth zone which would have a significant effect on the recovery of weakly floatable material i.e. the nature of the feed can have an influence on the relationship between recovery and air flowrate.

4.2.1.2 Rate Constant

Figure 4.15 is a graph of the flotation rate constant versus the bubble surface area flux. This graph shows the relationship between the overall flotation rate constant for the FCTR (i.e. all cells) and the average bubble surface area flux.

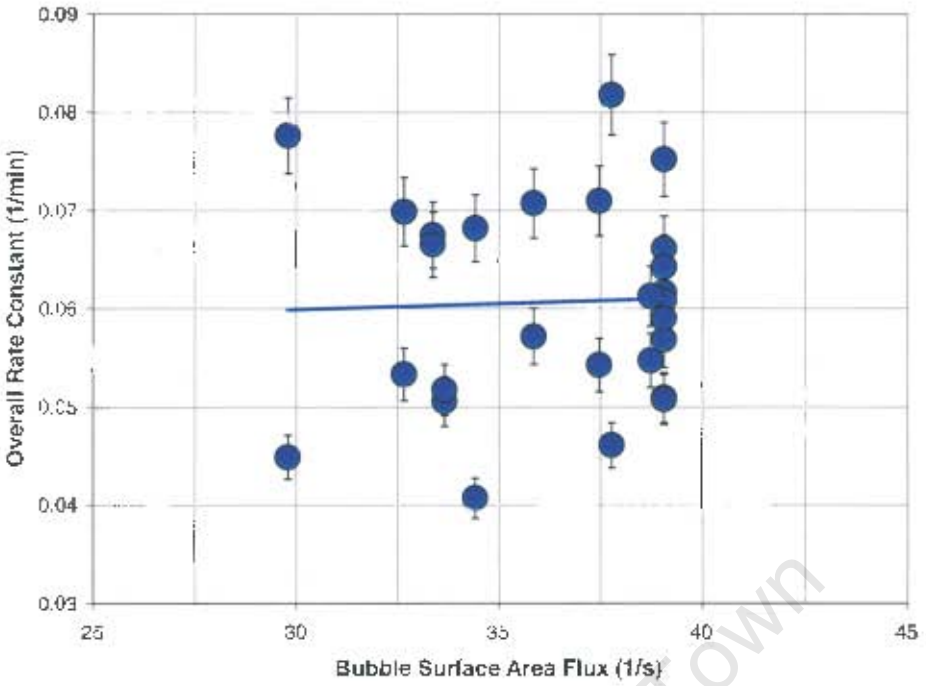

Figure 4.15 Flotation rate constant (overall) versus bubble surface area flux – rougher feed.

This figure shows that there is no relationship between the flotation rate constant and bubble surface area flux for the rougher feed testwork. The graph shows no increase in the flotation rate constant with increasing bubble surface area flux, which does not support the k-Sb relationship observed in the flotation literature. Figure 4.26 shows two major differences from the usual k-Sb relationships observed in the literature. Firstly, Gorain *et al* (1997) found that there was a strong linear relationship between the flotation rate constant and the bubble surface area flux for a number of different cell types, which is clearly not reflected here. Secondly, Gorain showed that the bubble surface area flux typically varies over a broad range, from around 50 to 200 s^{-1} for certain cells, which is also not reflected here. A typical bubble surface area flux range for an industrial flotation cell is between 40 and 80 s^{-1} (Deglon *et al*, 2000) which is far broader than the range of 30 to 40 s^{-1} observed in this testwork.

Figure 4.16 is a graph of the flotation rate constant versus the power intensity. This graph shows the relationship between the flotation rate constant in the first rougher cell and the power intensity at various constant air flowrates.

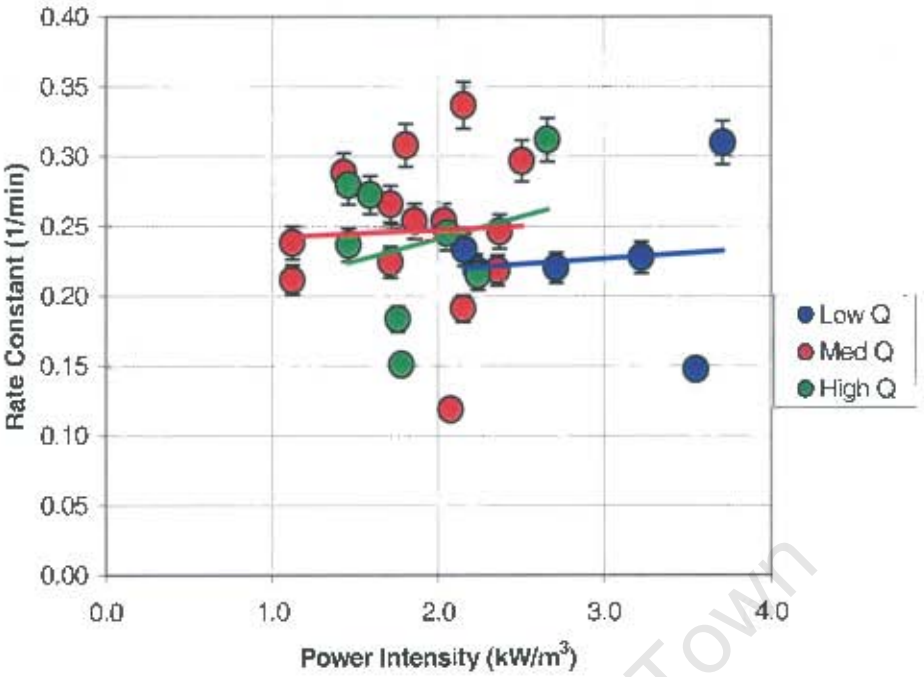

Figure 4.16 Flotation rate constant (first rougher cell) versus power intensity – rougher feed.

Figure 4.16 shows slight, or negligible, increases in the flotation rate constant with increasing power intensity, across all ranges of air flowrates used in the study. From this it would appear that power intensity has no effect on the flotation rate constant for the first rougher cell. This can be explained by the fact that the first rougher cell is full of fast floating material. Here, recovery is generally limited by the carrying capacity of the froth rather than by the actual rate of flotation in the cell i.e. mass transport limited rather than kinetically limited.

Figure 4.17 is a graph of the flotation rate constant versus the power intensity. This graph shows the relationship between the flotation rate constant in the third rougher cell and the power intensity at various constant air flowrates.

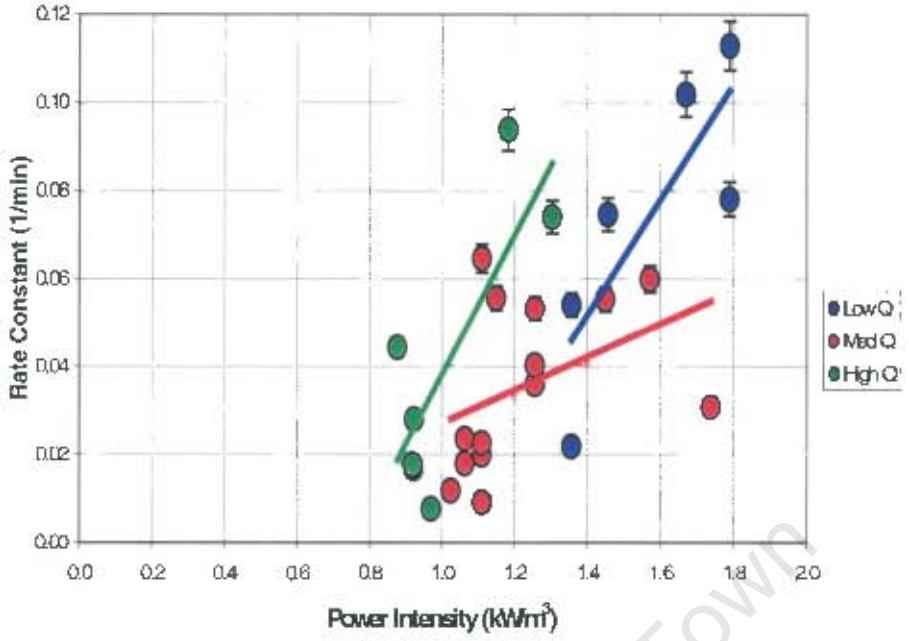

Figure 4.17 Flotation rate constant (third rougher cell) versus power intensity – rougher feed.

Figure 4.17 shows significant increases in the flotation rate constant with increasing power intensity across all ranges of air flowrates used in the study. In some instances, the flotation rate constant increases by up to 5 times for an increase in power intensity of less than 0.5 kW/m^3. This graph demonstrates that an increase in the power intensity strongly increases the flotation rate constant further down the bank in the rougher cells. This is an interesting finding but is expected as increasing the power intensity increases the turbulence in the cell. This should lead to improved particle-bubble contacting which will improve the flotation performance of the slower floating and finer particles. This increase in the flotation rate constant with increasing power intensity is not observed when analysing the overall FCTR performance. This is because most of the recovery occurs in the first two rougher cells, which do respond strongly to increasing power intensity, for reasons discussed previously. Hence, when analysing the overall FCTR performance, there is only a weak relationship between the flotation rate constant and the power intensity for the rougher feed testwork.

4.2.1.3 Grade

Figure 4.18 is a graph of the concentrate grade versus the impeller speed. This graph shows the relationship between the concentrate grade and the impeller speed at various constant feed grades.

It should be noted that the CCRD regression analysis yielded no relationship between the concentrate grade and the air flowrate i.e. the results are identical at all air flowrates.

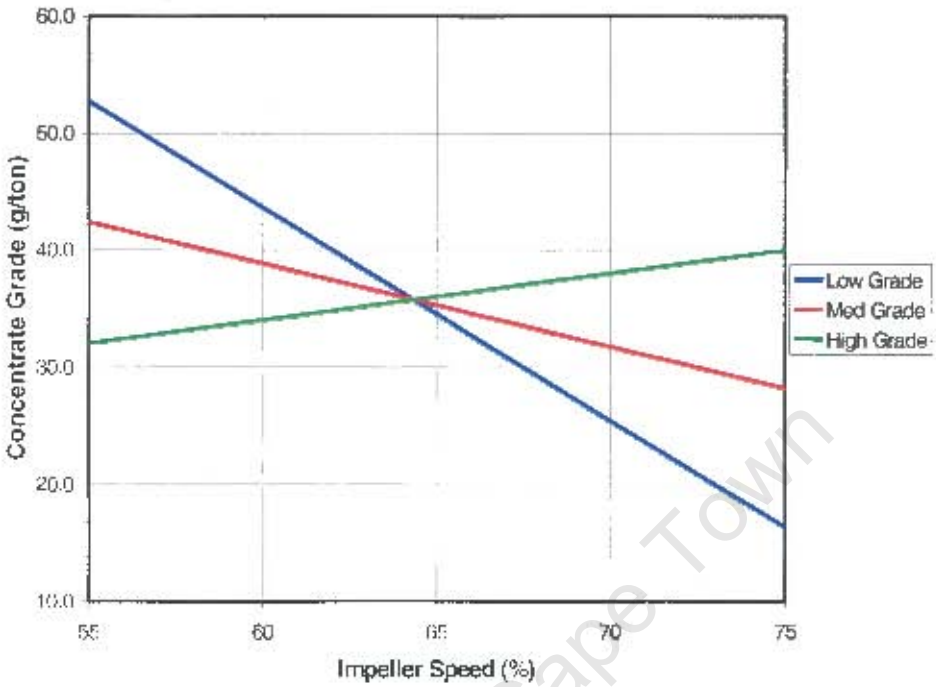

Figure 4.18 Concentrate grade versus impeller speed – rougher feed.

This figure shows that concentrate grade generally decreases with increasing impeller speed but that this is strongly dependent on the feed grade. The concentrate grade decreases by over 30 g/ton at low feed grades but increases slightly at high feed grades. The trends in Figure 4.18 are not in keeping with the flotation literature. Both Arbiter *et al* (1968) and Arbiter and Harris (1969) found that increasing the impeller speed increases the concentrate grade due to a reduction in the air flow number. However, Arbiter and Harris (1969) suggested that when the air flow number reached certain levels, both recovery and grade were reduced. Nonetheless, these results suggest that increasing impeller speed increases both recovery and grade for high feed grades and decreases both recovery and grade for low feed grades. This is surprising as increases in recovery are usually accompanied by decreases in grade, and visa versa. However, it should again be noted that there was significant error in the CCRD regression analysis of the rougher feed.

4.2.2 Cleaner Tails

This section presents the results of the tests performed on the cleaner tails stream on the FCTR. It concerns itself primarily with the effect of the various hydrodynamic parameters on recovery, concentrate grade and flotation rate constants. It should be noted that the "Low", "Medium" and "High" contours depicted in the figures in this section refer to impeller speeds of 50, 60 & 70%, to air flowrates of 140, 170 & 200 l/min and to feed grades of 3, 4 & 5 g/ton.

4.2.2.1 Recovery

Figure 4.19 is a graph of recovery versus feed grade. This graph shows the relationship between recovery and feed grade at various constant air flowrates and at an impeller speed of 60%. The same general trends observed in this figure occurred at all impeller speeds used in the study.

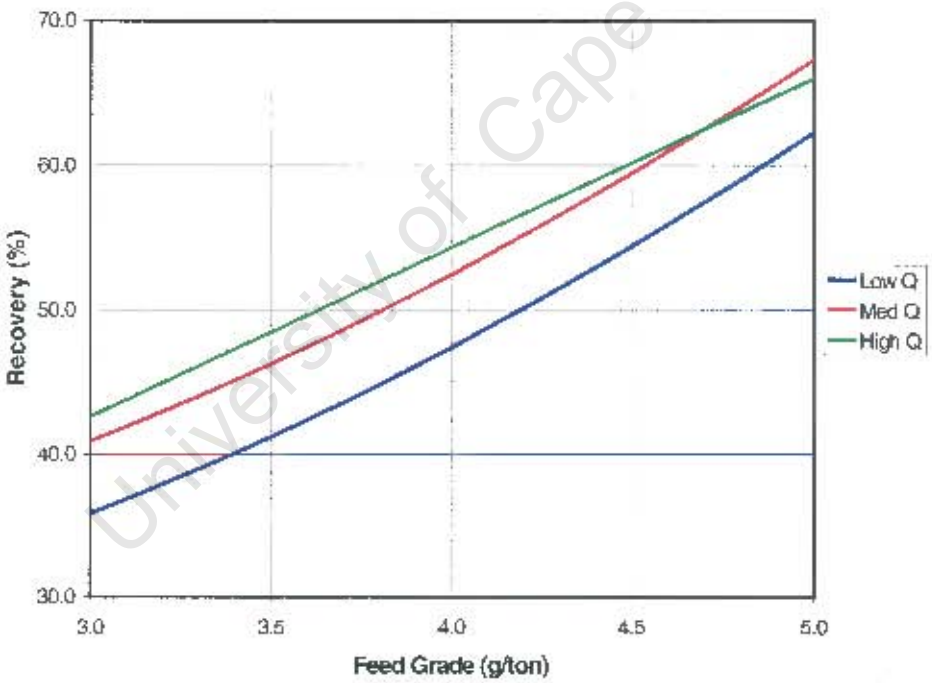

Figure 4.19 Recovery versus feed grade – cleaner tails.

This figure shows that recovery increases as feed grade increases across all ranges of air flowrates used in the study. This is a common finding in the flotation literature, and has been noted in a

number of studies, as discussed previously. This supports the general increase in recovery with increasing feed grade noted in the rougher feed testwork.

Figure 4.20 is a graph of recovery versus impeller speed. This figure shows the relationship between recovery and impeller speed at various constant feed grades and at an air flowrate of 170 l/min. The same general trends observed in this figure occurred at all air flowrates used in the study.

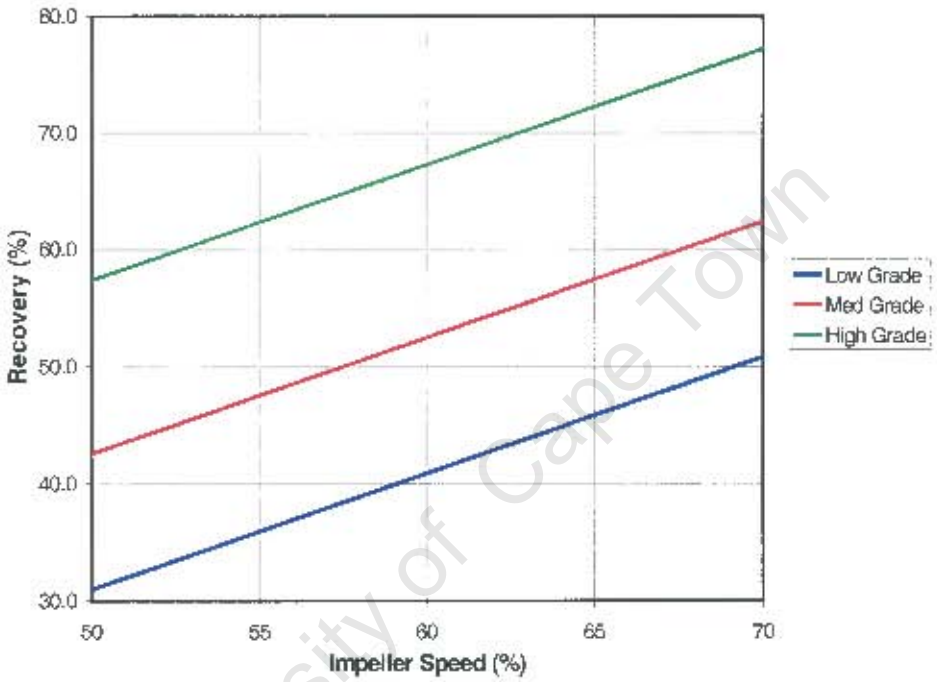

Figure 4.20 Recovery versus impeller speed – cleaner tails.

This figure shows that recovery increases steeply with increasing impeller speed across all feed grades. The recovery increases by approximately 20% over the range of impeller speeds used in the study. This increase in recovery with increasing impeller speed differs from the rougher feed results (cf. Figure 4.13) as it is largely independent of feed grade and no optimum is observed i.e. there is a steady and continuous increase. The increase in recovery can be explained in terms both the air flow number and improved particle-bubble contacting, as discussed in the rougher feed results. The steady increase in recovery with increasing impeller speed is more likely to occur with the cleaner tails material. This contains finer particles and produces more stable froths than the rougher feed, which would tend to reduce both particle-bubble detachment in the pulp zone and drop-back in the froth zone. However, one would have expected a general "leveling off" of recovery with increasing impeller speed which should be more pronounced with the low grade

feed. This is clearly not evident over the range of impeller speeds used in the study but must occur at higher impeller speeds. Nonetheless, it is interesting to see that the recovery of cleaner tails material can be significantly increased by increasing the impeller speed.

Figure 4.21 is a graph of recovery versus air flowrate. This figure shows the relationship between recovery and air flowrate at various constant feed grades and at an impeller speed of 60%. The same general trends observed in this figure occurred at all impeller speeds used in the study, but were more pronounced at the higher impeller speeds.

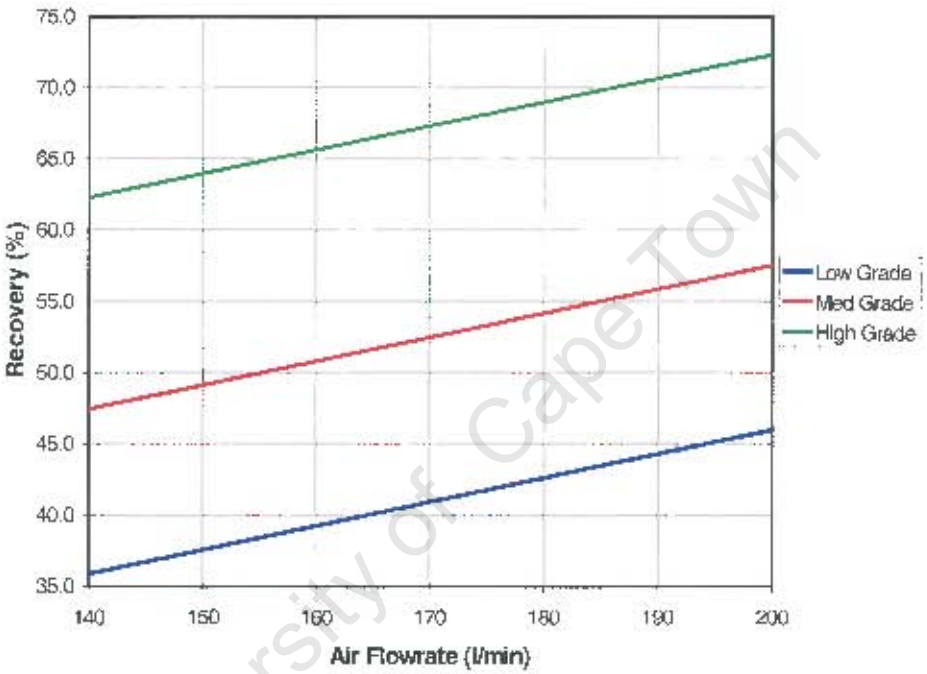

Figure 4.21 Recovery versus air flowrate – cleaner tails.

This figure shows that recovery increases with increasing air flowrate across all feed grades. The recovery increases by approximately 10% over the range of air flowrates used in the study. This is expected as increasing the air flowrate increases in the number of bubbles in the flotation cell which improves particle-bubble contacting, up to the point at which ability of the cell to effectively disperse gas is exceeded, as discussed previously. This finding is more convincing than the rougher feed results where recovery was found to decrease with increasing air flowrate for the low grade feed. However, as discussed previously, the cleaner tails contains finer particles and produces more stable froths than the rougher feed. This would tend to limit the "disruptive" effects of high air flowrates on the froth phase which would results in recovery responding more favourably to air flowrate.

4.2.2.2 Rate Constant

Figure 4.22 is a graph of the flotation rate constant versus the bubble surface area flux. This graph shows the relationship between the overall flotation rate constant for the FCTR (i.e. all cells) and the average bubble surface area flux.

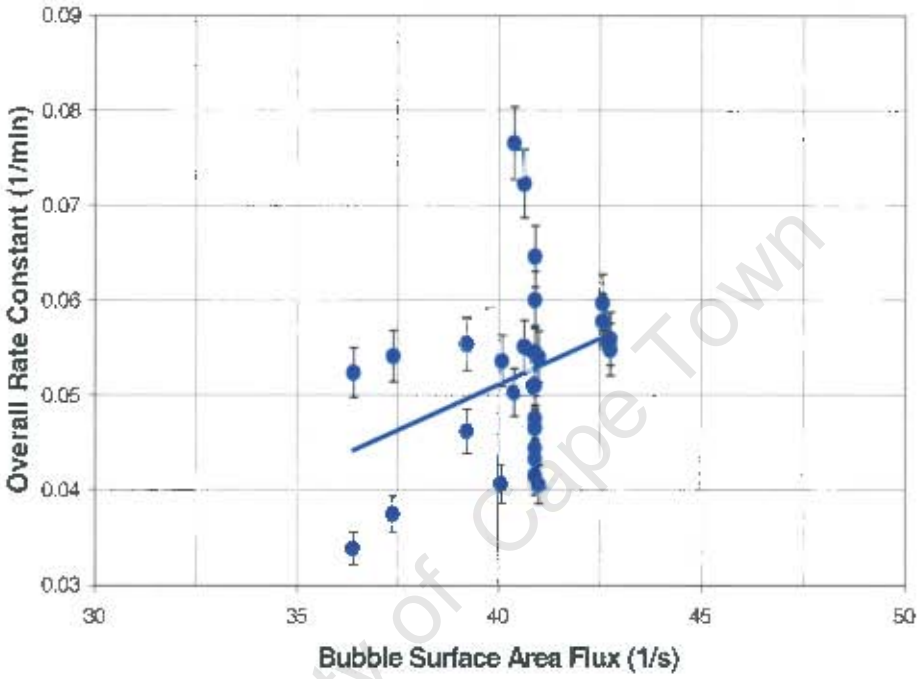

Figure 4.22 Flotation rate constant (overall) versus bubble surface area flux – cleaner tails.

This figure shows a very weak increase in the flotation rate constant with increasing bubble surface area flux. This is more promising that the rougher feed results where no increase was observed but still does not support the k-Sb relationship observed in the flotation literature. Figure 4.22 is more of a "scatter gram" with a general increasing trend than a linear relationship and straddles a fairly narrow range of bubble surface area fluxes. From this it would appear that the k-Sb relationship does not hold for platinum. However, it should be noted that only a fairly narrow range of bubble surface area fluxes was obtained in both the rougher feed and cleaner tails tests. Consequently, the lack of a clear k-Sb relationship in the experimental results might well be due to this narrow window of bubble surface area fluxes and might only be observed over a broad range.

Figure 4.23 is a graph of the flotation rate constant versus the power intensity. This graph shows the relationship between the flotation rate constant in the first rougher cell and the power intensity at various constant air flowrates.

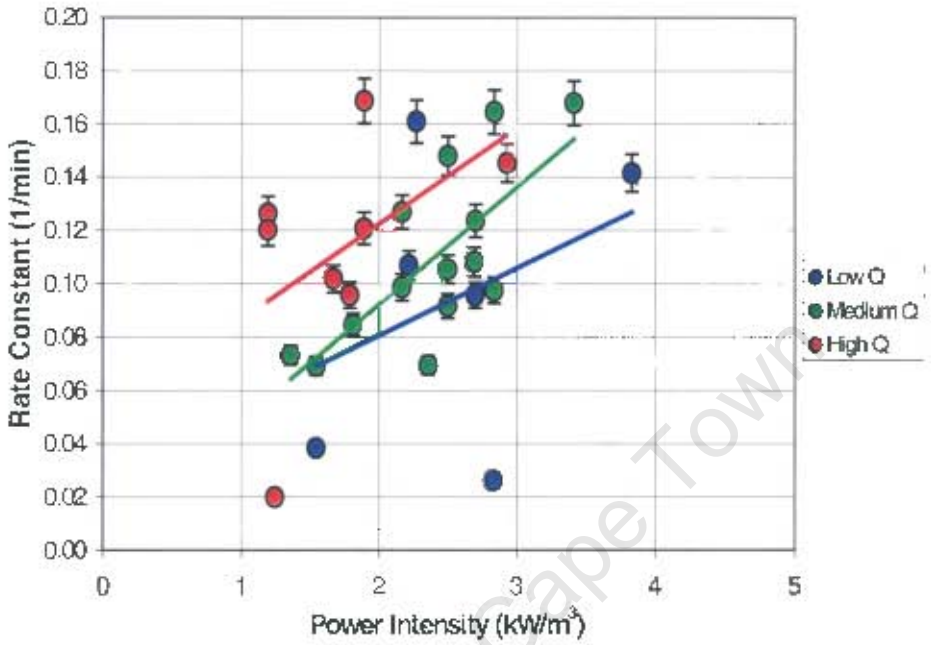

Figure 4.23 Flotation rate constant (first rougher cell) versus power intensity – cleaner tails.

This figure shows significant increases in the flotation rate constant with increasing power intensity across all ranges of air flowrates used in the study. The flotation rate constant almost doubles over the range of power intensities used in the study. This is dramatically different from the rougher feed results where only slight (or negligible) increases where observed. However, the cleaner tails stream is significantly different to the rougher feed as all the fast floating material would already have been removed in the cleaner bank. Recovery in the first rougher cell of the FCTR is unlikely to be limited by the carrying capacity of the froth, but rather by the actual rate of flotation in the pulp zone. Consequently, these results suggest that increasing the power intensity increases the rate of flotation of platinum through improved particle-bubble contacting.

Figure 4.24 is a graph of the flotation rate constant versus the power intensity. This graph shows the relationship between the flotation rate constant in the third rougher cell and the power intensity at various constant air flowrates.

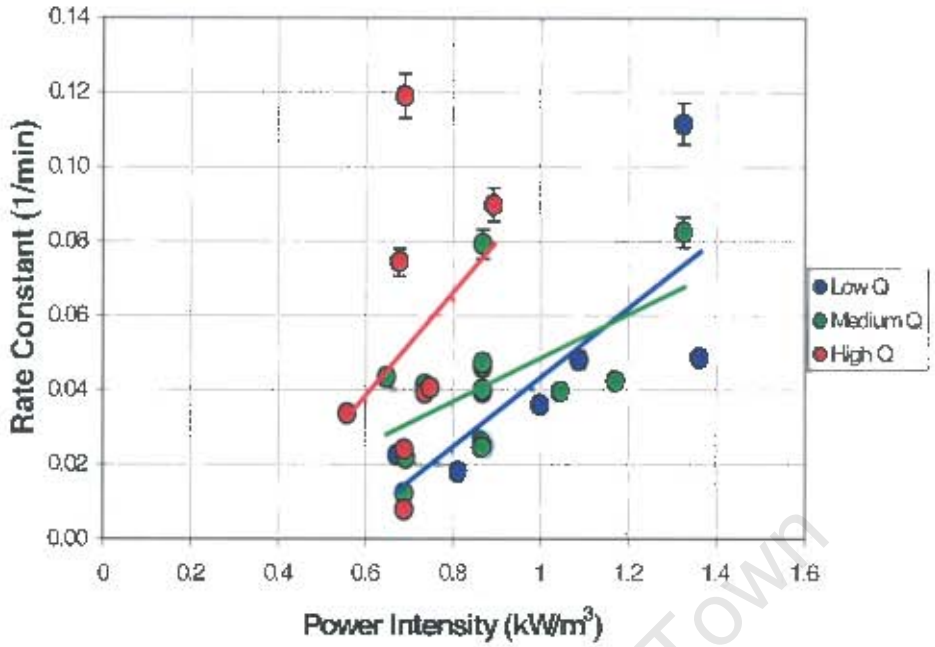

Figure 4.24 Flotation rate constant (third rougher cell) versus power intensity – cleaner tails.

This figure shows even more dramatic increases in the flotation rate constant with increasing power intensity than those observed in Figure 4.23. As per the rougher feed results, in some instances the flotation rate constant increases by up to 5 times for an increase in power intensity of less than 1 kW/m^3. These results again suggest that increasing the power intensity has a beneficial effect on the rate of flotation of platinum. However, it is interesting to note that increasing the power intensity has a more notable effect further down the bank i.e. in the third cell. This tends to suggest that increasing the power intensity improves the rate of flotation of finer or slow floating material which is the common opinion in the platinum industry. Here, increasing the power intensity increases the turbulence in the cell. This leads to improved particle-bubble contacting which will improve the flotation performance of the finer or slow floating particles.

4.2.2.3 Grade

Concentrate grade was found to increase steadily with increasing feed grade at all experimental conditions but to be strongly dependent on both impeller speed and air flowrate. Figures 4.25 is a graph of the concentrate grade versus the impeller speed. This graph shows the relationship between the concentrate grade and the impeller speed at various constant air flowrates and at a feed grade of 4 g/ton. The same general trends observed in this figure occurred at all feed grades encountered in the study.

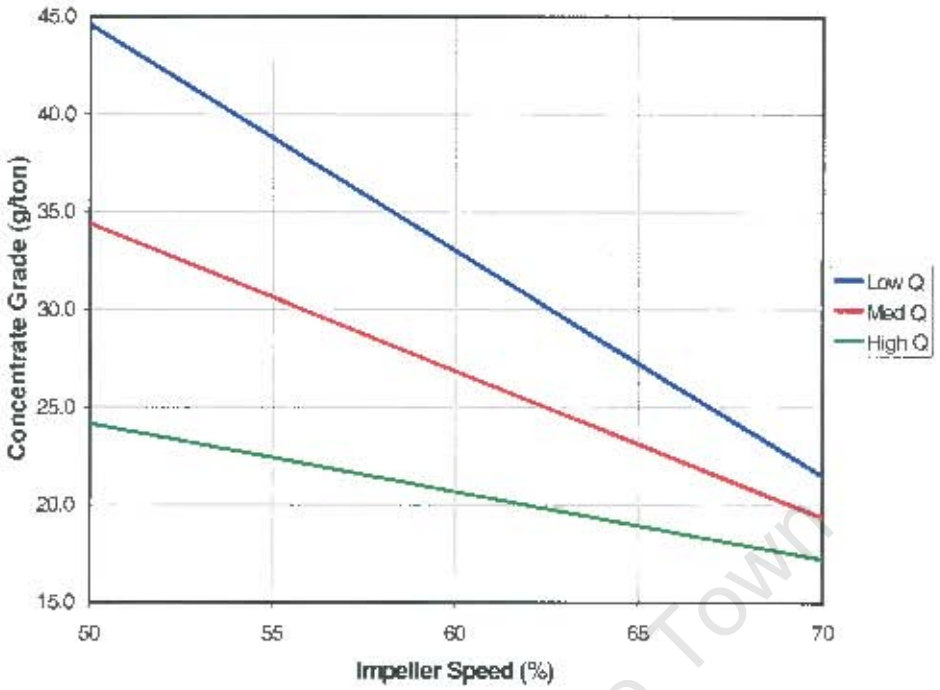

Figure 4.25 Concentrate grade versus impeller speed – cleaner tails.

Figure 4.25 shows that the concentrate grade decreases sharply with both increasing impeller speed and increasing air flowrate. In terms of the air flow number, concentrate grade should decrease with increasing air flowrate but should increase with increasing impeller speed due to improved flotation performance (Arbiter and Harris, 1969). However, as discussed previously, when the air flow number reaches certain levels both recovery and grade will decrease with increasing impeller speed. These dramatic decreases in concentrate grade with increasing impeller speed and air flowrate tend to counter the significant improvements in recovery observed with these two variables (cf. Figures 4.20 and 4.21). One would expect grade to decrease slightly with increasing recovery but not to the extent observed in Figure 4.25. In the worst case these dramatic decreases in concentrate grade suggest that material is simply being entrained to concentrate at high levels of agitation and aeration (i.e. over the lip of the cell). However, it is possible that this decrease is due to increases in the rate of flotation of poorly liberated, slow floating particles at higher levels of agitation and aeration. This would have to be ascertained through a mineralogical study of the flotation concentrate, which was not done as part of this study.

Chapter 5 Conclusions

The objective of this thesis was to perform an investigation into the effect of hydrodynamic parameters, driven by the central hydrodynamic variables of impeller speed and air flowrate, on the flotation of platinum ore in a pilot flotation plant. The conclusions regarding the findings of this thesis are presented in this chapter. They refer to results obtained using data from the Floatability Characterisation Test Rig (FCTR) campaign at Lonmin's Eastern Platinum concentrator. The conclusions presented here are broken down into hydrodynamic and flotation conclusions, in Sections 5.1 and 5.2 respectively.

5.1 Hydrodynamic Conclusions

The results for the hydrodynamics section of the study were obtained through a variety of techniques, including experimental measurements (e.g. bubble size, superficial gas velocity), calculations based on experimental variables (e.g. Froude number, power number) and experimental observation compared to examples in the flotation literature (e.g. efficiency of mixing). These results were interpreted, where possible, with reference to the major hydrodynamic variables of impeller speed and air flowrate.

Key dimensionless numbers (e.g. Power number, Froude number) and hydrodynamic parameters (e.g. tank-turnover time, air flow velocity) were found to lie within, or just outside, the ranges of values observed by other researchers. From this one may conclude that the mechanical flotation cells in the FCTR were operating under similar hydrodynamic conditions to typical industrial flotation cells.

Power Intensity

- Power intensities ranged between 1 and 4 kW/m^3 which is slightly above the power intensities found in industrial flotation cells but is within the range considered as typical for industrial platinum flotation cells.
- Power intensities increased with increasing impeller speed and decreased with increasing air flowrate (as expected).

Mixing

- A residence time distribution (RTD) test performed during the commissioning phase showed that the FCTR behaves as a series of well-mixed tanks

- Although mixing was not explicitly characterised, the ranges of Reynolds numbers, power intensities, impeller tip speeds and tank-turnover times observed during the study indicated that the FCTR cells were well mixed, in terms of both macro and micromixing.

Solids Suspension

- No sanding of the FCTR cells was observed under the hydrodynamic conditions used in the study, which indicates that the solids were reasonably well suspended.
- Although solids suspension was not explicitly characterised, the ranges of power intensities and tank-turnover times observed during the study indicated that solids were reasonably well suspended. In addition, the range of impeller speeds used in the study were found to be above the critical impeller speed for solids suspension.

Gas Dispersion

- Sauter mean bubble sizes ranged between 1.5 and 1.9 mm which is within the range considered as typical for industrial platinum flotation cells. Bubble size decreased with increasing impeller speed and increased with increasing air flowrate (as expected).
- Superficial gas velocities ranged between 0.90 and 1.15 cm/s which is towards the lower end of the range considered as typical for industrial platinum flotation cells. Superficial gas velocity increased with increasing air flowrate (as expected) but also increased with increasing impeller speed, which suggests that gas dispersion was not ideal at the lower impeller speeds.
- Bubble surface area fluxes ranged between 30 and 40 s^{-1} which is towards the lower end of the range considered as typical for industrial platinum flotation cells. Bubble surface area flux increased with increasing impeller speed and air flowrate (as expected), although the effects of air flowrate were less pronounced.
- In general, the gas dispersion results showed that the FCTR cells were operating under similar conditions to those encountered in industrial platinum flotation cells. However, gas dispersion parameters were generally towards the lower (poorer) end of this range and were fairly insensitive to changes in impeller speed and air flowrate.

5.2 Flotation Conclusions

The results for the flotation section of the study were obtained through a sampling campaign conducted on the FCTR and the subsequent assay, mass balancing and regression analysis of the data. The results from the statistical analysis of the flotation data were used to plot a number of relationships. The following conclusions were drawn based on these results:

Rougher Feed

- Considerable statistical error was observed in the CCRD regression analysis of the rougher feed (i.e. results are poor).
- Recovery increased with increasing feed grade, which is a common finding in the flotation literature. In general, recovery increased with increasing impeller speed and air flowrate, although this was strongly dependent on the feed grade.
- No relationship between the flotation rate constant and bubble surface area flux was observed. Increases in the power intensity had no effect on the flotation rate constant in the first rougher cell but had a significant effect on the flotation rate constant in the third rougher cell.
- No conclusions may be made regarding the effect of impeller speed and air flowrate on the concentrate grade as unexpected results were obtained. This is attributed to the high statistical error in the rougher feed data.

Cleaner Tails

- Minimal statistical error was observed in the in the CCRD regression analysis of the cleaner tails (i.e. results are good).
- As per the rougher feed results, recovery increased with increasing feed grade. However, recovery increased significantly with increasing impeller speed and air flowrate, for all feed grades.
- A weak relationship between the flotation rate constant and bubble surface area flux was observed. Increases in the power intensity led to significant increases in the flotation rate constant in both the first and third cleaner cells.
- Concentrate grade decreased significantly with increasing impeller speed and air flowrate.

In general, the results tend to follow the types of trends observed in the flotation literature. For example, increases in recovery with increasing feed grade, impeller speed and air flowrate are common findings. However, the results show (at best) a very weak relationship between the flotation rate constant and the bubble surface area flux. This does not support the k-Sb relationship observed in the flotation literature and suggest that this relationship does not hold for platinum. However, the results demonstrate clearly that increasing the power intensity has a beneficial effect on the rate of flotation of platinum, particularly in cells further down the bank. This suggest that increasing the power intensity improves the rate of flotation of finer or slow floating material which is the common opinion in the platinum industry. Unfortunately, these increases are generally accompanied by significant decreases in concentrate grade. This may be due to simple factors, such

as increases in entrainment, or due to increases in the rate of flotation of poorly liberated, slow floating particles at higher levels of agitation. This would have to be ascertained through a mineralogical study of the flotation concentrate, which was not done as part of this study.

REFERENCES

1. Abrahamson, J., 1975. Collision rates of small particles in a vigorously turbulent fluid. Chem. Eng. Sci., 30: 1371-1379.

2. Agar, G.E. and Kipkie, W.B., 1978. Predicting locked cycle flotation test results from batch data. CIM Bull., November 1978: 119-125.

3. Agar. G.E., Stratton-Crawley, R. and Bruce, T.J., 1980. Optimizing the design of flotation circuits. CIM Bulletin, December 1980: 1-9. In: Kalapudas, R., 1985. *Op cit.*

4. Ahmed, N. and Jameson, G.J., 1989. Flotation kinetics. Miner. Process. Extract. Metall. Rev., 5: 77-99.

5. Ahmed, N. and Jameson, G.J., 1985. The effect of bubble size on the rate of flotation of fine particles. Int. J. Miner. Process., 14: 195-215.

6. Amelunxen, R.L., 1990. Column flotation: New carrying capacity considerations for scale-up. Cominco Engineering Services Ltd report.

7. Anfruns, J.F. and Kitchener, J.A., 1977. The rate of capture of small particles in flotation. Trans. Inst. Min. Metall., 86: C9-C15.

8. Anon., 1999. AMIRA P9 Project Brief – The Optimisation of Mineral Processes by Modelling and Simulation.

9. Anon., 1999. AMIRA Project P9M: Minerals Processing 2000-2003. Project proposal.

10. Anon., 1982. Selective flotation: An art as well as a science. Miner. Eng., March 1982: 275-279.

11. Anon., 1998. Svedala Flotation Machines. Svedala marketing brochure.

12. Anon., 1999. Senmin marketing brochure.

13. Arbiter, N. *et al*, 1978. Mineral processing plant design. In Conceptual Design of Flotation Circuits. SME/AIME, New York. pp 447-465. In Arbiter, N., 1999. *Op cit.*

14. Arbiter, N., 1984. The flotation cell – a critique. Principles of Mineral Flotation: 301-311.

15. Arbiter, N., 1999. Development and scale-up of large flotation cells. In B.K. Parekh and J.D. Miller (Editors). Advances in Flotation Technology. SME, Colorado. pp 345-352

16. Arbiter, N. and Harris, C.C., 1969. Impeller speed and air rate in the optimization and scale-up of flotation machinery. Trans. S.M.E., 244: 115-117.

17. Arbiter, N., Harris, C.C. and Yap, R.F., 1968. A hydrodynamic approach to flotation scale-up. VIII International Mineral Processing Congress. Leningrad. Paper D19. In: Arbiter, N. and Harris, C.C., 1969. *Op cit.*

18. Arbiter, N., Harris, C.C. and Yap, R.F., 1969. Hydrodynamics of flotation cells. S.M.E. Trans., 244: 134-148.

19. Arbiter, N. and Steininger, J., 1965. Hydrodynamics of flotation machines. Miner. Process.: 595-608.

20. Arbiter, N. and Weiss, N.L., 1970. Design of flotation cells and circuits. S.M.E. Trans., 247: 340-347.

21. Arbiter, N., Harris, C.C. and Yap, R.F., 1976. The air flow number in flotation machine scale-up. International Journal Mineral Processing, 3: 257-280.

22. Armenante, P.M., Huang, Y-T and Li, T., 1992. Determination of the minimum agitation speed to attain the just dispersed state in solid-liquid and liquid-liquid reactors provided with multiple impellers. Chem. Eng. Sci., Vol.47 No. 9-11: 2685-2870

23. Barbery, G., Bourassa, M. and Maachar, A., 1986. Laboratory testing for flotation circuit design. In A.L. Mular and M.A. Anderson (Editors). Design and Installation of Concentration and Dewatering Circuits. SME, Colorado, pp 419-432.

24. Belugou, P. and Dru, G., 1958. The treatment of slurry by flotation. Third Int. Coal Prep. Conf. Proc., Liège 1958: 469:480

25. Bezuidenhout, G., 1998. Selection criteria for flotation equipment. In Minerals Processing Design School. SAIMM, Johannesburg.

26. Bojcevski, D., Vink, L., Johnson, N.W., Landmark, V., Johnston, M., Mackenzie, J. and Young, M.F., 1998. Metallurgical characterisation of George Fisher ore textures and implications for ore processing. Mine to Mill Conference Proceedings 1998. AusIMM, Melbourne. pp. 29-42.

27. Bourassa, M., Barbery, G., Broussard, A. and Conil, P., 1988. Flotation kinetics scale-up: Comparison laboratory batch tests to pilot plant processing. XVI Int. Miner. Process. Cong.: 579-588.

28. Box, G.E.P. and Hunter, J.S., 1957. Multi-factor experimental design for exploring response surfaces. Annals of Math. Stats., 28 (1), March: 195-241. In Napier-Munn, 2000b. *Op cit.*

29. Box, G.E.P. and Wilson, K.B., 1951. On the experimental attainment of optimum conditions. J. Royal Stat. Soc., Series B, 13 (1): 1-45. In Napier-Munn, 2000b. *Op cit.*

30. Bratby, J. and Marais, G.V.R., 1977. Flotation. In D.B. Purchas (Editor), Solid/Liquid separation equipment scale-up. Uplands Press, Croydon, pp 155-198

31. Cochran, W.G. and Cox, G.M., 1966. Experimental designs. Wiley (2nd Ed., 6th printing). In Napier-Munn, 2000b. *Op cit.*

32. Corrans, I.J., Brugman, C.F., Overbeek, P.J. and McRae, L.B., 1982. The recovery of platinum-group metals from ore of the UG-2 Reef in the Bushveld Complex. Proc. 12th CMMI Cong.: 629-634

33. Darley, P., 1998. Scale-up of flotation circuits. In Minerals Processing Design School. SAIMM, Johannesburg.

34. Deglon, D.A., 1998. A hydrodynamic investigation of fine particle flotation in a batch flotation cell. Ph.D. Thesis, University of Cape Town.

35. Deglon, D.A., 1999. Flotation cell operation and design – what the researchers think. University of Cape Town presentation.

36. Deglon, D.A. and Franzidis, J-P, 1999. Review of hydrodynamics and gas dispersion in flotation cells on South African PGM concentrators. AMIRA P9L Progress Report.

37. Deglon, D.A., Sawyerr, F. and O'Connor, C.T., 1999. A model to relate the flotation rate constant and the bubble surface area flux in mechanical flotation cells. Miner. Eng., 12: 599-608.

38. Deglon, D.A., Egya-Mensah, D. and Franzidis, J-P, 2000. Review of hydrodynamics and gas dispersion in flotation cells on South African platinum concentrators. Miner. Eng., 13: 235-244.

39. Degner, V.R., 1979. Design Consideration in Large Flotation Machine Development. Wemco Publication.

40. Degner, V.R., 1980. Engineering and design considerations in scale-up to 28.3 m^3 (1000 cu-ft) flotation machines. Transactions SME, 268: 1857-1865.

41. Degner, V.R., 1985. Hydrodynamic influences in flotation machine design. SME-AIME Preprint 85-41. In Barbery *et al*, 1986. *Op cit.*

42. Degner, V.R., Sabey, J.B. and MacGillivray, D., 1981. Coarse potash flotation machine design advances. Wemco Publication.

43. Diaz-Penafiel, P. and Dobby, G.S., 1994. Kinetic studies in flotation columns: Bubble size effect. Miner. Eng., 7: 465-478.

44. Dowling, E.C., Klimpel, R.R. and Aplan, F.F., 1985. Model discrimination in the flotation of a porphyry copper ore. Miner. Metall. Trans., 2: 87-101. In Barbery *et al*, 1986. *Op cit.*

45. Egya-Mensah, D., 1998. Hydrodynamics and gas dispersion in industrial flotation cells. MSc Thesis, University of Cape Town.

46. Ek, C., 1992. Flotation kinetics. In P. Mavros and K.A. Matis (Editors), Innovations in Flotation Technology. Kluwer Academic Publishers, Netherlands, pp. 183-210.

47. Fahrenweld, A.W., 1946. The submergence factor in the impeller type of flotation machines. Trans. A.I.M.E., 169: 440 in Arbiter and Steininger, 1962. *Op Cit.*

48. Fallenius, K., 1987. Turbulence in flotation cells. International Journal Mineral Processing, 21: 1-23.

49. Fichera, M.A. and Chudacek, M.W., 1992. Batch cell flotation models – a review. Miner. Eng., Vol. 5, No. 1: 41-55. In Harris, M.C., 1998. *Op cit.*

50. Forss, M. and Hindstrom, S., 1993. The role of mixing and energy consumption in the flotation of different size particles. Proc. Konferens in Mineralteknik, Lulea Uni. of Tech., Sweden: 185-194

51. Frew, J.A. and Trahar, W.J., 1982. Roughing and cleaning flotation behaviour and the realistic simulation of complete plant performance. Int. Jour. Miner. Process. 9. In: Manlapig, E.V., 1996. *Op cit.*

52. Gorain, B.K., 1998. Characterisation studies in a 154m^3 WEMCO flotation cell at the Ernest Henry concentrator. JKMRC Report.

53. Gorain, B.K., Franzidis, J.-P. and Manlapig, E.V., 1997. Bubble surface area flux: A new criterion to evaluate flottaion cell performance.

54. Gorain, B.K., Franzidis, J.-P. and Manlapig, E.V., 1995a. Effect of bubble size, gas holdup and superficial gas velocity on metallurgical performance in an industrial scale flotation cell. Colloquium on Downstream Processing. SAIMM, Randburg.

55. Gorain, B.K., Franzidis, J.-P. and Manlapig, E.V., 1995b. Effect of impeller type, impeller speed and air flow rate in an industrial scale flotation cell – Part 1: Effect on bubble size distribution. Miner. Eng. Vol. 8 No. 6: 615-635.

56. Gorain, B.K., Franzidis, J.-P. and Manlapig, E.V., 1995c. Effect of impeller type, impeller speed and air flow rate in an industrial scale flotation cell – Part 2: Effect on gas holdup. Miner. Eng. Vol. 8 No. 12: 1557-1570.

57. Gorain, B.K., Franzidis, J.-P. and Manlapig, E.V., 1996a. Effect of impeller type, impeller speed and air flow rate in an industrial scale flotation cell – Part 3: Effect on superficial gas velocity. Miner. Eng. Vol. 9 No. 6: 639-654.

58. Gorain, B.K., Manlapig, E.V. and Franzidis, J.-P., 1996b. The effect of gas dispersion properties on the kinetics of flotation. In: C.O. Gomez and J.A. Finch (Editors). Proceedings of the International Symposium of Column Flotation. Montreal: 299-313.

59. Gorain, B.K., Franzidis, J.-P. and Manlapig, E.V., 1997. Studies on impeller type, impeller speed and air flow rate in an industrial scale flotation cell - Part 4: Effect of bubble surface area flux on flotation kinetics. Miner. Eng., Vol. 10, No. 4: 367-379. In: Harris, M.C., 1998. *Op cit.*

60. Griffiths, M., 1998. Of Mines and Men: Australia's 20th Century Mining Miracle 1945-1985. Kangaroo Press, Sydney.

61. Harris, M.C., 1998. The use of flotation plant data to simulate flotation circuits. In Minerals Processing Design School. SAIMM, Johannesburg.

62. Hochreiter, R.C., Kennedy, D.C., Muir, W. and Woods, A.I., 1985. Platinum in South Africa. J. S. Afr. Inst. Min. Metall., Vol. 85, No. 6: 165-185.

63. Horst, W.E., 1958. Scale-up relationships in spodumene flotation. Trans. A.I.M.E., 211: 1182 in Arbiter and Steininger, 1962 *Op cit.*

64. Imaizumi, T. and Inoue, T., 1963. Kinetic considerations of froth flotation. Proceedings VI International Mineral Processing Congress, Pergamon. pp 581-593. In Barbery *et al*, 1986. *Op cit.*

65. Immink, R., 1999a. Personal communication. 23rd August, 1999.

66. Imminck, R., 1999b. Personal communication. 14th September, 1999.

67. Inoue, T., Nonaka, M. and Imaizumi, T., 1986. Flotation kinetics – Its macro and micro structure. In: P. Somasundran (Editor), Advances in Mineral Processing. S.M.E., Colorado, pp. 209-228.

68. Jameson, G.J., 1984. Physical aspects of fine particle flotation. In: R. Moore (Editor), Principles of Mineral Flotation (The Wark Symposium). Australas. Inst. Min. Metall., pp. 215-232.

69. Jameson, G.J. and Allum, P., 1984. A survey of bubble sizes in industrial flotation cells. Report prepared for AMIRA Ltd.

70. Jameson, G.J., Nam, S. and Moo Young, M., 1977. Physical factors affecting recovery rates in flotation. Min. Sc. Eng., 9: 103-118. In: Manlapig, E.V., 1996. *Op cit.*

71. Jonaitis, A.J., 1999. Design, development, application and operating benefits of $100m^3$+ Outokumpu TankCell flotation cells. In B.K. Parekh and J.D. Miller (Editors). Advances in Flotation Technology. SME, Colorado. pp 371-380

72. Kalapudas, R., 1985. A study on scaling-up of laboratory batch flotation data to industrial size flotation. Proceedings XV International Mineral Processing Congress, Cannes, Vol. 2. pp112-121

73. Kalapudas, R. and Kallioinen, J., 1988. The design of industrial flotation circuits on the basis of continuously operating laboratory-scale minipilot flotation machinery. In E. Forssberg (Editor). XVI International Mineral Processing Congress. Elsevier, Amsterdam. pp 469-480

74. Kerr, M., 1999. Personal communication. 24th August 1999.

75. Knopjes, B., 2000. Personal communication. 23rd February 2000.

76. Laplante, A.R., Kaya, M. and Smith, H.W., 1989. The effect of froth on flotation kinetics – a mass transfer approach. Miner. Process. Extr. Metall. Rev. Vol. 5:147 – 168.

77. Laskowski, J.S., 1989. Thermodynamic and kinetic flotation criteria. Miner. Process. Extr. Metall. Rev., 5: 25-41.

78. Lawes, G., 1999. Personal Communication. 24th August 1999.

79. Luttrell, G.H., Mankosa, M.J. and Yoon R-H., 1993. Design and scale-up criteria for column flotation. XVIII International Mineral Processing Congress. Sydney. pp785-791

80. Lynch, A.J., Johnson, N.W., Manlapig, E.V. and Thorne, C.G., 1982. Mineral and coal flotation circuits, their simulation and control. Elsevier, Amsterdam.

81. Manlapig, E., 2000. Personal communication. 4th April 2000.

82. Manlapig, E. (Editor), 1996. The optimisation of mineral processes by modelling and simulation. Vol. 2: Flotation. Julius Kruttschnitt Mineral Research Centre, Brisbane.

83. Mathe, Z.T., Harris, M.C., O'Connor, C.T. and Franzidis, J.-P., 1998. Review of froth modelling in steady state systems. Miner. Eng. Vol. 11, No. 5: 397-421. In: Harris, M.C., 1998. *Op cit.*

84. Mavros, P., 1992. Mixing and hydrodynamics in flotation cells. In *Innovations in Flotation Technology*, ed. P. Mavros and K.A. Matis, Kluwer Academic Publishers, Netherlands, pp. 211-234.

85. Mika, T.S. and Fuerstenau, D.W., 1968. A microscopic model of the flotation process. Proc. 8th Inter. Miner. Process. Conf., Leningrad: 246-269. In: Ahmed, N. and Jameson, G.J., 1989. *Op cit.*

86. Miller, K.J., 1988. Novel flotation technology – A survey of equipment and processes. S.M.E. Conf., Hidden Valley, Somerset: 347-363.

87. Napier-Munn, T., 2000a. Analysis of CCRD data from FCTR experiments. JKMRC Memorandum.

88. Napier-Munn, T., 2000b. The central composite rotatable experimental design. JKMRC Memorandum.

89. Niiti, T., 1999. Personal communication. 8th September, 1999.

90. Oyama, Y. and Endoh, K., 1955. Power correlations of gas-liquid contacting mixers. Chem. Eng., Tokyo, 19: 2 in Arbiter and Steininger, 1962. *Op cit.*

91. Pavlushenko, I.S., Kostin, N.M. and Mateev, 1957. Stirrer speeds in the stirring of suspension. Priklad. Khim. Vol. 30, No. 8: 1160-1169 in Arbiter *et al*, 1969. *Op cit.*

92. Rahal, K. R., 1999. The development of the Wemco Floatability Characterisation Test Rig (FCTR). In: AMIRA P9L Project Final Report. Volume 2: Flotation: 351-357.

93. Rahal, K.R., 2000.Flotation plant modelling and simulation using the Floatability Characterisation Test Rig (FCTR). AMIRA P9M Project First Progress Report, May 2000. Chapter 16: 209-221.

94. Read, T.A., 1933. An investigation into the mechanical efficiency of impellers for machines working the flotation process. Proc. Aust. Inst. Min. Metall., 91: 337 in Arbiter and Steininger, 1962. *Op cit.*

95. Rose, E.H., 1946. AIME Trans. Vol. 169: 93-94. In Arbiter, 1999. *Op cit.*

96. Rushton, J.H., Costich, E.W. and Everett, H.J., 1950. Power characteristics of mixing impellers. Chem. Eng. Porgress, 46: 395 in Arbiter and Steininger, 1962. *Op cit.*

97. Schubert, H. and Bischofberger, C., 1978. On the hydrodynamics of flotation machines. International Journal Mineral Processing, 5: 132-142.

98. Schubert, H., Bishofberger, C. and Koch, P., 1982. On the influence of hydrodynamics in flotation processes. XIV Int. Min. Proc. Cong., Toronto. Paper IV-15.

99. Schulz, N.F., 1970. Separation efficiency. Trans. SME/AIME 247, 81. In: Kalapudas, R., 1985. *Op cit.*

100. Schulze, H.J., 1984. Physico-chemical elementary processes in flotation. Elsevier, Amsterdam.

101. Schulze, H.J., 1989. Hydrodynamics of bubble-mineral particle collisions. Miner. Process. Extr. Metall. Rev., 5: 43-76.

102. Sivamohan, R., 1990. The problem of recovering very fine particles in mineral processing – A review. Int. J. Miner. Process., 28: 247-288

103. Skillen, A., 1993. Froth flotation – New technologies bubbling under. Ind. Miner., February: 48-54.

104. Spada, M., 1981. Essai de standardisation dans la determination d'un circuit de flottation. Rev. Ind. Miner. – Les Techniques, 63: 411-416. In: Bourassa *et al*, 1988. *Op cit.*

105. Strohmayr, S.J., Barns, K.E., Brindley, S.K. and Munro, P.D., 1998. Mineralogy controlling metallurgy at Ernest Henry Mining. Mine to Mill Conference Proceedings 1998. AusIMM, Melbourne. pp. 13-18.

106. Taggart, A.F., 1945. Handbook of Mineral Dressing: Ores and Industrial Minerals. J. Wiley and Sons, New York.

107. Trahar, W.J. and Warren, L.J., 1976. The floatability of very fine particles – A review. Int. J. Miner. Process., 3: 103-131.

108. Tomlinson, H.S. and Fleming, M.G., 1965. Flotation rate studies. Proceedings of the 6th Int. Miner. Process. Cong., Pergamon: 563-579. In: Inoue *et al*, 1986. *Op cit.*

109. Varbanov, R., Forssberg, E. and Hallin, E., 1993. On the modeling of the flotation process. Int. Jour. Miner. Process. 3: 27-43. In: Manlapig, E.V., 1996. *Op cit.*

110. Vermaak, C.F., 1995. Platinum-group metals, a global perspective. Mintek Publication: 8-20, 85-91.

111. Weber, A., Walker, C., Redden, L., Lelinski, D. and Ware, S., 1999. Scale-up and design of large-scale flotation equipment. In B.K. Parekh and J.D. Miller (Editors). Advances in Flotation Technology. SME, Colorado.. pp 353-370

112. Wills, B.A., 1988. Mineral processing technology (4th Edition). Pergamon, Oxford.

113. Wrigley, R., 1999. Personal communication. 22nd September, 1999.

114. Yoon, R.H., 1993. Microbubble flotation. Miner. Eng., 6: 619-630.

115. Yoon, R.H. and Luttrell, G.H., 1989. The effect of bubble size on fine particle flotation. Miner. Process. Extr. Metall. Rev., 5: 101-122.

116. Zwietering, T.N., 1958. Suspending of solid particles in liquids by agitators. Chem. Eng. Sci. 8: 244-253. In: Arbiter *et al*, 1969. *Op cit.*

APPENDIX A:

HYDRODYNAMIC DATA

SUPERFICIAL GAS VELOCITY MEASUREMENTS

ROUGHER FEED

Impeller Speed(%)	Air Flow(l/s)	Time (s)					Average (s)	Jg (cm/s)
55	120	40.65	38.73	41.58	41.01	41.66	40.73	1.02
57.9	100	41.88	42.54	40.87	42.31	40.70	41.66	1.00
	140	39.69	40.23	39.22	39.85		39.75	1.05
65	90	41.37	40.09	43.09	40.98		41.38	1.00
	120	38.12	36.65	38.27	36.65		37.42	1.11
	140	36.06	35.69	37.75	37.09		36.65	1.13
	150	36.16	35.24	36.06	37.85		36.33	1.14
72.1	100	45.70	45.71	43.59	45.98		45.25	0.92
	140	37.42	37.30	37.30	37.17		37.30	1.11
75	120	37.21	37.91	37.36	38.84		37.83	1.10

CLEANER TAILS

Impeller Speed(%)	Air Flow(l/s)	Time (s)					Average (s)	Jg (cm/s)
50	170	41.65	42.57	41.08	41.49		41.70	1.00
52.9	150	43.24	43.80	44.37	42.76		43.54	0.95
	190	38.50	39.23	39.61	39.57		39.23	1.06
60	140	41.31	39.31	42.08	41.96		41.17	1.01
	170	37.89	39.18	38.37	39.46	40.65	39.11	1.06
	190	36.91	36.03	37.51	36.37		36.71	1.13
	200	36.66	35.19	36.95	35.14		35.99	1.15
67.1	150	39.51	39.77	40.46	41.44		40.30	1.03
	190	36.52	35.95	36.79	37.40		36.67	1.13
70	170	37.65	37.06	38.27	40.00		38.25	1.09

BUBBLE SIZE MEASUREMENTS

ROUGHER FEED

Impeller	Air	Surface Area	Volume	Sauter Mean	Ave d32
55	120	11659.3	3.6	1.85	1.87
		11900.8	3.7	1.87	
		12497.7	3.9	1.87	
		12583	4	1.91	
		9937.7	3.1	1.87	

Impeller	Air	Surface Area	Volume	Sauter Mean	Ave d32
57.9	100	12257	3.7	1.81	1.78
		13158.7	4	1.82	
		12945.1	3.8	1.76	
		12334.5	3.6	1.75	
		12286.5	3.6	1.76	
		12067	3.6	1.79	

Impeller	Air	Surface Area	Volume	Sauter Mean	Ave d32
57.9	140	12922	4	1.86	1.83
		12058.8	3.6	1.79	
		11674	3.6	1.85	
		12094.8	3.65	1.81	
		12051	3.7	1.84	

Impeller	Air	Surface Area	Volume	Sauter Mean	Ave d32
65	90	10758.5	3.4	1.90	1.80
		13377.3	4	1.79	
		10409.5	3	1.73	
		8658.4	2.9	2.01	
		11535.9	3	1.56	

Impeller	Air	Surface Area	Volume	Sauter Mean	Ave d32
65	120	10723	3	1.68	1.71
		11164.6	3.1	1.67	
		11200.5	3.1	1.66	
		11275.2	3.4	1.81	
		10710	3	1.68	
		8296	2.4	1.74	

Impeller	Air	Surface Area	Volume	Sauter Mean	Ave d32
65	140	11218.1	3.1	1.66	1.79
		10810.2	3	1.67	
		10233.6	2.9	1.70	
		9855.2	2.9	1.77	
		9187.7	3	1.96	
		9839.6	3	1.83	
		9620.9	2.7	1.68	
		8309.8	2.9	2.09	

Impeller	Air	Surface Area	Volume	Sauter Mean	Ave d32
65	150	10729.2	3.1	1.73	1.77
		10877.2	3.2	1.77	
		11065.1	3.3	1.79	
		10231.2	3.1	1.82	
		10666.6	3	1.69	
		10658	3.2	1.80	

Impeller	Air	Surface Area	Volume	Sauter Mean	Ave d32
72.1	100	13081.9	4	1.83	1.85
		12712.2	4	1.89	
		12275.3	4	1.96	
		13349.5	3.9	1.75	
		11955	3.7	1.86	
		12786.3	3.9	1.83	

Impeller	Air	Surface Area	Volume	Sauter Mean	Ave d32
72.1	140	13175.1	4.1	1.87	1.86
		13368	4.1	1.84	
		14149.2	4.4	1.87	
		13022.9	4	1.84	
		12882.6	4	1.86	
		13906.3	4.3	1.86	
		14414.4	4.19	1.74	
		12438.7	4.1	1.98	

Impeller	Air	Surface Area	Volume	Sauter Mean	Ave d32
75	120	11830	3.4	1.72	1.76
		12300.2	3.8	1.85	
		13073.9	3.9	1.79	
		12934.3	3.65	1.69	
		13408.7	3.9	1.75	

CLEANER TAILS

Impeller	Air	Surface Area	Volume	Sauter Mean	Ave d32
50	170	9131.5	2.25	1.48	1.60
		9592.5	2.5	1.56	
		8804.2	2.5	1.70	
		9192.8	2.6	1.70	
		9151	2.4	1.57	
		8717.6	2.34	1.61	

Impeller	Air	Surface Area	Volume	Sauter Mean	Ave d32
52.9	150	9754	2.6	1.60	1.57
		8754	2.3	1.58	
		8219.3	2.2	1.61	
		8909.5	2.2	1.48	

Impeller	Air	Surface Area	Volume	Sauter Mean	Ave d32
52.9	190	7834.2	2.09	1.60	1.59
		9397.3	2.5	1.60	
		9475.5	2.5	1.58	
		9296.4	2.34	1.51	
		8600.5	2.4	1.67	
		8868.4	2.3	1.56	

Impeller	Air	Surface Area	Volume	Sauter Mean	Ave d32
60	140	10509.9	3	1.71	1.54
		11707.9	2.9	1.49	
		10361.8	2.8	1.62	
		10664	2.7	1.52	
		11617.7	2.8	1.45	
		10935.6	2.7	1.48	

Impeller	Air	Surface Area	Volume	Sauter Mean	Ave d32
60	170	11361.6	2.9	1.53	1.55
		10136.3	2.7	1.60	
		11922.7	3.1	1.56	
		12062.4	3.1	1.54	
		13043	3.4	1.56	
		13305.7	3.4	1.53	

Impeller	Air	Surface Area	Volume	Sauter Mean	Ave d32
60	190	9907.2	2.7	1.64	1.59
		12518.8	3.3	1.58	
		12512.1	3.3	1.58	
		11590.5	3	1.55	
		12463.3	3.3	1.59	
		11887.7	3.2	1.62	

Impeller	Air	Surface Area	Volume	Sauter Mean	Ave d32
60	200	11027.5	3.1	1.69	1.71
		10996.9	3.1	1.69	
		10636.7	3	1.69	
		10690.6	3	1.68	
		10390.2	3.1	1.79	

Impeller	Air	Surface Area	Volume	Sauter Mean	Ave d32
67.1	150	8709.4	2.2	1.52	1.51
		9120.5	2.2	1.45	
		9420.7	2.4	1.53	
		8462.2	2.2	1.56	
		10566.8	2.8	1.59	
		8927.8	2.09	1.40	

Impeller	Air	Surface Area	Volume	Sauter Mean	Ave d32
67.1	190	8652.3	2.5	1.73	1.67
		9599	2.5	1.56	
		8870.3	2.5	1.69	
		9171.8	2.6	1.70	
		9066.3	2.5	1.65	

Impeller	Air	Surface Area	Volume	Sauter Mean	Ave d32
70	170	8695.3	2.3	1.59	1.53
		8823.2	2.3	1.56	
		9144.2	2.25	1.48	
		9060.1	2.25	1.49	

POWER INTENSITY AND BUBBLE SURFACE AREA FLUX

Rougher Feed			Cleaner Tails		
Test	P/V	Sb	Test	P/V	Sb
A	2.19	33.7	*AC*	2.27	36.4
B	2.09	39.1	*AD*	2.51	40.9
C	1.62	34.4	*AE*	1.49	40.1
D	2.22	39.1	*AF*	2.51	40.9
E	2.45	35.9	*AG*	2.01	40.6
F	3.63	29.8	*AH*	2.78	41.0
G	1.67	37.8	*AI*	1.95	42.6
H	1.76	38.7	*AJ*	1.58	40.4
I	2.01	39.1	*AK*	2.51	40.9
J	1.46	39.1	*AL*	2.51	40.9
K	1.81	39.1	*AM*	2.51	40.9
L	2.97	33.4	*AN*	2.72	39.2
M	1.90	37.5	*AO*	2.47	42.8
N	1.72	32.7	*AP*	1.77	37.4
O	2.19	33.7	*AQ*	2.27	36.4
P	2.09	39.1	*AR*	2.51	40.9
Q	1.62	34.4	*AS*	1.49	40.1
R	2.22	39.1	*AT*	2.51	40.9
S	2.45	35.9	*AU*	2.01	40.6
T	3.63	29.8	*AV*	2.78	41.0
U	1.67	37.8	*AW*	1.95	42.6
V	1.76	38.7	*AX*	1.58	40.4
W	2.01	39.1	*AY*	2.51	40.9
X	1.46	39.1	*AZ*	2.51	40.9
Y	1.81	39.1	*BA*	2.51	40.9
Z	2.97	33.4	*BB*	2.72	39.2
AA	1.90	37.5	*BC*	2.47	42.8
AB	1.72	32.7	*BD*	1.77	37.4

APPENDIX B:

FLOTATION DATA

EXPERIMENTAL RAW DATA – ROUGHER FEED

Test A

Stream	Mass Flow (tph)	PGM (ppm)	Chrome (ppm)	% Solids	SG
Feed	1.274	2.47	25.44	40.11	3.63
Con 1	0.04392	36.87	10.73	16.11	3.5
Con 2	0.007014	37.20	6.59	23.80	3.3
Con 3	0.01068	20.50	9.50	29.20	3.36
Con 4	0.003496	24.53	7.91	20.20	3.42
Tail 4	1.294	1.21	27.15	42.62	3.78

Test B

Stream	Mass Flow (tph)	PGM (ppm)	Chrome (ppm)	% Solids	SG
Feed	1.192	2.34	25.31	36.24	3.66
Con 1	0.04239	33.00	11.00	14.37	3.39
Con 2	0.006541	35.73	7.77	26.90	3.29
Con 3	0.006575	26.20	8.58	26.40	3.3
Con 4	0.002399	24.80	8.29	13.60	3.61
Tail 4	1.412	1.3	25.93	38.81	3.7

Test C

Stream	Mass Flow (tph)	PGM (ppm)	Chrome (ppm)	% Solids	SG
Feed	1.260	2.59	24.72	37.51	3.68
Con 1	0.02361	42.00	8.61	14.90	3.29
Con 2	0.01173	27.00	9.90	19.20	3.32
Con 3	0.004944	23.20	8.50	28.80	3.28
Con 4	0.004625	19.13	8.56	34.20	3.35
Tail 4	1.434	1.29	26.90	39.25	3.68

Test D

Stream	Mass Flow (tph)	PGM (ppm)	Chrome (ppm)	% Solids	SG
Feed	1.240	2.55	24.68	36.83	3.61
Con 1	0.03648	33.87	9.72	14.60	3.38
Con 2	0.006957	30.73	6.02	28.10	3.26
Con 3	0.005675	21.27	7.94	21.80	3.29
Con 4	0.003057	18.93	9.02	23.40	3.35
Tail 4	1.595	1.19	27.39	39.13	3.71

Test E

Stream	Mass Flow (tph)	PGM (ppm)	Chrome (ppm)	% Solids	SG
Feed	1.252	2.24	24.46	37.07	3.59
Con 1	0.04192	31.47	10.94	12	3.35
Con 2	0.006934	28.73	7.23	33.3	3.26
Con 3	0.004454	19.90	9.00	26	3.29
Con 4	0.001679	23.53	7.70	14.5	3.35
Tail 4	1.390	1.37	24.35	40.26	3.65

Test O

Stream	Mass Flow (tph)	PGM (ppm)	Chrome (ppm)	% Solids	SG
Feed	1.230	2.16	25.83	36.74	3.44
Con 1	0.02961	47.10	7.15	30.5	3.25
Con 2	0.004820	42.67	5.25	26.3	3.22
Con 3	0.006487	18.50	9.55	33.3	3.36
Con 4	0.003215	19.70	8.02	17.9	3.27
Tail 4	1.337	1.54	28.02	37.11	3.61

Test P

Stream	Mass Flow (tph)	PGM (ppm)	Chrome (ppm)	% Solids	SG
Feed	1.226	2.32	25.77	37.16	3.43
Con 1	0.03291	38.40	9.05	16.09	3.34
Con 2	0.005968	35.30	5.93	28.5	3.25
Con 3	0.007539	23.80	8.54	29.5	3.3
Con 4	0.003583	26.60	7.63	35.6	3.27
Tail 4	1.644	0.98	27.63	38.73	3.67

Test Q

Stream	Mass Flow (tph)	PGM (ppm)	Chrome (ppm)	% Solids	SG
Feed	1.290	2.27	25.58	39.04	3.41
Con 1	0.03045	56.90	7.67	37.2	3.28
Con 2	0.009454	32.50	7.45	27.2	3.26
Con 3	0.008219	28.80	7.47	24.6	3.26
Con 4	0.004046	24.80	7.55	32.4	3.27
Tail 4	1.354	1.26	26.43	39.36	3.64

Test R

Stream	Mass Flow (tph)	PGM (ppm)	Chrome (ppm)	% Solids	SG
Feed	1.305	2.37	25.91	39.49	3.42
Con 1	0.03700	46.67	8.35	21.38	3.31
Con 2	0.006407	38.80	5.99	26	3.26
Con 3	0.01188	21.20	10.12	36.2	3.38
Con 4	0.004091	26.80	7.64	32.69	3.29
Tail 4	1.573	1.35	26.61	40.44	3.66

Test S

Stream	Mass Flow (tph)	PGM (ppm)	Chrome (ppm)	% Solids	SG
Feed	1.295	2.37	25.17	37.7	3.39
Con 1	0.04413	40.00	11.13	14.69	3.45
Con 2	0.008558	34.53	7.58	19	3.27
Con 3	0.008558	28.80	9.53	16.6	3.4
Con 4	0.002616	28.60	7.68	18.1	3.28
Tail 4	1.758	1.29	25.96	40.47	3.58

Test F

Stream	Mass Flow (tph)	PGM (ppm)	Chrome (ppm)	% Solids	SG
Feed	1.497	1.92	24.49	43.97	3.58
Con 1	0.04668	23.40	11.95	11.9	3.38
Con 2	0.006044	34.50	6.37	22	3.44
Con 3	0.006124	21.70	8.51	27.7	3.38
Con 4	0.002620	23.13	7.37	21.41	3.69
Tail 4	1.432	1.20	25.12	48.84	3.69

Test T

Stream	Mass Flow (tph)	PGM (ppm)	Chrome (ppm)	% Solids	SG
Feed	1.254	2.32	25.05	38.19	3.37
Con 1	0.03892	42.10	6.32	14.9	3.24
Con 2	0.006106	24.40	8.96	24.1	3.38
Con 3	0.01179	24.70	9.19	29.9	3.41
Con 4	0.005046	45.30	9.44	17.9	3.44
Tail 4	1.304	1.36	26.07	40.4	3.6

Test G

Stream	Mass Flow (tph)	PGM (ppm)	Chrome (ppm)	% Solids	SG
Feed	1.257	1.96	24.42	36.7	3.61
Con 1	0.02951	31.6	9.18	13.9	3.3
Con 2	0.007377	24.00	6.62	27.5	3.25
Con 3	0.004695	17.00	8.61	25.9	3.32
Con 4	0.002264	25.30	7.33	18.8	3.4
Tail 4	1.453	1.15	26.45	38.52	3.65

Test U

Stream	Mass Flow (tph)	PGM (ppm)	Chrome (ppm)	% Solids	SG
Feed	1.228	2.33	25.21	36.45	3.38
Con 1	0.04047	45.30	9.44	22.2	3.42
Con 2	0.008124	27.50	7.65	16.8	3.29
Con 3	0.008787	20.90	9.74	26.3	3.42
Con 4	0.004919	24.90	9.37	20.1	3.4
Tail 4	1.122	1.39	25.75	37.87	3.58

Test H

Stream	Mass Flow (tph)	PGM (ppm)	Chrome (ppm)	% Solids	SG
Feed	1.210	2.23	24.32	36.8	3.44
Con 1	0.03775	38.40	9.43	15.9	3.32
Con 2	0.01108	26.10	8.14	18.6	3.27
Con 3	0.008884	16.20	10.70	15.1	3.33
Con 4	0.003415	22.20	8.43	11.6	3.63
Tail 4	1.354	1.21	26.08	39.6	3.63

Test V

Stream	Mass Flow (tph)	PGM (ppm)	Chrome (ppm)	% Solids	SG
Feed	1.275	2.34	25.83	37.14	3.41
Con 1	0.03101	45.00	9.78	20.1	3.44
Con 2	0.009903	31.73	8.70	16.8	3.39
Con 3	0.005105	24.73	10.04	26.3	3.46
Con 4	0.005141	22.50	9.21	20.1	3.41
Tail 4	1.491	1.24	27.45	38.32	3.65

Test I

Stream	Mass Flow (tph)	PGM (ppm)	Chrome (ppm)	% Solids	SG
Feed	1.218	2.54	24.89	36.82	3.38
Con 1	0.04757	35.60	8.71	22.89	3.38
Con 2	0.006945	31.67	6.23	30.4	3.65
Con 3	0.005469	21.33	7.60	22.4	3.35
Con 4	0.003967	18.53	10.00	28.2	3.38
Tail 4	1.395	1.24	26.5	37.89	3.68

Test W

Stream	Mass Flow (tph)	PGM (ppm)	Chrome (ppm)	% Solids	SG
Feed	1.244	2.12	25.17	37.13	3.4
Con 1	0.03290	44.93	8.91	24.79	3.4
Con 2	0.006503	33.60	7.11	30	3.26
Con 3	0.005187	25.53	7.90	17.4	3.28
Con 4	0.003518	25.33	7.97	17.8	3.27
Tail 4	1.448	1.41	27	38.02	3.62

Test J

Stream	Mass Flow (tph)	PGM (ppm)	Chrome (ppm)	% Solids	SG
Feed	1.183	2.40	24.39	36.22	3.56
Con 1	0.03668	37.10	9.56	29.9	3.31
Con 2	0.006704	30.00	6.96	27.9	3.26
Con 3	0.005075	20.20	8.36	19.5	3.39
Con 4	0.003258	22.20	7.64	24	3.23
Tail 4	1.506	1.36	25.63	36.66	3.89

Test X

Stream	Mass Flow (tph)	PGM (ppm)	Chrome (ppm)	% Solids	SG
Feed	1.267	1.99	25.19	38.21	3.42
Con 1	0.04581	35.20	6.93	18.7	3.24
Con 2	0.006656	27.90	7.18	26.7	3.28
Con 3	0.003709	27.40	7.59	26.1	3.29
Con 4	0.003157	36.30	10.44	25.5	3.44
Tail 4	1.424	1.33	26.84	39.9	3.58

Test K

Stream	Mass Flow (tph)	PGM (ppm)	Chrome (ppm)	% Solids	SG
Feed	1.266	2.78	24.07	38.51	3.51
Con 1	0.02876	49.20	8.28	29.1	3.35
Con 2	0.006789	34.87	6.76	27.6	3.19
Con 3	0.005745	22.10	9.51	23.1	3.31
Con 4	0.004276	21.60	8.84	20.8	3.38
Tail 4	1.469	1.19	28.88	39.51	4.44

Test L

Stream	Mass Flow (tph)	PGM (ppm)	Chrome (ppm)	% Solids	SG
Feed	1.234	2.50	25.6	38.8	3.48
Con 1	0.03520	34.47	10.02	20	3.32
Con 2	0.006509	44.00	6.13	24.3	3.2
Con 3	0.006758	27.30	9.27	16.3	3.32
Con 4	0.004750	27.00	8.91	24.7	3.25
Tail 4	1.475	1.00	27.19	38.21	3.62

Test M

Stream	Mass Flow (tph)	PGM (ppm)	Chrome (ppm)	% Solids	SG
Feed	1.227	2.47	25.8	36.47	3.26
Con 1	0.04632	29.80	11.77	16.69	3.38
Con 2	0.005364	33.53	7.13	17.2	3.22
Con 3	0.007033	21.40	10.70	12.5	3.41
Con 4	0.002564	24.80	9.28	22.4	3.29
Tail 4	2.608	1.27	27.82	38.72	3.69

Test N

Stream	Mass Flow (tph)	PGM (ppm)	Chrome (ppm)	% Solids	SG
Feed	1.207	2.47	25.22	36.77	3.61
Con 1	0.03507	43.80	8.05	35.8	3.3
Con 2	0.007460	34.70	6.60	28.6	3.25
Con 3	0.005765	22.00	8.08	23.8	3.3
Con 4	0.002549	21.47	7.29	32.5	3.22
Tail 4	1.338	1.61	26.88	36.9	3.86

Test Y

Stream	Mass Flow (tph)	PGM (ppm)	Chrome (ppm)	% Solids	SG
Feed	1.269	2.51	24.66	40.62	3.4
Con 1	0.04120	36.30	10.44	17	3.45
Con 2	0.006264	39.70	6.79	24.6	3.25
Con 3	0.004757	28.10	7.63	18.4	3.3
Con 4	0.003672	27.50	8.03	22	3.32
Tail 4	1.436	1.40	26.89	43.01	3.6

Test Z

Stream	Mass Flow (tph)	PGM (ppm)	Chrome (ppm)	% Solids	SG
Feed	1.268	2.54	25.21	37.83	3.45
Con 1	0.02948	48.27	8.82	20.3	3.35
Con 2	0.004828	40.67	6.13	31.7	3.21
Con 3	0.007827	24.40	8.36	31.1	3.33
Con 4	0.003241	29.00	6.08	24.9	3.33
Tail 4	1.280	1.35	25.83	38.73	3.57

Test AA

Stream	Mass Flow (tph)	PGM (ppm)	Chrome (ppm)	% Solids	SG
Feed	1.209	2.38	25.12	36.26	3.46
Con 1	0.04468	36.60	10.86	17.5	3.48
Con 2	0.006609	36.73	7.24	22.3	3.24
Con 3	0.005811	21.20	10.32	19.9	3.43
Con 4	0.003282	24.67	10.23	18.7	3.41
Tail 4	1.615	1.33	28.42	38.17	3.6

Test AB

Stream	Mass Flow (tph)	PGM (ppm)	Chrome (ppm)	% Solids	SG
Feed	1.218	2.40	24.59	36.73	3.42
Con 1	0.02755	46.73	9.57	38	3.4
Con 2	0.006302	33.20	6.06	23.7	3.18
Con 3	0.005472	21.60	8.99	27.5	3.36
Con 4	0.003988	24.60	8.50	34.5	3.34
Tail 4	1.380	1.63	26.14	36.95	3.59

EXPERIMENTAL RAW DATA – CLEANER TAILS

Test AC

Stream	Mass Flow (tph)	PGM (ppm)	Chrome (ppm)	% Solids	SG
Feed	0.3442	4.08	9.40	13.49	3.3
Con 1	0.009142	31.3	1.03	3.41	3.31
Con 2	0.002326	57.5	4.01	2.54	3.24
Con 3	0.003732	15.30	11.29	2.72	3.27
Con 4	0.001819	33.00	10.40	2.42	3.34
Tail 4	0.3338	2.64	9.83	16.72	3.26

Test AD

Stream	Mass Flow (tph)	PGM (ppm)	Chrome (ppm)	% Solids	SG
Feed	0.3496	4.52	8.83	13.49	3.27
Con 1	0.02794	16.30	11.38	4.74	3.30
Con 2	0.01126	16	10.71	3.85	3.30
Con 3	0.008161	30.80	11.56	3.50	3.30
Con 4	0.005321	15.67	11.54	3.06	3.22
Tail 4	0.3572	1.84	8.72	24.17	3.30

Test AE

Stream	Mass Flow (tph)	PGM (ppm)	Chrome (ppm)	% Solids	SG
Feed	0.3263	4.28	9.12	12.88	3.3
Con 1	0.01835	20.7	11.01	4.03	3.30
Con 2	0.01373	15.80	11.18	3.98	3.30
Con 3	0.006661	19.60	12.29	3.13	3.28
Con 4	0.003178	21.65	12.08	2.58	3.24
Tail 4	0.3380	2.27	8.62	22.31	3.31

Test AF

Stream	Mass Flow (tph)	PGM (ppm)	Chrome (ppm)	% Solids	SG
Feed	0.3404	4.44	8.62	13.23	3.31
Con 1	0.02618	17.13	12.02	4.30	3.32
Con 2	0.01073	17.70	12.57	3.44	3.31
Con 3	0.002760	28.70	11.49	2.57	3.28
Con 4	0.004875	16.80	11.93	2.88	3.24
Tail 4	0.3194	1.97	9.28	21.70	3.34

Test AG

Stream	Mass Flow (tph)	PGM (ppm)	Chrome (ppm)	% Solids	SG
Feed	0.3446	4.13	9.24	13.98	3.28
Con 1	0.01286	46.90	11.64	3.51	3.27
Con 2	0.02183	17.87	11.57	5.08	3.29
Con 3	0.02272	10.10	11.43	5.12	3.32
Con 4	0.007686	10.60	11.60	3.77	3.27
Tail 4	0.3404	1.89	9.81	22.75	3.31

Test AQ

Stream	Mass Flow (tph)	PGM (ppm)	Chrome (ppm)	% Solids	SG
Feed	0.3519	4.55	8.95	13.25	3.27
Con 1	0.008217	36.70	10.87	3.67	3.26
Con 2	0.004335	34.60	10.61	3.20	3.25
Con 3	0.001829	39.00	9.95	2.86	3.22
Con 4	0.001232	41.60	9.70	2.53	3.21
Tail 4	0.3963	2.33	8.99	16.40	3.29

Test AR

Stream	Mass Flow (tph)	PGM (ppm)	Chrome (ppm)	% Solids	SG
Feed	0.3415	4.04	9.03	13.7	3.28
Con 1	0.01634	42.20	11.81	4.33	3.30
Con 2	0.009532	20.20	11.70	3.74	3.29
Con 3	0.005428	20.80	11.07	3.11	3.26
Con 4	0.002872	21.80	10.86	2.63	3.27
Tail 4	0.2853	2.33	9.07	19.15	3.28

Test AS

Stream	Mass Flow (tph)	PGM (ppm)	Chrome (ppm)	% Solids	SG
Feed	0.3385	3.93	8.94	13.4	3.30
Con 1	0.01360	22.93	11.41	3.86	3.28
Con 2	0.007046	21.33	11.15	3.22	3.28
Con 3	0.002267	29.53	10.35	2.63	3.25
Con 4	0.002014	23.20	10.53	2.56	3.27
Tail 4	0.3273	2.23	8.92	17.77	3.26

Test AT

Stream	Mass Flow (tph)	PGM (ppm)	Chrome (ppm)	% Solids	SG
Feed	0.3407	3.75	9.27	12.94	3.28
Con 1	0.01333	26.53	11.89	3.79	3.27
Con 2	0.01241	15.13	12.18	4.10	3.30
Con 3	0.006824	17.53	11.93	3.22	3.28
Con 4	0.002953	19.27	11.51	2.54	3.22
Tail 4	0.2913	1.99	8.93	18.82	3.27

Test AU

Stream	Mass Flow (tph)	PGM (ppm)	Chrome (ppm)	% Solids	SG
Feed	0.3469	3.74	8.93	13.68	3.26
Con 1	0.03326	14.00	11.89	4.76	3.28
Con 2	0.01932	17.23	12.04	4.70	3.30
Con 3	0.01184	10.70	12.05	3.98	3.30
Con 4	0.006496	8.00	12.15	3.41	3.26
Tail 4	0.3734	1.80	8.18	26.02	3.28

Test AH

Stream	Mass Flow (tph)	PGM (ppm)	Chrome (ppm)	% Solids	SG
Feed	0.3518	4.11	9.56	14.54	3.28
Con 1	0.002449	88.67	10.43	2.43	3.26
Con 2	0.002684	57.93	10.60	2.31	3.24
Con 3	0.02407	11.70	11.67	4.62	3.29
Con 4	0.004251	20.60	11.38	2.65	3.22
Tail 4	0.3550	2.11	8.98	18.80	3.28

Test AI

Stream	Mass Flow (tph)	PGM (ppm)	Chrome (ppm)	% Solids	SG
Feed	0.3494	4.26	8.79	12.99	3.32
Con 1	0.006261	48.60	11.37	3.09	3.32
Con 2	0.006123	30.40	11.29	3.18	3.29
Con 3	0.005942	20.00	11.63	3.37	3.33
Con 4	0.01706	10.50	11.92	4.71	3.27
Tail 4	0.2961	2.17	8.58	19.73	3.30

Test AJ

Stream	Mass Flow (tph)	PGM (ppm)	Chrome (ppm)	% Solids	SG
Feed	0.3562	4.03	8.89	13.69	3.29
Con 1	0.02415	16.20	12.02	4.91	3.28
Con 2	0.01549	14.53	12.47	4.81	3.30
Con 3	0.008566	13.93	12.30	3.86	3.27
Con 4	0.004930	14.07	12.03	3.35	3.24
Tail 4	0.3255	1.99	8.55	20.57	3.30

Test AK

Stream	Mass Flow (tph)	PGM (ppm)	Chrome (ppm)	% Solids	SG
Feed	0.3563	3.57	8.52	14.02	3.28
Con 1	0.01546	20.40	11.82	4.11	3.29
Con 2	0.002885	42.07	10.52	2.65	3.25
Con 3	0.002694	30.80	10.76	2.73	3.23
Con 4	0.005657	16.60	11.40	3.03	3.23
Tail 4	0.3944	2.05	8.35	18.44	3.28

Test AL

Stream	Mass Flow (tph)	PGM (ppm)	Chrome (ppm)	% Solids	SG
Feed	0.3434	3.67	7.83	13.77	3.29
Con 1	0.01814	19.20	12.30	4.20	3.28
Con 2	0.005795	23.93	12.08	3.39	3.27
Con 3	0.004061	22.73	12.06	2.79	3.30
Con 4	0.006619	15.00	12.06	3.32	3.28
Tail 4	0.3640	2.00	7.86	19.93	3.30

Test AV

Stream	Mass Flow (tph)	PGM (ppm)	Chrome (ppm)	% Solids	SG
Feed	0.3282	3.84	9.81	12.77	3.27
Con 1	0.02503	17.00	12.63	4.60	3.55
Con 2	0.005834	23.40	12.41	2.96	3.31
Con 3	0.009576	14.00	12.21	3.05	3.29
Con 4	0.002281	19.33	11.48	1.99	3.27
Tail 4	0.2708	2.07	9.23	22.11	3.29

Test AW

Stream	Mass Flow (tph)	PGM (ppm)	Chrome (ppm)	% Solids	SG
Feed	0.3333	4.04	10.16	12.79	3.28
Con 1	0.01709	22.07	12.98	4.13	3.36
Con 2	0.01573	13.80	13.37	4.52	3.30
Con 3	0.003893	21.30	12.47	2.99	3.28
Con 4	0.004185	17.00	12.52	2.87	3.24
Tail 4	0.2885	1.94	9.67	19.44	3.30

Test AX

Stream	Mass Flow (tph)	PGM (ppm)	Chrome (ppm)	% Solids	SG
Feed	0.3146	3.74	10.83	12.67	3.30
Con 1	0.02613	23.33	13.80	4.83	3.27
Con 2	0.01202	22.53	13.55	4.07	3.28
Con 3	0.004080	18.90	13.49	2.98	3.31
Con 4	0.002235	23.20	12.71	2.60	3.23
Tail 4	0.2959	2.07	10.37	20.76	3.32

Test AY

Stream	Mass Flow (tph)	PGM (ppm)	Chrome (ppm)	% Solids	SG
Feed	0.3189	4.21	10.84	11.76	3.27
Con 1	0.01558	16.40	12.61	3.96	3.36
Con 2	0.006025	14.60	11.81	3.36	3.31
Con 3	0.004067	12.00	12.39	2.99	3.29
Con 4	0.002131	12.70	11.73	2.52	3.26
Tail 4	0.2691	1.88	9.80	17.62	3.29

Test AZ

Stream	Mass Flow (tph)	PGM (ppm)	Chrome (ppm)	% Solids	SG
Feed	0.3301	4.19	10.80	12.61	3.28
Con 1	0.01877	20.80	11.96	4.91	3.31
Con 2	0.007084	16.20	12.11	3.33	3.31
Con 3	0.004390	23.30	11.83	2.98	3.27
Con 4	0.001938	25.73	11.92	2.33	3.27
Tail 4	0.3314	2.28	10.55	16.85	3.29

Test AM

Stream	Mass Flow (tph)	PGM (ppm)	Chrome (ppm)	% Solids	SG
Feed	0.3581	3.67	8.29	13.71	3.28
Con 1	0.01036	21.93	11.52	3.61	3.30
Con 2	0.006483	24.67	11.64	3.19	3.30
Con 3	0.001977	27.90	11.45	2.47	3.25
Con 4	0.002375	25.00	11.48	2.14	3.28
Tail 4	0.3500	2.04	8.09	18.45	3.31

Test BA

Stream	Mass Flow (tph)	PGM (ppm)	Chrome (ppm)	% Solids	SG
Feed	0.3425	3.82	9.87	13.23	3.26
Con 1	0.01093	26.80	10.78	3.52	3.31
Con 2	0.007855	20.40	11.35	3.40	3.26
Con 3	0.008448	14.60	11.10	3.47	3.26
Con 4	0.001908	25.73	11.05	2.34	3.24
Tail 4	0.3178	2.17	9.74	17.44	3.29

Test AN

Stream	Mass Flow (tph)	PGM (ppm)	Chrome (ppm)	% Solids	SG
Feed	0.3641	4.20	8.68	13.96	3.29
Con 1	0.008841	30.80	10.49	3.63	3.24
Con 2	0.003599	42.10	9.76	3.28	3.22
Con 3	0.007118	20.73	10.18	3.73	3.28
Con 4	0.003696	20.10	9.61	3.22	3.22
Tail 4	0.3779	2.32	8.58	17.81	3.35

Test BB

Stream	Mass Flow (tph)	PGM (ppm)	Chrome (ppm)	% Solids	SG
Feed	0.3359	4.08	9.80	13.15	3.27
Con 1	0.007327	96.13	13.49	3.19	3.24
Con 2	0.005020	41.50	13.72	3.18	3.23
Con 3	0.005700	21.00	13.25	3.45	3.24
Con 4	0.001750	29.70	12.49	2.81	3.24
Tail 4	0.3444	2.10	9.73	16.73	3.29

Test AO

Stream	Mass Flow (tph)	PGM (ppm)	Chrome (ppm)	% Solids	SG
Feed	0.3600	3.41	8.62	14.9	3.25
Con 1	0.004748	47.20	9.89	2.89	3.29
Con 2	0.01955	13.20	10.76	4.84	3.29
Con 3	0.02517	9.80	10.86	5.29	3.24
Con 4	0.005821	14.50	10.46	3.28	3.23
Tail 4	0.4575	2.04	8.40	23.00	3.27

Test BC

Stream	Mass Flow (tph)	PGM (ppm)	Chrome (ppm)	% Solids	SG
Feed	0.3519	4.26	9.32	13.48	3.25
Con 1	0.03316	14.90	13.65	5.19	3.26
Con 2	0.01780	12.47	13.47	4.81	3.25
Con 3	0.009436	11.60	13.33	4.07	3.22
Con 4	0.006199	11.20	12.54	3.40	3.20
Tail 4	0.3456	1.84	9.67	22.74	3.26

Test AP

Stream	Mass Flow (tph)	PGM (ppm)	Chrome (ppm)	% Solids	SG
Feed	0.3740	3.87	8.88	14.44	3.24
Con 1	0.007526	35.80	10.43	3.55	3.28
Con 2	0.005608	26.80	10.35	3.26	3.23
Con 3	0.001845	37.00	9.63	2.85	3.24
Con 4	0.001436	32.90	9.17	2.69	3.28
Tail 4	0.3979	2.46	8.93	17.41	3.27

Test BD

Stream	Mass Flow (tph)	PGM (ppm)	Chrome (ppm)	% Solids	SG
Feed	0.2839	4.72	10.60	11.61	3.28
Con 1	0.003100	63.07	12.83	2.96	3.21
Con 2	0.003755	35.70	12.83	3.04	3.21
Con 3	0.002465	28.90	11.39	2.94	3.26
Con 4	0.002730	22.40	12.15	2.76	3.24
Tail 4	0.3541	2.57	8.50	15.21	3.31

MASS BALANCED DATA – ROUGHER FEED

A

Stream	Mass Flow (tph)	PGM (ppm)	Chrome (ppm)	Cell PGM Recovery	Rate Constant	Overall Recovery (%)
Feed	1.27	2.69	25.85			
Con 1	0.0385	36.85	10.69	41.53	0.2085	
Tail 1	1.23	1.62	26.32			
Con 2	0.00818	37.19	8.59	15.27	0.04782	
Tail 2	1.23	1.39	26.45			
Con 3	0.01124	20.46	9.5	20.37	0.06727	
Tail 3	1.22	1.21	26.61			
Con 4	0.004326	24.49	7.91	7.18	0.02003	
Tail 4	1.21	1.13	26.67			60.27

O

Stream	Mass Flow (tph)	PGM (ppm)	Chrome (ppm)	Cell PGM Recovery	Rate Constant	Overall Recovery (%)
Feed	1.22	2.58	25.6			
Con 1	0.02726	47.01	7.15	41.03	0.2233	
Tail 1	1.2	1.54	28.02			
Con 2	0.004729	42.68	5.25	10.92	0.03828	
Tail 2	1.19	1.38	26.11			
Con 3	0.002042	18.49	9.55	3.26	0.01037	
Tail 3	1.19	1.35	26.13			
Con 4	0.003794	19.69	8.02	4.65	0.01505	
Tail 4	1.19	1.29	26.19			51.09

B

Stream	Mass Flow (tph)	PGM (ppm)	Chrome (ppm)	Cell PGM Recovery	Rate Constant	Overall Recovery (%)
Feed	1.24	2.68	25.18			
Con 1	0.03721	32.91	11	38.85	0.1923	
Tail 1	1.2	1.74	25.62			
Con 2	0.00554	35.69	7.77	9.47	0.03120	
Tail 2	1.19	1.59	25.7			
Con 3	0.01225	26.17	8.58	23.99	0.09305	
Tail 3	1.18	1.33	25.88			
Con 4	0.008659	24.78	8.29	13.87	0.04596	
Tail 4	1.17	1.16	26.01			58.90

P

Stream	Mass Flow (tph)	PGM (ppm)	Chrome (ppm)	Cell PGM Recovery	Rate Constant	Overall Recovery (%)
Feed	1.24	2.45	26.28			
Con 1	0.03248	38.37	9.04	41.02	0.2235	
Tail 1	1.21	1.49	26.75			
Con 2	0.009178	35.29	5.95	17.97	0.06506	
Tail 2	1.2	1.23	26.91			
Con 3	0.01026	23.79	8.54	23.81	0.09158	
Tail 3	1.19	1.03	27.08			
Con 4	0.00453	26.6	7.63	9.83	0.03153	
Tail 4	1.19	0.9355	27.14			63.68

C

Stream	Mass Flow (tph)	PGM (ppm)	Chrome (ppm)	Cell PGM Recovery	Rate Constant	Overall Recovery (%)
Feed	1.25	2.79	25.31			
Con 1	0.02356	41.97	8.6	28.35	0.1253	
Tail 1	1.23	2.04	25.63			
Con 2	0.01167	26.98	9.9	12.55	0.04290	
Tail 2	1.22	1.8	25.78			
Con 3	0.009175	23.19	8.5	14.42	0.04928	
Tail 3	1.21	1.64	25.91			
Con 4	0.02868	19.06	8.55	27.53	0.1099	
Tail 4	1.18	1.21	26.33			59.15

Q

Stream	Mass Flow (tph)	PGM (ppm)	Chrome (ppm)	Cell PGM Recovery	Rate Constant	Overall Recovery (%)
Feed	1.3	2.51	25.7			
Con 1	0.0213	56.86	7.67	37.12	0.1880	
Tail 1	1.28	1.6	28			
Con 2	0.004427	32.49	7.45	7.02	0.02334	
Tail 2	1.27	1.49	26.06			
Con 3	0.01009	28.78	7.47	24.75	0.1003	
Tail 3	1.26	1.27	26.21			
Con 4	0.006462	24.79	7.55	10.01	0.03345	
Tail 4	1.25	1.15	26.31			55.33

D

Stream	Mass Flow (tph)	PGM (ppm)	Chrome (ppm)	Cell PGM Recovery	Rate Constant	Overall Recovery (%)
Feed	1.28	2.62	25.61			
Con 1	0.03642	33.88	9.69	36.79	0.1940	
Tail 1	1.24	1.7	26.08			
Con 2	0.009511	30.7	8.02	13.85	0.04868	
Tail 2	1.23	1.46	26.24			
Con 3	0.01023	21.3	7.93	18.11	0.06613	
Tail 3	1.22	1.31	26.39			
Con 4	0.0102	18.9	9.01	12.06	0.04027	

R

Stream	Mass Flow (tph)	PGM (ppm)	Chrome (ppm)	Cell PGM Recovery	Rate Constant	Overall Recovery (%)
Feed	1.31	2.72	25.99			
Con 1	0.02875	45.02	8.35	36.32	0.1783	
Tail 1	1.26	1.76	28.39			
Con 2	0.006197	38.57	5.99	10.61	0.03509	
Tail 2	1.27	1.58	26.46			
Con 3	0.01205	21.09	10.08	20.43	0.07495	
Tail 3	1.26	1.4	26.84			
Con 4	0.00483	26.72	7.84	7.32	0.02278	

Tail 4	1.21	1.16	26.54			57.75

	3					
Tail 4	1.25	1.3	26.71			53.79

E

Stream	Mass Flow (tph)	PGM (ppm)	Chrome (ppm)	Cell PGM Recovery	Rate Constant	Overall Recovery (%)
Feed	1.29	2.59	24.08			
Con 1	0.04055	31.39	10.91	38.10	0.2051	
Tail 1	1.25	1.65	24.51			
Con 2	0.008077	28.68	7.23	11.23	0.03705	
Tail 2	1.24	1.48	24.62			
Con 3	0.008474	29.88	9	21.21	0.07802	
Tail 3	1.23	1.28	24.73			
Con 4	0.005064	23.49	7.7	7.56	0.02336	
Tail 4	1.23	1.19	24.8			56.17

S

Stream	Mass Flow (tph)	PGM (ppm)	Chrome (ppm)	Cell PGM Recovery	Rate Constant	Overall Recovery (%)
Feed	1.3	2.76	25.24			
Con 1	0.04223	39.88	11.1	46.60	0.2888	
Tail 1	1.26	1.54	25.71			
Con 2	0.00801	34.48	7.58	14.23	0.04935	
Tail 2	1.25	1.33	25.83			
Con 3	0.001646	28.8	9.53	4.48	0.01352	
Tail 3	1.25	1.29	25.85			
Con 4	0.00819	28.58	7.68	14.52	0.04920	
Tail 4	1.24	1.11	25.97			62.03

F

Stream	Mass Flow (tph)	PGM (ppm)	Chrome (ppm)	Cell PGM Recovery	Rate Constant	Overall Recovery (%)
Feed	1.52	2.19	24.45			
Con 1	0.04502	23.33	11.9	31.55	0.1423	
Tail 1	1.48	1.54	24.83			
Con 2	0.006712	34.49	6.37	10.16	0.02984	
Tail 2	1.47	1.39	24.91			
Con 3	0.01056	21.66	8.51	24.21	0.08310	
Tail 3	1.46	1.25	25.03			
Con 4	0.009817	23.09	7.37	12.42	0.03624	
Tail 4	1.45	1.1	25.15			52.19

T

Stream	Mass Flow (tph)	PGM (ppm)	Chrome (ppm)	Cell PGM Recovery	Rate Constant	Overall Recovery (%)
Feed	1.26	2.75	25.14			
Con 1	0.03551	41.99	6.32	43.03	0.2383	
Tail 1	1.22	1.61	25.66			
Con 2	0.005603	24.38	8.96	6.95	0.02121	
Tail 2	1.22	1.5	25.76			
Con 3	0.01163	24.68	9.19	23.73	0.08839	
Tail 3	1.21	1.28	25.92			
Con 4	0.00332	45.29	9.44	9.71	0.02991	
Tail 4	1.2	1.15	25.97			59.73

G

Stream	Mass Flow (tph)	PGM (ppm)	Chrome (ppm)	Cell PGM Recovery	Rate Constant	Overall Recovery (%)
Feed	1.28	2.08	25.15			
Con 1	0.0291	31.57	9.16	34.51	0.1765	
Tail 1	1.25	1.4	25.52			
Con 2	0.007835	23.99	6.62	10.74	0.03732	
Tail 2	1.24	1.25	25.64			
Con 3	0.001495	17	8.61	2.52	0.007920	
Tail 3	1.24	1.23	25.66			
Con 4	0.007577	25.29	7.33	12.56	0.04390	
Tail 4	1.23	1.09	25.78			49.72

U

Stream	Mass Flow (tph)	PGM (ppm)	Chrome (ppm)	Cell PGM Recovery	Rate Constant	Overall Recovery (%)
Feed	1.24	2.92	25.01			
Con 1	0.03632	45.14	9.45	45.28	0.2735	
Tail 1	1.2	1.64	25.48			
Con 2	0.008753	27.46	7.65	12.21	0.04312	
Tail 2	1.19	1.45	25.61			
Con 3	0.01445	20.84	9.74	24.71	0.09974	
Tail 3	1.18	1.22	25.8			
Con 4	0.005722	24.88	9.37	9.89	0.03280	
Tail 4	1.17	1.1	25.88			64.17

H

Stream	Mass Flow (tph)	PGM (ppm)	Chrome (ppm)	Cell PGM Recovery	Rate Constant	Overall Recovery (%)
Feed	1.22	2.54	24.81			
Con 1	0.03239	36.33	9.42	40.06	0.2141	
Tail 1	1.19	1.57	25.23			
Con 2	0.01067	26.08	8.14	14.89	0.05179	
Tail 2	1.18	1.34	25.38			
Con 3	0.01199	16.17	10.7	17.07	0.05966	
Tail 3	1.17	1.19	25.53			
Con 4	0.005623	22.19	8.43	8.96	0.02756	
Tail 4	1.16	1.09	25.62			59.33

V

Stream	Mass Flow (tph)	PGM (ppm)	Chrome (ppm)	Cell PGM Recovery	Rate Constant	Overall Recovery (%)
Feed	1.3	2.52	26.35			
Con 1	0.03021	44.96	9.77	41.46	0.2390	
Tail 1	1.27	1.51	26.74			
Con 2	0.006407	31.69	8.7	10.59	0.03789	
Tail 2	1.26	1.35	26.83			
Con 3	0.008676	24.69	10	19.99	0.07822	
Tail 3	1.25	1.19	26.95			
Con 4	0.00161	22.5	9.21	2.74	0.008700	
Tail 4	1.25	1.16	26.97			55.44

I

Stream	Mass Flow (tph)	PGM (ppm)	Chrome (ppm)	Cell PGM Recovery	Rate Constant	Overall Recovery (%)
Feed	1.24	2.73	25.27			
Con 1	0.04675	35.54	8.7	49.08	0.3143	
Tail 1	1.2	1.45	25.92			
Con 2	0.005355	31.69	6.23	9.75	0.03290	
Tail 2	1.19	1.32	26.01			
Con 3	0.001468	21.3	7.8	2.82	0.008718	
Tail 3	1.19	1.29	26.03			
Con 4	0.008597	18.49	10	10.35	0.03449	
Tail 4	1.18	1.17	26.15			59.71

W

Stream	Mass Flow (tph)	PGM (ppm)	Chrome (ppm)	Cell PGM Recovery	Rate Constant	Overall Recovery (%)
Feed	1.27	2.54	25.78			
Con 1	0.03056	44.8	8.9	42.44	0.2433	
Tail 1	1.24	1.5	28.2			
Con 2	0.004226	33.59	7.11	7.63	0.02596	
Tail 2	1.23	1.39	26.27			
Con 3	0.003025	25.49	7.9	6.62	0.02283	
Tail 3	1.23	1.33	26.31			
Con 4	0.008304	25.27	7.97	12.83	0.04562	
Tail 4	1.22	1.17	26.44			55.74

J

Stream	Mass Flow (tph)	PGM (ppm)	Chrome (ppm)	Cell PGM Recovery	Rate Constant	Overall Recovery (%)
Feed	1.2	2.65	24.68			
Con 1	0.03574	37.04	9.55	41.63	0.2284	
Tail 1	1.17	1.59	25.15			
Con 2	0.003559	29.99	6.96	5.74	0.01680	
Tail 2	1.18	1.51	25.2			
Con 3	0.002131	20.2	6.36	3.31	0.01045	
Tail 3	1.16	1.47	25.23			
Con 4	0.006349	22.19	7.64	8.26	0.02747	
Tail 4	1.15	1.38	25.33			50.77

X

Stream	Mass Flow (tph)	PGM (ppm)	Chrome (ppm)	Cell PGM Recovery	Rate Constant	Overall Recovery (%)
Feed	1.29	2.58	25.57			
Con 1	0.04392	35.03	6.92	46.23	0.2788	
Tail 1	1.25	1.43	26.23			
Con 2	0.007867	27.87	7.18	11.95	0.04008	
Tail 2	1.24	1.27	26.35			
Con 3	0.003532	27.39	7.59	9.45	0.03051	
Tail 3	1.24	1.2	26.4			
Con 4	0.003316	36.29	10.4	6.09	0.02552	
Tail 4	1.23	1.1	26.44			59.17

K

Stream	Mass Flow (tph)	PGM (ppm)	Chrome (ppm)	Cell PGM Recovery	Rate Constant	Overall Recovery (%)
Feed	1.27	2.89	26			
Con 1	0.0288	49.18	8.24	38.59	0.1963	
Tail 1	1.24	1.81	26.41			
Con 2	0.01069	34.89	8.75	16.62	0.05983	
Tail 2	1.23	1.52	26.58			
Con 3	0.01021	22.09	9.49	18.25	0.06626	
Tail 3	1.22	1.35	26.72			
Con 4	0.01168	21.59	8.82	15.31	0.05261	
Tail 4	1.21	1.16	26.9			61.77

Y

Stream	Mass Flow (tph)	PGM (ppm)	Chrome (ppm)	Cell PGM Recovery	Rate Constant	Overall Recovery (%)
Feed	1.28	2.77	25.46			
Con 1	0.04019	38.23	10.38	41.07	0.2047	
Tail 1	1.24	1.68	25.94			
Con 2	0.007761	39.69	6.79	14.79	0.04609	
Tail 2	1.23	1.44	26.07			
Con 3	0.002461	28.1	7.63	5.95	0.01651	
Tail 3	1.23	1.39	26.1			
Con 4	0.005036	27.49	8.03	8.10	0.02285	
Tail 4	1.22	1.28	26.18			55.63

L

Stream	Mass Flow (tph)	PGM (ppm)	Chrome (ppm)	Cell PGM Recovery	Rate Constant	Overall Recovery (%)
Feed	1.26	2.38	26.05			
Con 1	0.03563	34.53	9.99	41.03	0.2297	
Tail 1	1.22	1.45	26.52			
Con 2	0.004855	44	8.13	12.08	0.04240	
Tail 2	1.22	1.28	26.6			
Con 3	0.008651	27.31	9.27	22.52	0.08929	
Tail 3	1.21	1.09	26.73			

Z

Stream	Mass Flow (tph)	PGM (ppm)	Chrome (ppm)	Cell PGM Recovery	Rate Constant	Overall Recovery (%)
Feed	1.29	2.69	25.18			
Con 1	0.02565	48.28	8.82	35.89	0.1809	
Tail 1	1.26	1.76	25.51			
Con 2	0.003765	40.7	8.13	6.91	0.02300	
Tail 2	1.26	1.65	25.57			
Con 3	0.01049	24.39	8.36	19.54	0.07520	
Tail 3	1.25	1.45	25.72			

Con 4	0.002612	27	8.91	5.35	0.01700	
Tail 4	1.21	1.04	26.77			58.38

Con 4	0.007287	28.99	8.08	11.66	0.04026	
Tail 4	1.24	1.29	25.82			53.56

M

Stream	Mass Flow (tph)	PGM (ppm)	Chrome (ppm)	Cell PGM Recovery	Rate Constant	Overall Recovery (%)
Feed	1.26	2.81	26.31			
Con 1	0.04461	29.76	11.77	40.37	0.2284	
Tail 1	1.22	1.61	26.85			
Con 2	0.007173	33.49	7.13	12.23	0.04269	
Tail 2	1.21	1.42	26.96			
Con 3	0.00155	21.4	10.7	2.83	0.008638	
Tail 3	1.21	1.4	26.96			
Con 4	0.00926	24.79	9.26	13.55	0.04649	
Tail 4	1.2	1.22	27.12			55.66

AA

Stream	Mass Flow (tph)	PGM (ppm)	Chrome (ppm)	Cell PGM Recovery	Rate Constant	Overall Recovery (%)
Feed	1.25	2.75	25.38			
Con 1	0.04331	36.49	10.89	45.97	0.2846	
Tail 1	1.21	1.54	25.9			
Con 2	0.006814	36.68	7.24	13.41	0.04737	
Tail 2	1.2	1.34	26.01			
Con 3	0.00189	21.2	10.3	3.59	0.01119	
Tail 3	1.2	1.31	26.03			
Con 4	0.007713	24.68	10.2	12.11	0.04150	
Tail 4	1.19	1.18	26.13			59.95

N

Stream	Mass Flow (tph)	PGM (ppm)	Chrome (ppm)	Cell PGM Recovery	Rate Constant	Overall Recovery (%)
Feed	1.23	2.78	25.63			
Con 1	0.03378	43.73	8.04	43.20	0.2442	
Tail 1	1.19	1.62	26.13			
Con 2	0.001117	34.7	6.6	2.01	0.006351	
Tail 2	1.19	1.59	26.14			
Con 3	0.002604	21.99	6.08	4.29	0.01388	
Tail 3	1.19	1.55	26.18			
Con 4	0.008453	21.49	7.19	7.52	0.02511	
Tail 4	1.18	1.44	26.29			50.06

AB

Stream	Mass Flow (tph)	PGM (ppm)	Chrome (ppm)	Cell PGM Recovery	Rate Constant	Overall Recovery (%)
Feed	1.23	2.79	25.03			
Con 1	0.02574	46.63	9.56	34.96	0.1743	
Tail 1	1.21	1.86	25.36			
Con 2	0.007304	33.18	6.06	10.77	0.03839	
Tail 2	1.2	1.67	25.48			
Con 3	0.01077	21.57	8.99	16.69	0.06279	
Tail 3	1.19	1.49	25.63			
Con 4	0.004234	24.59	8.5	5.87	0.01925	
Tail 4	1.19	1.4	25.69			51.84

MASS BALANCED DATA – CLEANER TAILS

AC

Stream	Mass Flow (tph)	PGM (ppm)	Chrome (ppm)	Cell PGM Recovery	Rate Constant	Overall Recovery (%)
Feed	0.3451	4.08	9.47			
Con 1	0.01173	31.3	1.03	28.08	0.1069	
Tail 1	0.3334	3.12	9.77			
Con 2	0.001124	57.5	4.01	8.21	0.01715	
Tail 2	0.3322	2.94	9.79			
Con 3	0.004227	15.3	11.3	6.62	0.01797	
Tail 3	0.328	2.78	9.77			
Con 4	0.001482	33	10.4	5.38	0.01323	
Tail 4	0.3265	2.84	9.78			38.73

AD

Stream	Mass Flow (tph)	PGM (ppm)	Chrome (ppm)	Cell PGM Recovery	Rate Constant	Overall Recovery (%)
Feed	0.3502	4.47	9.00			
Con 1	0.02751	18.31	11.39	28.66	0.1236	
Tail 1	0.3227	3.46	8.8			
Con 2	0.01131	16.01	10.69	18.22	0.04532	
Tail 2	0.3114	3.01	8.73			
Con 3	0.008738	30.8	11.8	28.71	0.07924	
Tail 3	0.3028	2.2	8.65			
Con 4	0.007702	15.7	11.5	18.18	0.03658	
Tail 4	0.2949	1.85	8.58			85.15

AE

Stream	Mass Flow (tph)	PGM (ppm)	Chrome (ppm)	Cell PGM Recovery	Rate Constant	Overall Recovery (%)
Feed	0.3316	4.57	9.08			
Con 1	0.01831	20.64	11.00	24.94	0.1018	
Tail 1	0.3132	3.63	8.95			
Con 2	0.01371	15.78	11.2	19.00	0.05838	
Tail 2	0.2995	3.07	8.85			
Con 3	0.01253	19.56	12.3	26.66	0.07440	
Tail 3	0.287	2.35	8.7			
Con 4	0.002594	21.59	12.1	8.30	0.01392	
Tail 4	0.2844	2.18	8.66			59.07

AF

Stream	Mass Flow (tph)	PGM (ppm)	Chrome (ppm)	Cell PGM Recovery	Rate Constant	Overall Recovery (%)
Feed	0.3429	4.21	9.19			
Con 1	0.02733	17.16	11.95	32.49	0.1480	
Tail 1	0.3156	3.09	8.95			
Con 2	0.01075	17.72	12.58	19.53	0.05510	
Tail 2	0.3048	2.58	8.62			
Con 3	0.004954	28.71	11.49	18.09	0.04134	

AQ

Stream	Mass Flow (tph)	PGM (ppm)	Chrome (ppm)	Cell PGM Recovery	Rate Constant	Overall Recovery (%)
Feed	0.3568	4.48	9.03			
Con 1	0.01458	36.71	10.9	33.48	0.1609	
Tail 1	0.3422	3.11	8.95			
Con 2	0.004757	34.6	10.8	15.47	0.04924	
Tail 2	0.3375	2.87	8.92			
Con 3	0.001905	39	9.95	8.24	0.02248	
Tail 3	0.3356	2.48	8.92			
Con 4	0.001034	41.8	9.7	5.21	0.01327	
Tail 4	0.3345	2.34	8.92			51.12

AR

Stream	Mass Flow (tph)	PGM (ppm)	Chrome (ppm)	Cell PGM Recovery	Rate Constant	Overall Recovery (%)
Feed	0.3375	4.89	9.18			
Con 1	0.01357	42.1	11.79	38.09	0.1645	
Tail 1	0.3239	3.12	9.07			
Con 2	0.009279	20.13	11.7	18.48	0.05701	
Tail 2	0.3146	2.62	8.99			
Con 3	0.006131	20.75	11.1	15.43	0.04013	
Tail 3	0.3085	2.28	9.95			
Con 4	0.002857	21.78	10.9	8.92	0.01909	
Tail 4	0.3058	2.07	8.93			59.86

AS

Stream	Mass Flow (tph)	PGM (ppm)	Chrome (ppm)	Cell PGM Recovery	Rate Constant	Overall Recovery (%)
Feed	0.3383	3.87	9.02			
Con 1	0.01386	22.91	11.4	24.25	0.09580	
Tail 1	0.3245	3.06	8.92			
Con 2	0.007388	21.3	11.1	15.85	0.04779	
Tail 2	0.3171	2.84	8.87			
Con 3	0.003701	29.5	10.4	13.04	0.03384	
Tail 3	0.3134	2.32	8.85			
Con 4	0.001004	23.2	10.5	3.20	0.006831	
Tail 4	0.3124	2.25	8.85			46.39

AT

Stream	Mass Flow (tph)	PGM (ppm)	Chrome (ppm)	Cell PGM Recovery	Rate Constant	Overall Recovery (%)
Feed	0.3393	3.85	9.26			
Con 1	0.01246	28.48	11.9	25.26	0.1054	
Tail 1	0.3268	2.98	9.15			
Con 2	0.01239	15.08	12.2	19.19	0.06414	
Tail 2	0.3145	2.51	9.03			
Con 3	0.004541	17.49	11.9	10.08	0.02590	

Tail 3	0.2999	2.14	8.77			
Con 4	0.002343	16.81	11.9	6.14	0.01062	
Tail 4	0.2975	2.03	8.75			58.26

Tail 3	0.3099	2.29	8.99			
Con 4	0.005934	19.29	11.5	16.13	0.04105	
Tail 4	0.304	1.96	8.94			54.40

AG

Stream	Mass Flow (tph)	PGM (ppm)	Chrome (ppm)	Cell PGM Recovery	Rate Constant	Overall Recovery (%)
Feed	0.3587	4.83	9.64			
Con 1	0.01044	46.84	11.59	29.44	0.1264	
Tail 1	0.3483	3.37	9.58			
Con 2	0.02176	17.78	11.58	32.96	0.1301	
Tail 2	0.3265	2.41	9.44			
Con 3	0.02359	9.97	11.37	29.89	0.08979	
Tail 3	0.3029	1.82	9.29			
Con 4	0.002118	10.59	11.6	4.06	0.008468	
Tail 4	0.3008	1.76	9.28			68.25

AU

Stream	Mass Flow (tph)	PGM (ppm)	Chrome (ppm)	Cell PGM Recovery	Rate Constant	Overall Recovery (%)
Feed	0.3473	4.07	8.91			
Con 1	0.03325	13.86	11.9	32.60	0.1453	
Tail 1	0.3141	3.03	8.6			
Con 2	0.01929	17.12	12	34.70	0.1129	
Tail 2	0.2948	2.11	8.37			
Con 3	0.0116	10.65	12.1	20.20	0.04060	
Tail 3	0.283	1.75	8.22			
Con 4	0.001879	7.99	12.1	3.03	0.003636	
Tail 4	0.2811	1.71	8.19			65.92

AH

Stream	Mass Flow (tph)	PGM (ppm)	Chrome (ppm)	Cell PGM Recovery	Rate Constant	Overall Recovery (%)
Feed	0.3507	3.32	9.38			
Con 1	0.00157	86.69	10.4	11.98	0.03850	
Tail 1	0.3492	2.94	9.35			
Con 2	0.001249	57.9	10.6	7.04	0.02084	
Tail 2	0.3479	2.74	9.35			
Con 3	0.02412	11.81	11.71	29.38	0.11157	
Tail 3	0.3238	2.08	9.17			
Con 4	0.001502	20.59	11.4	4.59	0.009716	
Tail 4	0.3223	2	9.18			44.88

AV

Stream	Mass Flow (tph)	PGM (ppm)	Chrome (ppm)	Cell PGM Recovery	Rate Constant	Overall Recovery (%)
Feed	0.3279	4.09	9.73			
Con 1	0.02507	16.92	12.81	31.63	0.1415	
Tail 1	0.3029	3.03	9.49			
Con 2	0.005262	23.36	12.4	13.40	0.03670	
Tail 2	0.2976	2.87	9.44			
Con 3	0.01042	13.97	12.2	18.32	0.04809	
Tail 3	0.2872	2.26	9.34			
Con 4	0.004502	19.29	11.5	13.38	0.02636	
Tail 4	0.2827	1.98	9.3			58.13

AI

Stream	Mass Flow (tph)	PGM (ppm)	Chrome (ppm)	Cell PGM Recovery	Rate Constant	Overall Recovery (%)
Feed	0.3444	4.21	8.89			
Con 1	0.001773	48.6	11.4	5.94	0.01991	
Tail 1	0.3426	3.98	8.87			
Con 2	0.005607	30.4	11.3	12.50	0.04395	
Tail 2	0.337	3.54	8.83			
Con 3	0.01755	20.01	11.59	29.44	0.1191	
Tail 3	0.3194	2.63	8.66			
Con 4	0.01712	10.51	11.9	21.42	0.05964	
Tail 4	0.3023	2.19	8.5			54.33

AW

Stream	Mass Flow (tph)	PGM (ppm)	Chrome (ppm)	Cell PGM Recovery	Rate Constant	Overall Recovery (%)
Feed	0.3325	4.04	10.15			
Con 1	0.01705	22.1	13	28.05	0.1207	
Tail 1	0.3154	3.06	9.99			
Con 2	0.0157	13.8	13.4	22.45	0.07438	
Tail 2	0.2997	2.5	9.81			
Con 3	0.003558	21.3	12.5	10.11	0.02398	
Tail 3	0.2962	2.28	9.78			
Con 4	0.006614	17	12.5	16.65	0.03951	
Tail 4	0.2895	1.94	9.72			58.19

AJ

Stream	Mass Flow (tph)	PGM (ppm)	Chrome (ppm)	Cell PGM Recovery	Rate Constant	Overall Recovery (%)
Feed	0.3561	3.91	9.0			
Con 1	0.0241	18.23	11.99	28.09	0.1202	
Tail 1	0.332	3.01	8.78			
Con 2	0.015	14.52	12.5	21.79	0.06850	
Tail 2	0.317	2.47	8.6			
Con 3	0.008995	13.91	12.3	15.98	0.03922	
Tail 3	0.308	2.13	8.5			
Con 4	0.002697	14.1	12.0	5.80	0.01086	

AX

Stream	Mass Flow (tph)	PGM (ppm)	Chrome (ppm)	Cell PGM Recovery	Rate Constant	Overall Recovery (%)
Feed	0.3101	4.81	10.84			
Con 1	0.02382	22.94	13.8	36.63	0.1686	
Tail 1	0.2863	3.3	10.59			
Con 2	0.01188	22.32	13.8	28.07	0.08949	
Tail 2	0.2744	2.47	10.46			
Con 3	0.00141	18.88	13.5	3.93	0.007864	
Tail 3	0.273	2.39	10.44			
Con 4	0.00893	23.06	12.7	31.58	0.08592	

Tail 4	0.3053	2.03	8.46			55.45

Tail 4	0.2641	1.69	10.37			70.00

AK

Stream	Mass Flow (tph)	PGM (ppm)	Chrome (ppm)	Cell PGM Recovery	Rate Constant	Overall Recovery (%)
Feed	0.3566	3.63	8.55			
Con 1	0.01557	20.39	11.6	24.53	0.09751	
Tail 1	0.341	2.86	8.4			
Con 2	0.003	42.1	10.5	12.95	0.03749	
Tail 2	0.338	2.51	8.36			
Con 3	0.003921	30.8	10.6	14.23	0.03941	
Tail 3	0.3341	2.16	8.35			
Con 4	0.003511	18.6	11.4	8.00	0.01906	
Tail 4	0.3306	2.03	8.32			48.11

AY

Stream	Mass Flow (tph)	PGM (ppm)	Chrome (ppm)	Cell PGM Recovery	Rate Constant	Overall Recovery (%)
Feed	0.3188	3.49	10.4			
Con 1	0.01565	16.53	12.62	23.27	0.09861	
Tail 1	0.303	2.82	10.27			
Con 2	0.006815	14.66	11.61	11.69	0.03646	
Tail 2	0.2961	2.55	10.24			
Con 3	0.002935	12.02	12.4	4.67	0.01221	
Tail 3	0.2932	2.45	10.21			
Con 4	0.0103	12.79	11.71	18.34	0.05316	
Tail 4	0.2629	2.07	10.16			47.27

AL

Stream	Mass Flow (tph)	PGM (ppm)	Chrome (ppm)	Cell PGM Recovery	Rate Constant	Overall Recovery (%)
Feed	0.343	3.77	8.08			
Con 1	0.01812	19.18	12.26	26.88	0.1062	
Tail 1	0.3249	2.91	7.85			
Con 2	0.005895	23.89	12.09	14.90	0.04192	
Tail 2	0.319	2.52	7.77			
Con 3	0.006209	22.89	12.09	17.53	0.04619	
Tail 3	0.3128	2.12	7.68			
Con 4	0.003705	15	12.1	8.38	0.01727	
Tail 4	0.3091	1.96	7.83			52.96

AZ

Stream	Mass Flow (tph)	PGM (ppm)	Chrome (ppm)	Cell PGM Recovery	Rate Constant	Overall Recovery (%)
Feed	0.3296	4.13	10.77			
Con 1	0.01892	20.81	12	26.92	0.1269	
Tail 1	0.3107	3.11	10.89			
Con 2	0.0084	16.21	12.1	14.09	0.04315	
Tail 2	0.3023	2.75	10.65			
Con 3	0.005218	23.3	11.8	14.62	0.03956	
Tail 3	0.2971	2.38	10.63			
Con 4	0.001027	25.7	11.9	3.73	0.008084	
Tail 4	0.296	2.3	10.63			49.80

AM

Stream	Mass Flow (tph)	PGM (ppm)	Chrome (ppm)	Cell PGM Recovery	Rate Constant	Overall Recovery (%)
Feed	0.3589	3.58	8.31			
Con 1	0.01074	21.91	11.5	18.31	0.06941	
Tail 1	0.3482	3.02	8.21			
Con 2	0.007414	24.71	11.8	17.42	0.05731	
Tail 2	0.3407	2.55	8.14			
Con 3	0.005086	27.91	11.4	18.34	0.04724	
Tail 3	0.3357	2.16	8.09			
Con 4	0.001503	25	11.5	5.18	0.01177	
Tail 4	0.3342	2.06	8.07			46.54

BA

Stream	Mass Flow (tph)	PGM (ppm)	Chrome (ppm)	Cell PGM Recovery	Rate Constant	Overall Recovery (%)
Feed	0.3442	3.74	9.86			
Con 1	0.01099	26.81	10.8	22.89	0.09169	
Tail 1	0.3332	2.98	9.82			
Con 2	0.009353	20.41	11.4	19.23	0.06404	
Tail 2	0.3239	2.48	9.78			
Con 3	0.005225	14.81	11.1	9.50	0.02458	
Tail 3	0.3187	2.28	9.76			
Con 4	0.001003	25.7	11.1	3.55	0.007899	
Tail 4	0.3176	2.2	9.75			45.65

AN

Stream	Mass Flow (tph)	PGM (ppm)	Chrome (ppm)	Cell PGM Recovery	Rate Constant	Overall Recovery (%)
Feed	0.3641	4.19	8.69			
Con 1	0.01487	30.8	10.5	30.02	0.1321	
Tail 1	0.3492	3.08	8.61			
Con 2	0.003554	42.1	9.76	14.00	0.04301	
Tail 2	0.3457	2.66	8.6			
Con 3	0.004684	20.7	10.2	10.54	0.02641	

BB

Stream	Mass Flow (tph)	PGM (ppm)	Chrome (ppm)	Cell PGM Recovery	Rate Constant	Overall Recovery (%)
Feed	0.3326	4.06	9.87			
Con 1	0.001127	96.1	13.5	6.02	0.02620	
Tail 1	0.3315	3.75	9.88			
Con 2	0.005237	41.5	13.7	17.48	0.06272	
Tail 2	0.3263	3.14	9.6			
Con 3	0.00584	21	13.2	11.57	0.03595	

Tail 3	0.341	2.41	8.57			
Con 4	0.001776	20.1	8.58	4.34	0.01022	
Tail 4	0.3392	2.32	8.57			48.52

	4					
Tail 3	0.3206	2.83	9.74			
Con 4	0.008423	29.7	12.5	27.57	0.09674	
Tail 4	0.3122	2.11	9.66			51.42

AO

Stream	Mass Flow (tph)	PGM (ppm)	Chrome (ppm)	Cell PGM Recovery	Rate Constant	Overall Recovery (%)
Feed	0.3799	3.66	8.66			
Con 1	0.005541	47.18	9.69	18.80	0.06921	
Tail 1	0.3754	3.14	8.65			
Con 2	0.01952	13.13	10.8	21.74	0.07746	
Tail 2	0.3559	2.59	8.53			
Con 3	0.02521	9.71	10.5	26.56	0.08245	
Tail 3	0.3307	2.05	8.36			
Con 4	0.00292	14.49	10.5	6.24	0.01118	
Tail 4	0.3278	1.94	8.36			57.88

BC

Stream	Mass Flow (tph)	PGM (ppm)	Chrome (ppm)	Cell PGM Recovery	Rate Constant	Overall Recovery (%)
Feed	0.3542	4.03	9.96			
Con 1	0.03337	14.98	13.84	35.02	0.1678	
Tail 1	0.3208	2.89	9.56			
Con 2	0.0178	12.54	13.47	24.08	0.07308	
Tail 2	0.303	2.32	9.33			
Con 3	0.0113	11.83	13.28	16.70	0.04223	
Tail 3	0.2917	1.96	9.17			
Con 4	0.002184	11.21	12.5	4.26	0.006641	
Tail 4	0.2896	1.89	9.15			61.58

AP

Stream	Mass Flow (tph)	PGM (ppm)	Chrome (ppm)	Cell PGM Recovery	Rate Constant	Overall Recovery (%)
Feed	0.3756	3.93	8.94			
Con 1	0.006939	35.79	10.4	21.67	0.08469	
Tail 1	0.3667	3.15	8.9			
Con 2	0.005674	28.8	10.4	14.15	0.04518	
Tail 2	0.361	2.75	8.88			
Con 3	0.002126	37	9.83	7.92	0.02167	
Tail 3	0.3589	2.54	8.87			
Con 4	0.001283	32.9	9.17	4.63	0.01175	
Tail 4	0.3576	2.43	8.87			40.93

BD

Stream	Mass Flow (tph)	PGM (ppm)	Chrome (ppm)	Cell PGM Recovery	Rate Constant	Overall Recovery (%)
Feed	0.2855	4.89	9.57			
Con 1	0.004393	63.09	12.82	19.85	0.07320	
Tail 1	0.2811	3.98	9.52			
Con 2	0.00418	35.69	12.81	13.27	0.04229	
Tail 2	0.277	3.5	9.47			
Con 3	0.004816	28.89	11.42	14.35	0.04339	
Tail 3	0.2721	3.05	9.44			
Con 4	0.007433	22.39	12.13	20.05	0.05967	
Tail 4	0.2647	2.51	9.38			52.37

ROUGHER FEED REGRESSION EQUATIONS

$$\text{PGM Recovery} = 272 - 1.13*Q - 132*(\text{Feed Grade}) - 0.0253*N^2 + 0.445*Q*(\text{Feed Grade}) + 1.37*N*(\text{Feed Grade})$$

$$\text{Concentrate PGM Grade} = 439 - 6.26*N - 143*(\text{Feed Grade}) + 2.22*N*(\text{Feed Grade})$$

CLEANER TAILS REGRESSION EQUATIONS

$$\text{PGM Recovery} = -62.2 + 0.168*Q + 0.994*N + 1.65*(\text{Feed Grade})^2$$

$$\text{Concentrate PGM Grade} = 231 - 1.01*Q - 3.04*N + 0.510*(\text{Feed Grade})^2 + 0.0135*(Q*N)$$